



UNIVERSITAT ROVIRA I VIRGILI

CARBON DIOXIDE TO METHANOL: STOICHIOMETRIC CATALYTIC HYDROGENATION UNDER HIGH PRESSURE CONDITIONS

Rohit Gaikwad

ADVERTIMENT. L'accés als continguts d'aquesta tesi doctoral i la seva utilització ha de respectar els drets de la persona autora. Pot ser utilitzada per a consulta o estudi personal, així com en activitats o materials d'investigació i docència en els termes establerts a l'art. 32 del Text Refós de la Llei de Propietat Intel·lectual (RDL 1/1996). Per altres utilitzacions es requereix l'autorització prèvia i expressa de la persona autora. En qualsevol cas, en la utilització dels seus continguts caldrà indicar de forma clara el nom i cognoms de la persona autora i el títol de la tesi doctoral. No s'autoritza la seva reproducció o altres formes d'explotació efectuades amb finalitats de lucre ni la seva comunicació pública des d'un lloc aliè al servei TDX. Tampoc s'autoritza la presentació del seu contingut en una finestra o marc aliè a TDX (framing). Aquesta reserva de drets afecta tant als continguts de la tesi com als seus resums i índexs.

ADVERTENCIA. El acceso a los contenidos de esta tesis doctoral y su utilización debe respetar los derechos de la persona autora. Puede ser utilizada para consulta o estudio personal, así como en actividades o materiales de investigación y docencia en los términos establecidos en el art. 32 del Texto Refundido de la Ley de Propiedad Intelectual (RDL 1/1996). Para otros usos se requiere la autorización previa y expresa de la persona autora. En cualquier caso, en la utilización de sus contenidos se deberá indicar de forma clara el nombre y apellidos de la persona autora y el título de la tesis doctoral. No se autoriza su reproducción u otras formas de explotación efectuadas con fines lucrativos ni su comunicación pública desde un sitio ajeno al servicio TDR. Tampoco se autoriza la presentación de su contenido en una ventana o marco ajeno a TDR (framing). Esta reserva de derechos afecta tanto al contenido de la tesis como a sus resúmenes e índices.

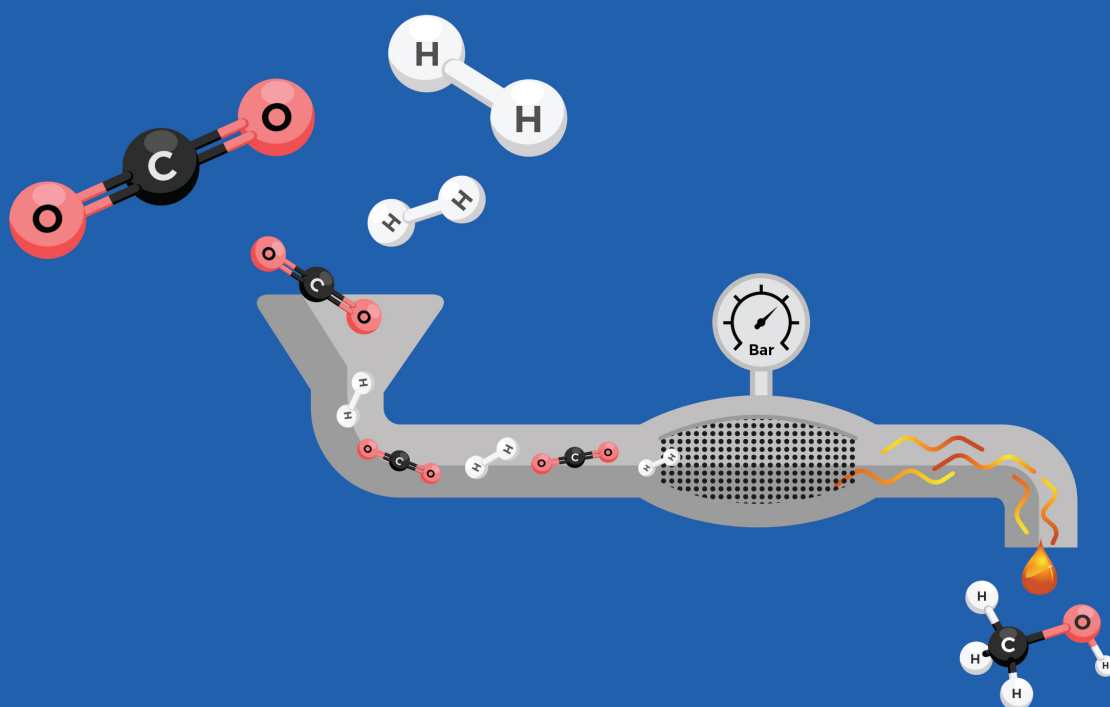
WARNING. Access to the contents of this doctoral thesis and its use must respect the rights of the author. It can be used for reference or private study, as well as research and learning activities or materials in the terms established by the 32nd article of the Spanish Consolidated Copyright Act (RDL 1/1996). Express and previous authorization of the author is required for any other uses. In any case, when using its content, full name of the author and title of the thesis must be clearly indicated. Reproduction or other forms of for profit use or public communication from outside TDX service is not allowed. Presentation of its content in a window or frame external to TDX (framing) is not authorized either. These rights affect both the content of the thesis and its abstracts and indexes.



UNIVERSITAT
ROVIRA I VIRGILI

Carbon Dioxide to Methanol: Stoichiometric Catalytic Hydrogenation under High Pressure Conditions

ROHIT VILAS GAIKWAD



DOCTORAL THESIS

2018

Doctoral thesis

**Carbon Dioxide to Methanol: Stoichiometric
Catalytic Hydrogenation under High
Pressure Conditions**

ROHIT VILAS GAIKWAD

Supervised by:

Prof. Dr. Atsushi Urakawa

ICIQ-URV



Tarragona
2018

UNIVERSITAT ROVIRA I VIRGILI

CARBON DIOXIDE TO METHANOL: STOICHIOMETRIC CATALYTIC HYDROGENATION UNDER HIGH PRESSURE CONDITIONS

Rohit Gaikwad

Prof. Dr. Atsushi Urakawa
Group Leader
Institute of Chemical Research of Catalonia (ICIQ)
Av. Països Catalans 16
43007 Tarragona, Spain

Tarragona, 5th February 2018

CERTIFY THAT:

The present work, entitled “Carbon Dioxide to Methanol: Stoichiometric Catalytic Hydrogenation under High Pressure Conditions” by Rohit Vilas Gaikwad for the award of the degree of doctor, has been carried out under my supervision at Institute of Chemical Research of Catalonia (ICIQ), and that it fulfils all the requirements to obtain the degree of Doctor in Chemical Science and Technology.

Sincerely,

Prof. Dr. Atsushi Urakawa



UNIVERSITAT ROVIRA I VIRGILI

CARBON DIOXIDE TO METHANOL: STOICHIOMETRIC CATALYTIC HYDROGENATION UNDER HIGH PRESSURE CONDITIONS

Rohit Gaikwad

Acknowledgement

I owe my deepest thanks to my supervisor Prof. Dr. Atsushi Urakawa for allowing me to do PhD in his group. Your continuous support, exceptional inspiration, and constructive criticism enabled me to improve my scientific and personal skills giving me feeling of a second adolescence. Thank you for being a sounding board for my crazy ideas and all kind of problems. Discussion with you always resulted in great solutions, new perspectives in retrieved data. Your inspiring word “100 percent” extend not only my capabilities but reactor system too, to deliver maximum from both of us. The opportunity you gave me to work with you is a milestone in my life that changed everything. Just thanks word will not be enough to express my sincere gratitude, a special word “Arigatou Gozaimasu Atsushi Sensei”.

I would like to thanks to all scientific and non-scientific staff at ICIQ and URV. A special thanks to Dr. Jordi Benet, Marta, and Eduardo from X-ray diffraction unit and Dr. Miguel Gonzalez, Dr. Georgiana Stoica and Dr. Dolores Gonzalez Candela from Heterogeneous Catalysis Unit for all their valuable time and patience while training on instruments. Their freedom in the unit and trust allowed me to handle all instruments independently. The help and guidance from Dr. Marta Gimenez Pedros and Cristina Rivero from Chemical Reaction Technology unit for using different reactors and facility is highly appreciated. I would like to give special thanks to Jose Luis Leon from the Mechanical Workshop and Xavier Asensio from Glass Blowing Workshop for their remarkable and quick fabrication of any reactor design with high precision. Thanks to Marc, Jesus and Alex for delivering parcel with happiness every day in the morning. Many thanks to Aurora and Noelia for the easy and uncomplicated handling of administrative and bureaucratic processes especially arranging trips and visas.

This Journey started 4 years back, when I entered in lab P2.11 and get introduced to Atul, Jordi, Antonio and Dina. Thank you very much guys for your helping hand with effective knowledge and experience transfer. Thanks Antonio (Chutano) for initial outdoor insane activities, and Jordi (Purdilla) for weekend parties and long lasting drinks. Thanks to Dina (Pirri) for inspiration and very effective discussion on how to enjoy life with work. A special thanks to Atul for your endless support, trust, critical inputs, directing the research and improving personal and professional skills.

I would like to express my gratitude to former members, Luis Bobadilla, Ta Corrales, Yi Zhang, Sergio Roso, Muralidhar Chourashiya, Damien Cornu, Reza Taheraslani and Joan Giner for their help, support and providing pleasant and friendly atmosphere over the years. I want to thank Sergio Lima and Andrea Alvarez for sharing their experience on methanol synthesis, especially those critical comments and discussions were really admirable. I would like to express my sincere appreciation to Dragos Stoian, Marta Borges and Dana Crivoi for patience, motivation and attitude to always help and care for each other, helped me to survive all those years. The fun, jokes, mocking and romantic moments (Titanic) were truly unforgettable memories. I would like to thank to Juan Jose Corral, Lungjun Hu, Rui Huang, Silvia Caminero, Nat Phongprueksathat, Sorin Bunea for keeping lab atmosphere fresh and energetic. A list cannot complete without mentioning Japanese community. A special thanks to Tsuyoshi Hyakutake, Takuya Suganuma, Prof. Tetsuya Kida and Satoshi Hinokuma for those keep smiling attitude, and Shunsaku Yasumura, and Shintaro Hara for the never ending house parties with Keisho Okura. I thank all my friends and country-mates in Tarragona for their love, support and encouragement.

Furthermore, I would like to thanks to Prof. Dorota Koziej and Prof. Markus Niederberger from ETH for making my research stay possible and enjoyable. I am much obliged to the members of multimat for all the help, support during my stay. Unfortunately, my thesis would burst to acknowledge

all friends I made during that short stay. Thank you for great help and all possible support from Nikalaus, Rupali, Alessandro, Mario, Elena, Ofer, Dipan. A special thanks to Philipp, Christoph, and Murielle for outdoor activities, especially skiing weekend. I furthermore thank to Prof. Philipp Rudolf von Rohr and Helena Raymond for collaboration and constructive scientific discussion during Raman experiments.

I also would like to thank to my previous mentor Dr. Sunil Joshi and all my colleagues and friends from NCL. I am also grateful to my manager and colleagues from Shell, for supporting and encouraging me to do PhD. Thanks to Mary, Makarand, Asif, and Abhilash for introducing me to industrial research. A special thanks to my old friends and colleagues Mahesh, Amit, Ajay, Praveen, Yogesh, Deepak, Sagar, Vinayak for being true friends, from whom I have received invaluable help, encouragement and moral support at all time.

Finally, I wish to thank my family, without my parents support and blessings this thesis could not have been completed. A constant love and care from Manisha, Rupali, Sujay gave me a solid and stable backbone which enabled me to do the things that I liked.

I also want to acknowledge, “Rovira i Virgili” University, ICIQ foundation, Ministry of Economy and Competitiveness (MINECO), Spain for financial support (FPI predoctoral fellowship) and mobility grant.



UNIVERSITAT ROVIRA I VIRGILI

CARBON DIOXIDE TO METHANOL: STOICHIOMETRIC CATALYTIC HYDROGENATION UNDER HIGH PRESSURE CONDITIONS

Rohit Gaikwad

Table of contents

Chapter 1: Introduction and overview.....	1
1.1 Carbon Dioxide: Current scenario.....	2
1.1.1 CO ₂ emission and the impact on lifestyle	2
1.1.2 CO ₂ mitigation strategies	5
1.1.2.1 CO ₂ capture and storage (CCS).....	6
1.1.2.2 CO ₂ capture and utilization (CCU)	7
1.2 Methanol: History and current status.....	12
1.2.1 Methanol synthesis history.....	13
1.2.2 Catalyst development	15
1.2.3 Active sites and reaction pathways	17
1.2.4 Methanol synthesis: Technology and aspects.....	19
1.3 Aim and outline of the thesis.....	26
Bibliography.....	28
Chapter 2: Methods and materials	33
2.1 Catalyst synthesis.....	34
2.1.1 Chemicals and catalyst synthesis	36
2.2 Experimental setup and catalytic tests.....	43
2.2.1 Working principle of flow reactor	44
2.2.2 Analytical system	48
2.2.3 Reactor automation.....	49
2.2.4 Safety	51
2.3 Working with the reactor	53
2.3.1 Catalyst loading	53
2.3.2 Reactor operation	54

Table of contents

2.4	Conclusions.....	56
	Bibliography.....	57
Chapter 3: High pressure advantages in stoichiometric CO₂ hydrogenation to methanol.....		59
3.1	Introduction.....	60
3.2	Experimental.....	61
3.3	Thermodynamic calculations	63
3.4	Results and discussion	63
3.4.1	Effect of temperature under high pressure conditions	63
3.4.2	Effect of GHSV under high pressure conditions	67
3.4.3	Evaluation of internal mass transfer limitations	75
3.5	Conclusions.....	80
	Bibliography.....	82
Chapter 4: Space-resolved gas analysis of high pressure CO₂ hydrogenation to methanol.....		83
4.1	Introduction.....	84
4.2	Experimental.....	85
4.2.1	High pressure reactor for operando Raman spectroscopy	85
4.2.2	Space-resolved gas analysis using SS reactor	87
4.3	Results and discussion	89
4.3.1	Equilibrium conversion and selectivity.....	89
4.3.2	Space-resolved gas analysis by GC	90
4.3.3	Space-resolved gas analysis by Raman spectroscopy.....	94
4.4	Conclusions.....	98
	Bibliography.....	99

Chapter 5: Cu-ZnO core-shell catalysts preparedd by non- aqueous sol-gel method.....	101
5.1 Introduction.....	102
5.2 Experimental.....	103
5.2.1 Chemicals.....	103
5.2.2 Catalyst synthesis.....	103
5.2.3 Catalyst characterization.....	103
5.2.4 Catalytic test.....	106
5.3 Results and discussion.....	107
5.3.1 Material structure.....	107
5.3.2 <i>Ex situ</i> XRD.....	110
5.3.3 <i>In situ</i> XRD during thermal pretreatment in H ₂	111
5.3.4 H ₂ -TPR.....	112
5.3.5 Catalyst evaluation: Effects of Cu-Zn ratio.....	114
5.3.6 Catalyst evaluation: Effects of Cu-Zn proximity.....	119
5.3.7 Catalyst evaluation: Effects of pre-reduction temperature.....	120
5.3.8 <i>Operando</i> XRD.....	123
5.3.9 Relation between ZnCO ₃ formation and catalytic activity.....	124
5.4 Conclusions.....	128
Bibliography.....	130
Chapter 6: Conclusions and Outlook.....	131
6.1 General conclusions.....	132
6.2 Outlook.....	135
Bibliography.....	137

Table of contents

Appendix A: Supplementary information of Chapter 3	139
Appendix B: Supplementary information of Chapter 5	145
Shorthand glossary	151
List of publications	155
Curriculum vitae	157

UNIVERSITAT ROVIRA I VIRGILI

CARBON DIOXIDE TO METHANOL: STOICHIOMETRIC CATALYTIC HYDROGENATION UNDER HIGH PRESSURE CONDITIONS

Rohit Gaikwad

UNIVERSITAT ROVIRA I VIRGILI

CARBON DIOXIDE TO METHANOL: STOICHIOMETRIC CATALYTIC HYDROGENATION UNDER HIGH PRESSURE CONDITIONS

Rohit Gaikwad

1.

Introduction and overview

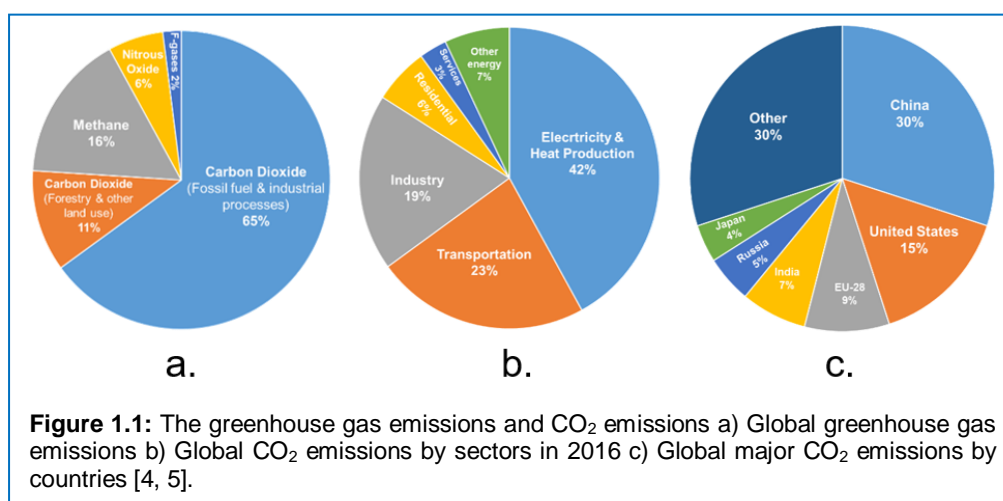
Chapter 1

1.1 Carbon dioxide: Current scenario

Global energy consumption is constantly increasing as a result of population and economic growth. Presently, the primary and major energy source are the fossil fuels (coal, gas, petroleum). The energy production from fossil fuels accounts for two-thirds of world's greenhouse gas emissions which mainly consist of carbon dioxide. A major consensus in efforts to combat climate change was the Paris agreement, on 12th December 2015, with an aim to keep the rise in global average temperatures below 2 °C compared to pre-industrial level, by the end of the century. Several countries have taken initiative steps to achieve the agreement goals [1].

1.1.1 CO₂ emission and the impact on lifestyle

Carbon dioxide emission has been constantly increasing worldwide after the pre-industrial era and reached 35.9 Gt in 2014 [2]. The global total primary energy supply has been increased by 150% from 1971 to 2013 due to increasing worldwide energy demand for economic growth and development [3]. Greenhouse gas emissions from the energy sector represent roughly two-thirds of all anthropogenic greenhouse gas emissions. Despite huge developments in renewable and nuclear energy sources over the last decades (which are considered as less, or zero, carbon-emitting sources of energy),



fossil fuels still remain the world's primary energy supply, thereby continuously contributing to CO₂ emissions. In 2016, CO₂ contributed 76% to global greenhouse gas emissions, followed by methane (16%) (Figure 1.1a data). The major CO₂ emissions sources are power plants, petroleum, chemical and cement industries. Electricity and heat generation contributes up to 42% of global CO₂ emissions while transportation (23%) is the second major CO₂ emissions source (Figure 1.1b data from year 2016) [4, 5]. The CO₂ emissions from power plants are associated with high consumption of coal, which has highest carbon content per unit of energy released compared to other fossil fuels. This trend is expected to persist in the coming years, as many countries such as Australia, China, India, Poland and South Africa are producing over two-thirds of their total electricity and heat from the fossil fuels combustion [4].

The global CO₂ emissions depend on the geopolitical location of the region or country, as well as its economy, and also on the type of fuel used for energy production. The top 10 CO₂ emitting countries are China, USA, India, Russia, Japan, Germany, Iran, South Korea, Canada and Saudi Arabia, with an overall share of 78% in the global CO₂ emissions (Figure 1.1c) [4].

Until late 17th century, the CO₂ concentration in the atmosphere was stable, maintaining the natural carbon cycle. After the Industrial Revolution, the anthropogenic CO₂ emission rate gradually increased and reached 403 ppm to date [4, 6]. It took around 200 years for first 50 ppm increase from stable CO₂ concentration, 33 years for the next 50 ppm (1973 to 2006) [7], while the further 20 ppm was increased in the last 11 years. Table 1.1 summarizes the change in CO₂ concentration over the last 1000 years. At first glance, it is strange to call CO₂ a threat for plants and animals, however, a "sudden" (in terms of the Earth's long climate history) increase in CO₂ concentration can adversely affect the climate, and consequently the ecosystem. Annually, the natural carbon cycle emits ca. 120 Gt of CO₂ into the atmosphere from the respiration of living beings and from the decomposition of the soil organic matter. It is supposed that the natural photosynthesis process

Chapter 1

utilizes a similar amount of CO₂, which helps to maintain a comparatively stable CO₂ concentration of approximately 280±10 ppm. However, this is the ideal scenario where the population growth would be limited and deforestation would not occur.

Table 1.1: Variation of CO₂ concentration of over the last 1000 years [6, 7].

Year	Period (years)	Concentration (ppm)	Increase (ppm)	Increase rate (ppm yr ⁻¹)
1000-1800	800	270-280	10	0.01
1800-1950	150	280-310	30	0.2
1958-1973	15	315-330	15	1
1973-2006	33	330-380	50	1.5
2006-2017	11	380-402	21	1.9

The effect of atmospheric CO₂ on the average global temperature was first outlined by Svante Arrhenius in 1896. He was the first scientist who proposed the idea of the contribution of CO₂ to the greenhouse gas effect.

The heat trapped by greenhouse gases (CO₂, CH₄, N₂O, SF₆) from solar radiation helped to maintain the earth's temperature. However, an increase in heat trapping gases (especially CO₂) in the atmosphere has increased the average global temperature and is causing global warming. The present concentration of atmospheric CO₂ accounts for 9-26% of the natural greenhouse gas effect. Thus, CO₂ is the most important climate regulator besides water vapor which mainly comes from the energy sector [8]. Hence, as estimated from Arrhenius's model [5] and recent modern studies, there will be a significant temperature rise over the next 100 years if the concentration of CO₂ increases at the current rate. The International Panel of Climate Change (IPCC), which monitors the global climate change, predicted that a doubling of CO₂ concentration will most likely result in a rise of the global average temperature between 2 and 4.5 °C. Although long-term climate changes

cannot be accurately predicted, most scientists agree that observations such as the melting of Arctic Ocean ice and glacier retreats, and the rise in sea level have been triggered by this phenomenon [9]. An increase in the average global temperature by 2 °C is expected to cause life-threatening effects such as droughts and other extreme weather phenomena worldwide. Coping with the anthropogenic CO₂ emissions and the utilization of CO₂ are the major challenges for mankind.

1.1.2 CO₂ mitigation strategies

The social, scientific and industrial opinion about carbon dioxide has drastically changed in the last few decades and is no longer considering it as waste. Many research activities are focusing on the development of new technologies for CO₂ abatement, specifically in the energy and transportation sectors. There are four main possible pathways:

- i) increasing efficiency by technological improvement in the power and industrial sectors;
- ii) substitution of fossil fuel resources by renewable energy resources;
- iii) chemical or physical capture and storage of CO₂ (CCS);
- iv) utilization of CO₂ for synthesis of chemicals and fuels (CCU);

There is a significant scope for the technical improvement of reducing CO₂ emissions in the energy and chemical sectors that can help to increase the energy efficiency of the overall industrial process (for instance, the use of nuclear energy for producing electricity). The second option, the one of renewable energy resources, is still in primitive stage. Although ongoing research shows that it has potential to substitute fossil fuel resources, it is far away from industrial applications. Although i) and ii) can represent future scenarios in the process and energy sectors, still, they do not offer short or mid-term sustainable solutions. Hence, an effective and robust pathway to control overall global CO₂ emissions is needed. The last two aforementioned

Chapter 1

options (CCS and CCU) certainly do have potential for controlling and reducing the overall CO₂ concentration to a satisfactory level.

1.1.2.1 CO₂ capture and storage (CCS)

There has been continuous advancement in CO₂ capture technology over the last decades. It will be soon applied on large-scale at stationary sources of emissions [10]. The main targets for implementation of CO₂ capture technologies are power plants, fuel processing plants and several large scale industrial process facilities, such as iron, steel and cement production plants. The CO₂ capture and separation processes are broadly divided into physical and chemical processes, such as absorption, membrane adsorption, cryogenic separation and chemical looping. The well-developed CO₂ capture process helps to dispose off CO₂ in different forms or places.

Enhanced oil recovery (EOR) by injection of CO₂ into depleted oil wells to force the leftovers of oil out of the wells is one of the most popular methods to make use of CO₂, as more oil can be recovered in this way. Although the process is widely applicable at industrial scale, it is still limited by geographical conditions. An alternative storage technology is the storage of the captured CO₂ in empty oil fields (e. g., 2 million tons of CO₂ was stored by Quest by July 2017 in Canada). Similarly, Illinois Basin Decatur Project in US has a CO₂ storage capacity of 1 Mtpa. Moreover, the CO₂ capture and injection from biofuel plants has already began since April 2017 [10]. However, the CO₂ captured from big plants has to be close to storage wells, to avoid energy-intensive transportation to the storage location. After CO₂ storage, special care needs to be taken to maintain and isolate the reservoirs from any accidental leak and addition of stored CO₂ to the atmosphere. Beside these technical challenges, significant financial investment is required, along with public awareness [11]. Besides storage in wells, mineralization, or reactions of minerals with CO₂ to form carbonates is another potential large scale CO₂ storage strategy.

1.1.2.2 CO₂ Capture and utilization (CCU)

In case of CCU, the CO₂ is used as a chemical precursor to make valuable products instead of storing it. This process can be considered as a complementary technology to CCS, serving similar goals, while additionally providing economic benefits. CCU is a broad field which can be mainly classified into two categories:

- (A) direct CO₂ utilization based on physical properties;
- (B) chemical uses, comprising conversion of CO₂ into various valuable chemicals and fuel;

Carbon dioxide utilization mainly depends on the purity of available CO₂. CO₂ streams from production of some fertilizers, natural gas processing and cement production are considered pure and clean sources [12]. The CO₂ produced from power plants requires an extra purification step, since it frequently contains additional impurities.

Table 1.2: Industrial processes which produce CO₂ [13].

No.	Industry	CO ₂ produced (Mt yr ⁻¹)
1	Oil Refining	850-900
2	Cement Production	1000
3	Iron+Steel Production	870
4	Fermentation	200
5	Ammonia Synthesis	160
6	Ethene Synthesis	155
7	LNG Sweetening	20-25
8	Ethylene Oxide Synthesis	10

Chapter 1

On the contrary, CO₂ emitted from smaller sources (shown in Table 1.2) is cleaner and produced in manageable quantities. The global warming impact of many of these high economic value processes will be minimized, if CO₂ captured from these pure and clean CO₂ producing sources is utilized in an energy efficient manner.

A) Direct use of CO₂

CO₂ alone without any conversion or chemical transformation has certain uses such as food processing, preservation, beverage carbonation, coffee decaffeination, fire suppression, production of pharmaceuticals and enhanced oil recovery. Carbonation of CO₂ in beverage industry comprises CO₂ injection to water, cold drinks, beer and dairy products, provides their sparkling appearance, astringency and refreshing feel after consumption. In food industry, the *Modified Atmosphere Packaging* technique is used to increase shelf life of fresh and chilled products, such as meat, fish, fruits and vegetables. The pressurized supercritical CO₂ is used for the decaffeination of coffee beans and for the extraction of bitter flavours. The use of CO₂ as a fire suppressor decreases oxygen concentration near the fire area and also lowers the flame temperature and flame speed.

Although the direct use of CO₂ has wide applications, many of them are used in small-scale processes or less demanding products. Therefore, the overall CO₂ utilization is less, compared to the amount of CO₂ released into the atmosphere. The transformation of CO₂ into chemicals and fuel-alternatives or fuel additives would be an excellent option to achieve large scale CO₂ reduction.

B) Conversion of CO₂

As mentioned in the above subsection, CO₂ has already found number of direct applications, however, the potential of CO₂ in the direct use is very low compared to another approach, where CO₂ is converted to chemicals and fuels via carboxylation or reduction for synthesis of polycarbonate, synthesis

gas, methanol, salicylic acid and urea [14]. The CO₂ utilization towards these products has advantages such as production of value added chemicals, environment friendly processing and non-hazardous chemical process.

Until today, CO₂ was never used at its fullest potential even for chemicals or fuel synthesis because of its high thermodynamic and kinetic stability. The use of efficient catalysts and selective reaction pathways are needed to promote the reaction rate. According to current estimates, the chemical industry can only make minor direct contribution towards reducing the overall amounts of CO₂ emissions and could contribute to convert around 1% of global CO₂ emissions into chemical products and 10% into synthetic fuels [15]. Table 1.3 shows the major routes of CO₂ utilization in various chemical conversion processes.

Table 1.3: Commercial processes producing chemicals from CO₂.

No.	Chemical process	Company
1	Production of ethylene oxide (C ₃ -PEO)	RTI International, USA
2	CO ₂ to chemicals and fuels	Liquid Light, USA
3	Dimethyl carbonate from CO ₂ and CH ₃ OH	E3Tec Service, LLC, USA
4	Acetic acid synthesis from CO ₂ and CH ₄	Gas Technology Institute, USA
5	CO ₂ to polyol for polyurethane	Bayer with CAT, Germany

The fixation of CO₂ into organic compounds refers to reactions that use the entire molecule. In case of catalytic CO₂ reduction reactions, the CO₂ is reduced to other C1 chemicals (CO, methanol). The CO₂ conversion to fuels, rather than organic chemicals, will play a major role in CO₂ emissions management strategies. Firstly, because fuel market demand is higher than for organic chemicals. Secondly, CO₂ emissions are primarily associated with consumption of fossil fuels, thus fuels synthesized from CO₂ can substitute the fossil fuels and contribute towards the closing of the open carbon cycle.

Chapter 1

It should be noted that the chemical industry uses only around 10% of the global crude oil consumption, while the rest of it is used as liquid fuels such as gasoline, diesel and heavy oil. Hence, an effective use of CO_2 with regard to a noticeable reduction of the global net emissions of CO_2 can only be reached if the CO_2 is utilized for fuels, *e. g.*, by reverse water gas shift reaction and subsequent Fischer-Tropsch synthesis for alcohol synthesis. CO_2 conversion to methanol is a promising way that might offer a comprehensive solution to the issues of greenhouse gas control and depletion of fossil fuels. Methanol is a starting material for a number of valuable chemicals, as well, it can act as a fuel. Additionally, some reports already suggested that CO_2 can be converted into C1 to C10 hydrocarbon fuels via methanol, hence it has a great potential for industrial applications [16, 17]. The hydrogen used for methanol synthesis is mainly produced from hydrocarbon reforming, which is an energy-intensive process. Therefore, the methanol synthesis process would not contribute to the overall CO_2 concentration reduction, unless the H_2 is produced from renewable resources or processes that use waste or nuclear (carbon-free) energy.

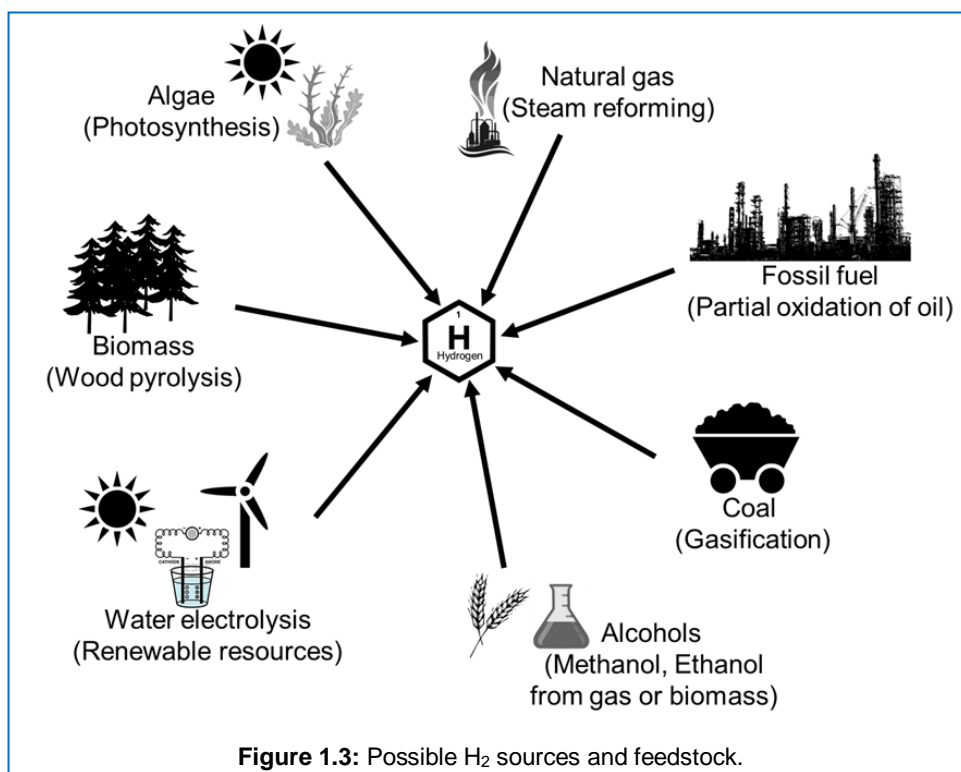
C) H_2 sources and concern

Hydrogen is an energy carrier, not an energy source. It acts as a medium to store and deliver energy in a usable form [18]. It is also considered a clean, carbon-free, future energy vector [19]. Hydrogenation of CO_2 allows for the synthesis of various products such as CO, methane, formic acid, methanol or formaldehyde. As mentioned in [Table 1.3](#), currently, several products are synthesized at industrial scale by CO_2 hydrogenation and there will be more products in demand in the coming decades [20]. It is also important to evaluate the sources of H_2 for CO_2 hydrogenation. The conventional hydrogen production by steam reforming reaction has high energy requirements and is associated with increased CO_2 emissions, therefore, it is not desirable to be used. The hydrogen production technology varies with the amount of H_2

produced and depends on the cost of available feedstock and final product market value.

Although there are various hydrogen resources available, fossil fuels still act as the main feedstock (96%) for H_2 production. Currently, H_2 is mainly produced from methane steam reforming, partial oxidation and autothermal reforming reactions. Along with these, water electrolysis and renewable liquid reforming (ethanol with high-temperature steam) are also used to produce H_2 . However, these are small-scale H_2 production processes, and are usually located near the feedstock site. Nevertheless, there are other emerging technologies which are considered to be carbon (CO_2) free, for example water splitting using solar light, photoelectrochemical water splitting and photobiological water splitting. However, these technologies are still in the developing stage.

Currently, hydrogen is mainly used for chemical synthesis. Ammonia and



Chapter 1

methanol synthesis together consume approximately 63% of the total produced H₂. Following chemical synthesis, approximately 33% of pure H₂ is used in the refineries. Along with this, pure H₂ is also used for a number of hydrogenation reactions (4% of total consumption), such as hydrogenation of unsaturated hydrocarbons and aromatics. Very little (1%) pure H₂ is used in metallurgy, semiconductor and food industry [21]. [Figure 1.3](#) shows an overview of different resources and feedstocks, along with current process technologies used for H₂ production. The availability of local feedstock, market demand and technologic maturity have influence on the H₂ production process.

In case of high pressure CO₂ hydrogenation to methanol process, the energy efficiency is almost independent of pressure and relies mostly on hydrogen cost [22]. Therefore, the cost of pressurized pure H₂ can be a critical point for large-scale methanol synthesis, considering that high H₂ partial pressure boosts the catalytic activity [23].

1.2 Methanol: History and current status

Methanol is a very important bulk commodity chemical. In 1985 the methanol production was 12.4 million Mt and reached 85 million Mt in 2016 [24]. The major part of produced methanol is used for formaldehyde production. Next to that is the production of *tert*-butyl methyl ether (MTBE), which is widely used as a fuel or blended with gasoline, as mentioned in [Figure 1.4](#) [25]. In addition, methanol is also used for plastics, paints and polymers synthesis. Methanol applications in fuel cells and as a direct fuel (M100) or blended with petrol (M85) are gaining importance. The high energy density and hydrogen storage capacity of methanol make it a suitable candidate for convenient energy storage. Being liquid, methanol is easier to transport and store compared to hydrogen.

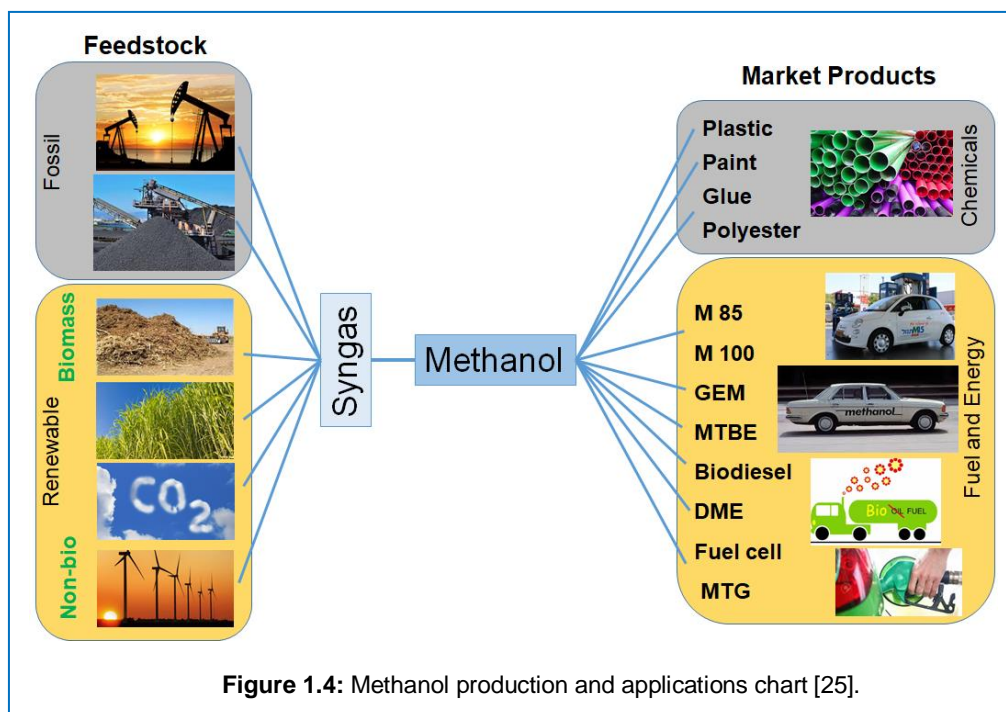


Figure 1.4: Methanol production and applications chart [25].

1.2.1 Methanol synthesis history

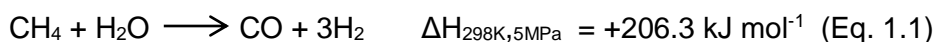
Methanol was discovered by the ancient Egyptians, by wood pyrolysis. But it was not known until 1661 when pure methanol was isolated by the Irish chemist Robert Boyle. Until 19th century, methanol did not have any special use. In 1835 J. B. Dumas and E. M. Peligot gave it a chemical and molecular identity and introduced the terms “methyl” and “methyl alcohol”. In 1892, the name was shortened to methanol, in accordance with IUPAC nomenclature. Since then, various efforts have been made to synthesize methanol [26].

In early 1913, the German chemist A. Mittasch and M. Pier at BASF successfully produced methanol from CO and H₂ using an iron-based catalyst. In 1920s, M. Pier and coworkers started working on the development of large scale methanol production using a sulfur resistant ZnO on Cr₂O₃-based catalyst [24]. Later, in 1923, the process was successfully converted from development stage to production stage at the BASF Leuna Work. This synthesis process was based on high pressure (250-350 bar) and high

Chapter 1

temperature (320-450 °C). For the next 40 years, this process was used to produce methanol at industrial scale.

In early 1960s, ICI introduced a highly selective copper-zinc oxide based catalyst for methanol synthesis. This technology was owned and licensed by Johnson Matthey. The process was operated at moderate reaction conditions of 50-100 bar pressure and 200-300 °C temperature [27]. This catalytic process was possible due to the use of higher purity synthesis gas, which was free from sulphur and carbonyl contaminants, primarily responsible for catalyst deactivation. Currently, 90% of world methanol is produced by this technology. Natural gas is the main feedstock for this process, as methane is the major ingredient of natural gas [28].



As shown in Eq. 1.1, methane decomposes and produces CO and H₂, a mixture called syngas, which is further used for methanol synthesis. It was found that the addition of small amounts of CO₂ in the syngas mixture enhances the catalytic activity and methanol yield. Nowadays, up to 30% CO₂ is added to the syngas mixture for commercial methanol synthesis processes [29]. The production of syngas from methane is a highly endothermic reaction and an energy demanding step in the overall process. The Nobel Prize winner G. A. Olah and coworkers explored direct methane to methanol synthesis routes, but it was found that the process gives very low yield due to the decomposition of produced methanol to CO₂ and water at the high reaction temperature (300 °C) [30].

The production of methanol via CO₂ hydrogenation represents an interesting approach for CO₂ mitigation, as well as for switching dependency from fossil fuels to renewable energy sources. In this aspect, the overall closed carbon cycle can be envisioned as “Methanol Economy”, as proposed by G. A. Olah. In methanol economy, CO₂ can be captured from any natural, industrial or other human activities and directly be converted into methanol,

which is an efficient fuel substitute, with a high capacity for hydrogen storage and ease in safe transportation. For this to be a sustainable process, the H_2 has to be produced from renewable resources, e. g., water electrolysis or photocatalytic water splitting.

1.2.2 Catalyst development

As mentioned in the previous section, the first industrial methanol synthesis process used a ZnO on Cr_2O_3 -based catalyst. Later, in 1966, copper-based catalysts were introduced for methanol synthesis [31]. Although elemental copper is not very promising for direct use as a catalyst due to its low thermal stability, studies on single crystal and polycrystalline copper still demonstrate its high activity towards methanol synthesis [32]. The high copper surface area was also found to be an important factor that enhances the catalytic activity [33-35]. The specific copper surface area and copper particle size are important factors which affect the catalytic performance. The smaller the particles, the higher the dispersion and lower the agglomeration, which helps to enhance catalytic activity. Thus, in order to maintain high activity and stability at the same time, the catalyst was supported on a metal oxide. Hence, copper stabilization and higher dispersion were reported by addition of Zr [36, 37], Ga [38-43], Si, B [44], Cr [45], Ti [46], Ce [36, 47], and ZnO [33]. The ZnO-supported catalyst showed high activity, as it improved the copper dispersion and product selectivity. Furthermore, ICI developed a highly active and thermally stable copper-based catalyst using copper and zinc oxide supported on aluminum oxide [48]. Since then, Cu, ZnO and Al_2O_3 are still the integral components of most methanol synthesis catalysts. The purpose and exact role of each component in methanol synthesis reaction is still one of the widely debated topic in the scientific community [49-51]. As an example, neither ZnO itself, nor mixtures of ZnO with Al_2O_3 show any activity, however, its presence in copper-based catalysts boosts the catalytic activity and enhances the methanol yield. It was reported that high catalytic activity and selectivity in the Cu/ZnO catalyst resulted from high copper dispersion. To

Chapter 1

further improve the high dispersion of copper on zinc oxide, modifications have been investigated on conventional Cu/ZnO/Al₂O₃ catalysts using Pd, Rh, Pt, Co, Mn, Ti, Zr, Y [33, 52-58]. It was reported that apart from the metallic active sites, the support also plays a crucial role in modulating and enhancing catalytic performance [59]. Al₂O₃, SiO₂, ZrO₂, and Ga₂O₃ are also well known as supports in catalysis. Cu/SiO₂ was less active for methanol synthesis [60]. Doping with Ca, La and Zn oxide slightly improved the activity. Maniecki and his group compared CrAl₃O₆, FeAlO₃, and ZnAl₂O₄, however, apart from zinc oxide, none of the other materials showed any catalytic activity [61]. In addition to copper oxide, Ga, In₂O₃ [62, 63] and Pd oxides [64] were also found as active metal oxides to improve catalytic activity towards methanol synthesis.

Along with proper combination of metal and support material, the catalyst preparation method plays an important role. Many different routes have been investigated for the synthesis of copper-based catalyst systems. The commercially available Cu/ZnO/Al₂O₃ catalyst, which shows high activity and selectivity, is prepared by a co-precipitation method with an approximate ratio of Cu:ZnO:Al₂O₃ 60:30:10 [65]. Metal nitrate salts are preferred as precursors over more common sulfate and chloride salts, as the latter could diminish the catalytic activity by poisoning the catalyst. It is not only the ratio of different components that plays a crucial role in forming the selective precursor, leading to a highly selective, stable and active catalyst, but also the intimate mixing and uniform distribution of individual component phases are highly desirable. The careful control of variables such as pH, ionic strength, mixing and aging procedure during the precipitation step is of utmost importance. These parameters need to be optimized carefully when preparing a co-precipitated catalyst.

Apart from the co-precipitation catalyst synthesis method, other methods like impregnation, sol-gel matrix and combustion were also investigated,

however coprecipitation remains the most preferred method for methanol synthesis catalysts.

1.2.3 Active sites and reaction pathways

As mentioned earlier, despite research efforts on finding other active metals and supports for methanol synthesis catalysts, Cu/Zn/Al₂O₃ still remains the most popular and efficient choice at industrial scale.

Knowing how the catalyst functions and where the reaction exactly occurs (active site) and the possible reaction mechanism is of utmost importance for rational design of catalysts. In case of Cu/Zn/Al₂O₃, Klier suggested that Cu is incorporated in the ZnO phase on interstitial sites, assuming three possible valence states Cu, Cu⁺ and Cu²⁺ and stated that the bulk of the catalysts determine the catalytic activity. The formation of Cu⁺ has also been reported by several authors [66-68]. In particular, the study reported by Fujitani et al. on the interaction between the support and metal in the catalyst suggested that the active component is not only Cu⁺ but also Cu⁰ [68]. Later, Burch and Bartley found that the support effect pronounces the catalytic activity when they tested different copper catalysts for methanol synthesis from both CO/H₂ and CO₂/H₂ mixture. In particular, Burch et al. and Spencer have proposed that the ZnO acts as a reservoir for hydrogen and promotes the hydrogen spill-over [69-71]. Chinchén et al. used a Cu/ZnO system and reported that the methanol synthesis reaction happens exclusively on the Cu surface, and ZnO acts as a spacer and keeps the copper particles away from each other to avoid agglomeration [48, 72].

Another perspective was proposed by other researchers, in which the morphology of Cu and ZnO particles was found to be responsible for higher catalytic activity [32, 73-75]. In methanol synthesis and methanol steam reforming, the activity of binary Cu/ZnO catalysts can be related to the microstrain in the copper particles [76, 77]. Cu/ZnO stabilized by a series of bulkhead defects, surface species [49] and incomplete copper reduction

Chapter 1

and/or ZnO orientation can cause strain, which modifies the copper active surface area, thereby influencing the catalytic activity [76]. Along with the strain, the formation of Cu/ZnO alloy also helped to increase the catalytic activity [78, 79].

In 1970s, Russian scientists showed that methanol was formed from CO₂ rather than CO using kinetic and experimental evidence supported by labeled carbon oxide isotope experiments using Cu/ZnO based catalysts [80]. In early 1980s Klier et al. studied the methanol synthesis mechanism using syngas with CO₂ and concluded that CO was the primary source and the active site was Cu⁺ dissolved in ZnO [81]. Later, Chinchin et al. performed the reaction using an isotope-labelled feed (¹⁴CO or ¹⁴CO₂) with a commercial catalyst and claimed that CO₂ was the primary source of methanol [82]. Similar results were also reported for methanol synthesis using Cu/ZrO₂ by investigating the reaction intermediates formed from CO and CO₂ species adsorbed on the catalyst surface [83, 84]. Extensive research has been carried out to obtain an understanding of the the intermediates and adsorbed species on the surface by various techniques, as IR, DRIFTS, TDS, TPD and chemical trapping, investigating all possible species that may adsorb on the surface of the catalyst such as CO, CO₂, H₂, H₂O, CH₃OH, formaldehyde and methyl formate on Cu/ZnO or Cu/ZrO₂ catalysts [85-89]. The experimental evidence demonstrated the existence of three surface species: formyl, formate and methoxy. The IR spectroscopy studies have shown the formation of formyl species on the surface of ZnO, Cu/ZnO and Cu/ZnO/Al₂O₃ from CO and H₂ [71, 81, 90, 91]. The formyl species are unstable and readily undergo hydrogenation to form methoxy species, which were also observed on the catalyst surface [92]. These methoxy species were found to be more stable than formyl but less stable than formates. Hence, many reports have shown the existence of formate species on Cu (100) [93, 94], ZnO doped Cu (111) [95]. Millar et al. reported that bidentate formates were the intermediate species in methanol synthesis and the hydrogenation of these species was the

rate determining step in the CO₂ hydrogenation reaction [96]. Formate species are subsequently hydrogenated via methoxy to methanol, and Cu gets partially oxidized. Similar formate species are also observed on Cu-ZnO interface during CO hydrogenation to methanol reaction [97].

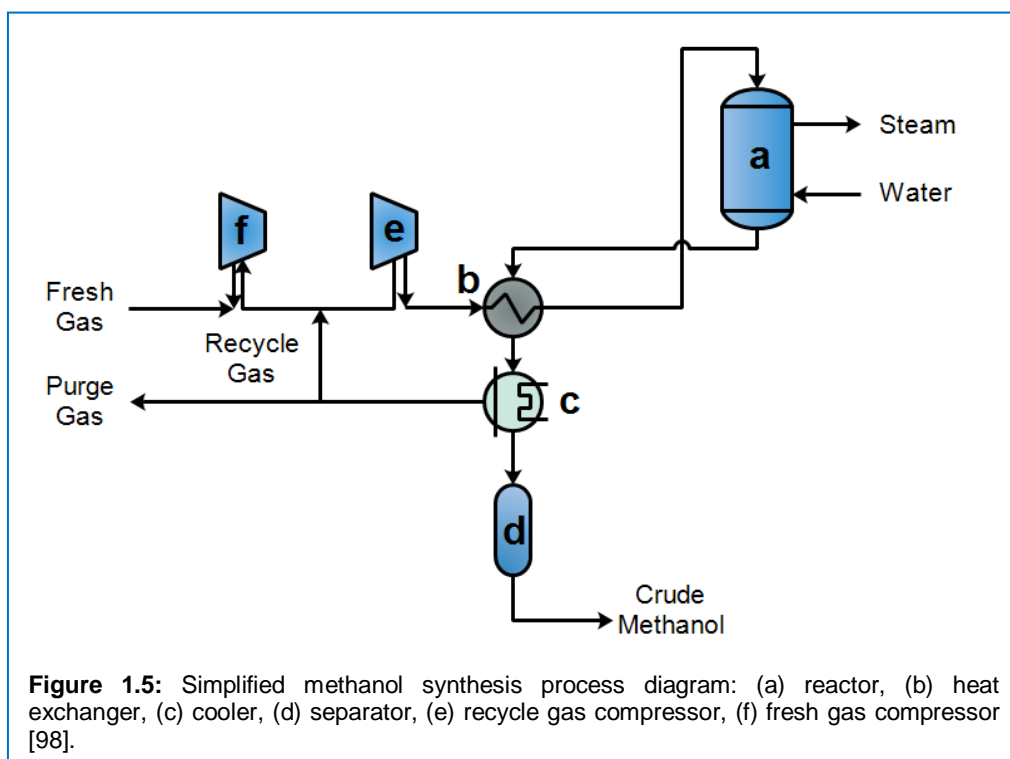
1.2.4 Methanol synthesis: Technology and aspects

The first commercialised (1920s) syngas to methanol production process was operating at pressures of 250-350 bar and 320-450 °C temperature and using Cr₂O₃-ZnO based catalysts [83, 98]. In 1960s, feedstock switchover from coal to natural gas allowed the development of the low-pressure methanol synthesis process. Overall, the industrial methanol synthesis process is divided into three stages: first, the synthesis gas production, then the conversion of synthesis gas into methanol and finally crude distillation to obtain the desired product [98]. Natural gas is the primary source of syngas via the steam reforming process. Additionally, methane can be obtained from biomass and coal gasification. The obtained cooled synthesis gas has to pass through the gas purification stage, in order to remove the sulfur-containing, catalyst-poisoning components. The purified gas is mixed with recycled gas and then fed to the reactor, by maintaining a specific H₂/CO feed ratio of 3:1 to 5:1.

Figure 1.5 illustrates the typical methanol production flow diagram. As stated earlier, methanol synthesis is favored by high pressure, however, most of the industrial processes use low pressure, due to which a large fraction of unreacted syngas has to pass through the recycling loop, because of the low conversion at low pressures [98]. A compressor (f) is used to pressurize the feed depending on the desired pressure (50 to 100 bar). Unreacted gas from the recycling loop and fresh gas are mixed together and transferred to the reactor (a). A purge gas is generally used to keep a certain feed composition ratio and to remove the impurities from the synthesis gas. After the reaction, the produced methanol and water are separated using a separator (d), and the

Chapter 1

remaining synthesis gas is recycled and compressed in the compressor (e). The methanol synthesis reaction is exothermic, and is typically carried out at 200-300 °C. The gas passing through the reactor (a) carries heat released



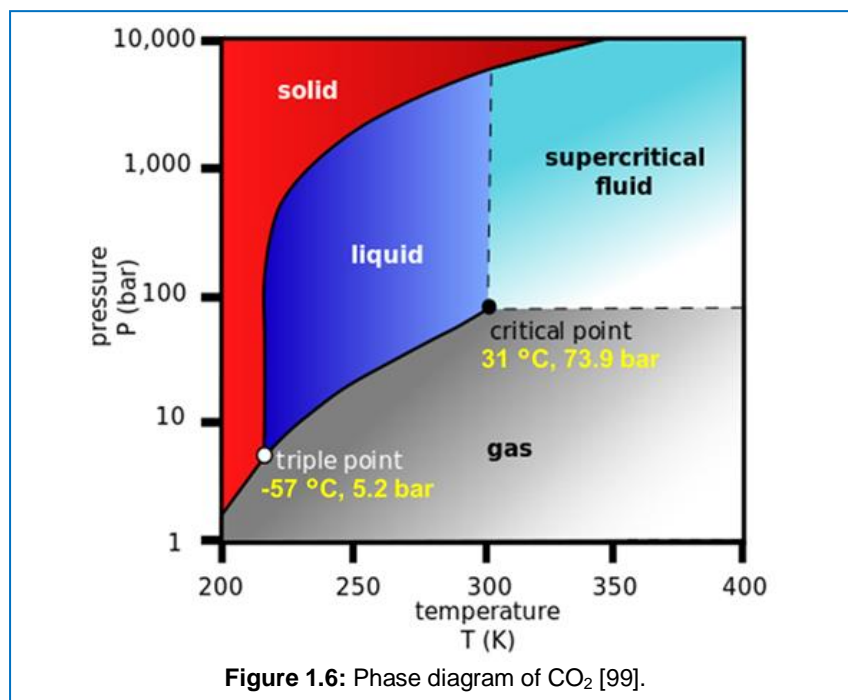
during the reaction and transfers it to the feed gas mixture via the heat exchanger (b) before the reactor inlet. The outlet product mixture is cooled further by a cooler (c) [99].

Currently, the commercial methanol production process uses Cu/ZnO/Al₂O₃-based catalysts, which have high catalytic activity, product selectivity and thermal stability. The catalysts are synthesized by co-precipitation and are available from various suppliers, as KATALCO_{JM} 51-8 (Johnson Matthey Catalysts), MegaMax 700[®] (Süd-Chemie) and S3-86 (BASF). Although the ratio of main components changes from manufacturing company to company, the main ingredients, Cu, ZnO and Al₂O₃ remain the same. Furthermore, dopants like rare earth metals and/or stabilizers are also added, varying from manufacturer to manufacturer. Although these catalysts

have a lifetime of 2-5 years, sulfur and chlorine-containing impure gas feeds and the sintering of copper due to prolonged exposure to high temperature certainly contribute to a reduction of the catalytic activity over the period.

A) High pressure approach

Pressure can have a dramatic impact on chemical reactions. By altering it, the reaction rate can be increased, and therefore the product yield. An increase in the pressure changes the physical properties of compounds, for example, carbon dioxide is a gas at normal temperature and pressure and liquefies easily at elevated pressures. During the liquefaction process it is removing produced heat at temperatures between triple point and critical point, where it reaches its supercritical state, as shown in Figure 1.6 [100]. The supercritical state is reached at reasonably mild conditions, at temperatures higher than 31.1 °C and pressures above 73.9 bar. The main advantage of the supercritical condition is that the substance exhibits liquid phase-like density and gas-like transport properties at the same time. Therefore, high pressure CO₂ has great industrial applications in solvent extraction, food processing,



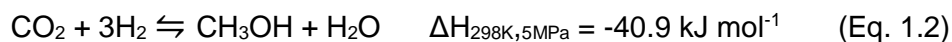
Chapter 1

and most importantly, as solvent or reactant in chemical reactions.

CO and/or CO₂ hydrogenation are exothermic reactions and proceed with a reduction in the total number of molecules. Hence, low temperatures and high pressures are favored for achieving the highest catalytic activity. Besides that, high pressure has several other advantages such as allowing to cross the thermodynamic barrier and to achieve very high CO₂ conversion, thereby avoiding the need for recycling. Beside thermodynamic benefits, due to high pressure, the reactants and/or products are compressed and the total reaction area plant is reduced, and consequently the capital cost. Additionally, small reactor volumes also helps to handle dangerous chemicals like hydrogen more safely. As stated earlier, the methanol synthesis reaction is exothermic, thus, use of small reactor sizes is also beneficial for efficient mass and heat management. The high surface to volume ratio allows for better heat management and restricts the formation of hot spots across the catalyst bed. The CO₂ at high pressure is in supercritical state and together with methanol and hydrogen forms multiphase reaction mixtures, which can result in mass transfer limitations that can be avoided or minimized by using small reactor sizes. The advantages of the high pressure process may results in shifting the equilibrium conversion towards products side and therefore enhance the catalytic yield [101].

B) Thermodynamic aspects

Carbon dioxide is a linear molecule with a double bond between the carbon and each oxygen atom. Due to the high stability of CO₂ molecule ($\Delta G^\circ = -394.38 \text{ kJ}\cdot\text{mol}^{-1}$), its activation requires substantial energy input, highly active and stable catalysts and optimized reaction conditions.

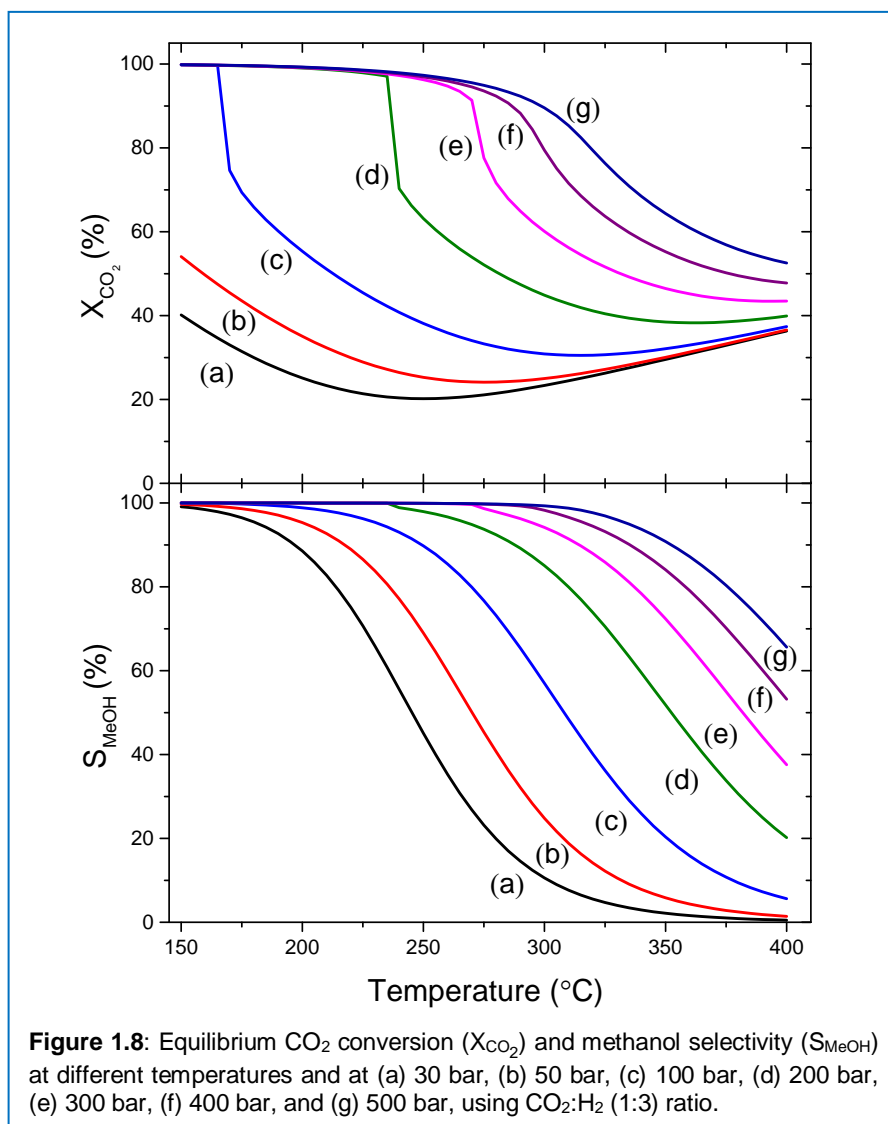


As shown in Eq. 1.2, CO_2 and H_2 can react together to form methanol and water. The formed water consumes one third of the hydrogen, which is more than in the reaction of methanol formation from syngas (Eq. 1.4). The reactions shown by Eq. 1.2 and 1.4 are exothermic and take place with loss of reactant volume. It is also possible that the reverse water gas shift reaction to take place on the catalyst surface using CO_2 as feed (Eq. 1.3). In this case, the produced CO undergoes hydrogenation to yield methanol as per Eq. 1.4. The reaction of CO_2 hydrogenation to methanol (Eq. 1.2) is exothermic and proceeds with loss of volume, hence, high pressure and low temperature should help to achieve the higher conversion as per Le Châtelier's principle. Thermodynamic aspects of a chemical reaction are important for understanding and predicting the stability of the desired chemical species, the yield, conversion and selectivity of the targeted products. Thermodynamics also provides information about reaction mixture phases, impact of temperature, pressure and feed ratio. Graaf et al. performed the thermodynamic study on methanol synthesis using CO, CO_2 and H_2 . They also calculated chemical equilibria for methanol synthesis using equilibrium constants. The non-ideality of the gas mixture was taken into account by including the fugacity coefficients in the equilibrium constants, which were calculated using Soave-Redlich-Kwong (SRK) equation of state (EOS) [102]. Furthermore, Graaf et al. refined the equation by using experimental data [103]. The deviation at equilibrium was fitted using Gibbs energy; they established a highly reliable expression for the equilibrium constant. The thermodynamic and kinetic aspects of methanol synthesis using CO_2 and H_2 were not studied much, compared to the conventional feed of CO, CO_2 and H_2 . The model developed by Graaf et al. and Van den Bussche and Froment are often applied to model the reaction of methanol synthesis using $\text{Cu/ZnO/Al}_2\text{O}_3$ catalysts. These widely applied kinetic expressions were primarily based on different assumptions. Graaf et al. stated that CO and CO_2 were the main sources of methanol synthesis. On the other hand, Bussche

Chapter 1

and Froment assumed that CO_2 , obtained from CO by WGS, is the main source of carbon for methanol synthesis and that the dissociative adsorption of H_2 and CO_2 was the rate-determining step.

At high pressure, CO_2 conversion is induced by the phase transition and separation (formation of liquid), associated with condensation of the products when the reaction temperature is lower than the transition point, as precisely



described and demonstrated by van Bennekom et al. [104]. The reported model is based on a modified Soave–Redlich–Kwong equation of state, which

enabled the simultaneous calculation of phase and chemical equilibria that occur during high-pressure methanol synthesis (200 bar, 190 to 280 °C). The calculated equilibrium CO₂ conversion and methanol selectivity as a function of pressure and temperature is shown in [Figure 1.8](#). (The other product is CO and only Eq. 1.2 to 1.4 were assumed. The calculations were performed with the same method described in ref [105]). The CO₂ conversion equilibrium profile shows a sudden decrease in the CO₂ conversion in the case of 100 to 300 bar pressure, due to phase separation and liquid phase formation. A similar phase change was also reported by van Bennekom et al. at 200 bar, where it was observed at 240 °C. At pressures of 400 and 500 bar, the CO₂ conversion decreases, which indicates the existence of a single phase at high pressure [106].

C) The need for stoichiometric ratio

Carbon dioxide hydrogenation to methanol requires one mole of CO₂ and three moles of H₂. This stoichiometric (1:3) ratio avoids the excess use of reactants and recycling of unreacted feed. It is reported that under high pressure conditions, an excess of hydrogen partial pressure is required to achieve almost full single pass conversion of CO₂ and high methanol yield [22, 23]. Additionally, energy efficiency towards methanol formation is increased, because of the suppressed competitive RWGS reaction.

However, the excess of unreacted pressurized hydrogen needs to be separated from the product stream and reused for the reaction. In commercial methanol synthesis plants, the accumulation of inert gases during recycling is avoided by a purge system, but the purge gases change the feed composition for recycling, which causes loss of chemicals and operational costs. The H₂ separation is commercially done by membrane separation, cryogenic distillation or pressure swing adsorption, which brings additional costs to the process [107]. Furthermore, as stated before, hydrogen production is the energy-intensive process in high pressure methanol synthesis, compared to

Chapter 1

the operational cost of a high pressure system. Hence, achieving full CO₂ conversion at stoichiometric ratio is beneficial from an economic point of view. This could be achieved by designing highly active catalysts, as well as optimizing the process parameters carefully at CO₂:H₂ (1:3) ratio.

1.3 Aim and outline of the thesis

Recently, our research group showed the advantages of using high pressure in the CO₂ hydrogenation reaction, where almost full one pass CO₂ conversion and extraordinary methanol yield under high H₂ partial pressure was obtained. However, full CO₂ and H₂ conversion at stoichiometric CO₂:H₂ ratio (1:3) was not achieved. The aim of this doctoral thesis was to achieve complete conversion of reactants and high methanol yield at stoichiometric ratio (1:3) of CO₂:H₂. Controversies still exist on the mechanistic approach of CO₂ hydrogenation to methanol, hence realistic features of gas phase reaction intermediates were also studied at high pressure by space resolved gas analysis. To design the model catalyst, comprehensive microstructural knowledge is required. Core-shell catalysts were developed to elucidate the structure-activity relationship of Cu-ZnO catalyst.

Chapter 2 describes the setup of high pressure (500 bar) tubular continuous flow lab scale reactor used for the high-pressure methanol synthesis process. The overview of a Labview-programmed system, which controls the complete reactor system with all safety measures is explained in detail along with the analytical system.

Chapter 3 shows the experimental results of the high-pressure CO₂ hydrogenation reaction where all process parameters were carefully optimized to achieve extraordinary methanol yield. Thermodynamic calculations were performed to estimate the theoretical conversion. The effect of mass transfer limitation is shown by varying catalyst particle size. The quantitative analysis of the degree of internal mass transfer is explained in detail.

Chapter 4 deals with space resolved gas analysis was studies to investigate the high pressure CO₂ hydrogenation to methanol reaction pathway. The space resolved study was performed using a stainless steel and sapphire reactor tube with gas analysis at different space intervals. The details of the reactor setup and experimental results are explained in this chapter.

Chapter 5 includes the Cu₂O-ZnO core-shell nanomaterial development and its activity for methanol synthesis. The synthesis methods were varied to obtain different Cu₂O and ZnO morphology and to understand the structure-activity relationship. Detailed investigation of ZnCO₃ phase formation at high pressure and its effect on catalytic activity was studied by high-pressure *operando* experiments.

Chapter 6 summarizes the key conclusions of the thesis and highlights its relevance and is complemented by an outlook for future research directions.

Chapter 1

Bibliography

- [1] UNFCCC. Decision 1/CP.21: Adoption of the Paris Agreement. Paris Climate Change Conference; Paris, France, (2015) Nov 30–Dec 11.
- [2] R. B. Jackson, J.G. Canadell, C. Le Quere, R.M. Andrew, J.I. Korsbakken, G.P. Peters, N. Nakicenovic, *Nat. Clim. Change*, 6 (2015), pp. 7-10.
- [3] D. A. N. Ussiri, R. Lal, *Carbon Capture and Storage in Geologic Formations, Carbon Sequestration for Climate Change Mitigation and Adaptation*, Springer International Publishing, Cham, (2017), pp. 497-545.
- [4] I.E. Agency, CO₂ emission from fuel combustion, IECD/IEA, France, (2016), pp. 166.
- [5] S. Arrhenius, *Philosophical Magazine Series* 5, 41 (1896) pp. 237-276.
- [6] E. Dlugokencky, P. Tans, in, *Global Monitoring Division, The National Oceanic and Atmospheric Administration, USA*, 2017.
- [7] L. Lemay, in, *National ready mixed concrete association*, 2010.
- [8] J.T. Kiehl, K.E. Trenberth, *Bull. Am. Meteorol. Soc.*, 78 (1997) pp. 197-208.
- [9] C. Brahic, *The impacts of rising global temperatures*, *New Scientist*, US, 2007.
- [10] Large-scale CCS facilities. Retrieved February 1, (2018), from <http://www.globalccsinstitute.com/projects/large-scale-ccs-projects>.
- [11] M.L. Szulczewski, C.W. MacMinn, H.J. Herzog, R. Juanes, *Proceedings of the National Academy of Sciences*, 109 (2012), pp. 5185-5189.
- [12] G. V. Last, M.T. Schmick, in: *Richland (Ed.)*, University of North Texas Libraries, Digital Library, Washington, 2011.
- [13] D. Minett, Department of Chemical Engineering, University of Bath, 2013.
- [14] E. Alper, O. Yuksel Orhan, *Petroleum*, 3 (2017), pp. 109-126.
- [15] VCI and DECHEMA, 2009, *Position Paper: Utilisation and Storage of CO₂*, Version 12: January 2009.
- [16] S. S. Nam, H. Kim, G. Kishan, M.J. Choi, K. W. Lee, *Appl. Catal., A*, 179 (1999), pp. 155-163.
- [17] T. Inui, K. Kitagawa, T. Takeguchi, T. Hagiwara, Y. Makino, *Appl. Catal., A*, 94 (1993) 31-44.
- [18] V. A. Goltsov, T.N. Veziroglu, L.F. Goltsova, *Int. J. Hydrog. Energy*, 31 (2006), pp. 153-159.
- [19] J. R. Rostrup-Nielsen, T. Rostrup-Nielsen, *CATTECH*, 6 (2002), pp. 150-159.
- [20] A.U., J. Sa, CO₂ to Fuels, in: J. Sa (Ed.) *Fuel Production with Heterogeneous Catalysis*, Taylor and Francis Group, Boca Raton, (2014), pp. 318.
- [21] D. Fraile, J. C. Lanoix, P. Maio, A. Rangel, A. Torres, in, *Belgium*, (2015).
- [22] B. Tidona, C. Koppold, A. Bansode, A. Urakawa, P. Rudolf von Rohr, *J Supercrit Fluids*, 78 (2013) pp. 70-77.
- [23] A. Bansode, A. Urakawa, *J. Catal.*, 309 (2014), pp. 66-70.
- [24] D. Sheldon, *Johnson Matthey Technology Review*, 61 (2017), pp. 172-182.
- [25] The Methanol Institute, <http://www.methanol.org/wp-content/uploads/2016/07/6-Combined-Side-Deck-GFBC-1.pdf> (accessed on 28/12/2017).

- [26] A. Basile, F. Dalena, *Methanol: Science and Engineering*, Elsevier Science & Technology Books, 2017.
- [27] L. Lloyd, *Ammonia and Methanol Synthesis*, in: *Handbook of Industrial Catalysts*, Springer US, Boston, MA, (2011), pp. 397-437.
- [28] W. Balthasar, D.J. Hambleton, *Int. J. Hydrog. Energy*, 5 (1980) pp. 21-33.
- [29] K.A. Ali, A.Z. Abdullah, A.R. Mohamed, *Renew. Sust. Energ. Rev.*, 44 (2015) pp. 508-518.
- [30] C. Shekhar, in: *MIT Technology Review*, Technology Review, 2006.
- [31] F.F.S. P. Davies, Patent no. 3326956, US (Ed.), UK, 1967.
- [32] J. Yoshihara, C.T. Campbell, *J. Catal.*, 161 (1996) pp. 776-782.
- [33] J.S. Lee, K.I. Moon, S.H. Lee, S.Y. Lee, Y.G. Kim, *Catal. Lett.*, 34 (1995) pp. 93-99.
- [34] E.I. Solomon, P.M. Jones, J.A. May, *Chem. Rev.*, 93 (1993) pp. 2623-2644.
- [35] C. Baltes, S. Vukojevic, F. Schüth, *J. Catal*, 258 (2008) pp. 334-344.
- [36] F. Arena, G. Mezzatesta, G. Zafarana, G. Trunfio, F. Frusteri, L. Spadaro, *J. Catal*, 300 (2013) pp. 141-151.
- [37] P. Gao, H. Yang, L. Zhang, C. Zhang, L. Zhong, H. Wang, W. Wei, Y. Sun, *J. CO₂ Util*, 16 (2016) pp. 32-41.
- [38] T. Inui, H. Hara, T. Takeguchi, J.B. Kim, *Catalysis Today*, 36 (1997) pp. 25-32.
- [39] A. Garcia-Trenco, E.R. White, A. Regoutz, D.J. Payne, M.S.P. Shaffer, C.K. Williams, *ACS Catal.*, 7 (2017) pp. 1186-1196.
- [40] M. M. J. Li, Z. Zeng, F. Liao, X. Hong, S.C.E. Tsang, *J. Catal.*, 343 (2016) pp. 157-167.
- [41] J. Toyir, P.R. de la Piscina, J. Llorca, J.L.G. Fierro, N. Homs, *Phys. Chem. Chem. Phys.*, 3 (2001) pp. 4837-4842.
- [42] J. Toyir, P.R. de la Piscina, J.L.G. Fierro, N.s. Homs, *Appl. Catal., B.*, 29 (2001) pp. 207-215.
- [43] J. Toyir, P. Ramírez de la Piscina, J.L.G. Fierro, N.S. Homs, *Appl. Catal. B.*, 34 (2001) pp. 255-266.
- [44] J. Wu, M. Saito, H. Mabuse, *Catal. Lett.*, 68 (2000) pp. 55-58.
- [45] L. Ma, T. Tran, M.S. Wainwright, *Topics in Catalysis*, 22 (2003) pp. 295-304.
- [46] G.X. Qi, X.M. Zheng, J.H. Fei, Z.Y. Hou, *Catal. Lett.*, 72 (2001) pp. 191-196.
- [47] J. Graciani, K. Mudiyansele, F. Xu, A.E. Baber, J. Evans, S.D. Senanayake, D. J. Stacchiola, P. Liu, J. Hrbek, J. F. Sanz, J. A. Rodriguez, *Science*, 345 (2014) pp. 546-550.
- [48] G.C. Chinchu, P.J. Denny, J.R. Jennings, M.S. Spencer, K.C. Waugh, *Appl. Catal.*, 36 (1988) pp. 1-65.
- [49] M. Behrens, F. Studt, I. Kasatkin, S. Kühl, M. Hävecker, F. Abild-Pedersen, S. Zander, F. Girgsdies, P. Kurr, B.-L. Knief, M. Tovar, R.W. Fischer, J.K. Nørskov, R. Schlogl, *Science*, 18, (2012), pp. 893-897.
- [50] T. Lunkenbein, F. Girgsdies, T. Kandemir, N. Thomas, M. Behrens, R. Schlogl, E. Frei, *Angew. Chem. Int. Ed.*, 55 (2016) pp. 12708-12712.
- [51] A. Karelavic, P. Ruiz, *Catal. Sci. Technol.*, 5 (2015) pp. 869-881.
- [52] X. An, J. Li, Y. Zuo, Q. Zhang, D. Wang, J. Wang, *Catal. Lett.*, 118 (2007) pp. 264-269.

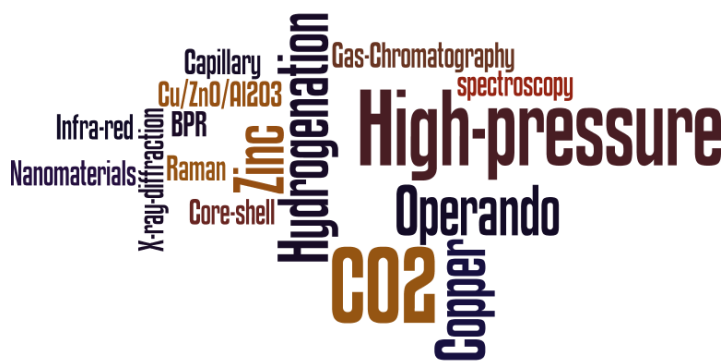
Chapter 1

- [53] I. Meliancabrera, J. Catal., 210 (2002) pp. 273-284.
- [54] I. Melian-Cabrera, M. Lopez Granados, J.L.G. Fierro, J. Catal., 210 (2002) pp. 273-284.
- [55] I. Melian-Cabrera, M.L. Granados, J.L.G. Fierro, J. Catal., 210 (2002) pp. 285-294.
- [56] I. Melian-Cabrera, M. Lopez Granados, J.L.G. Fierro, Catal. Lett., 79 (2002) pp. 165-170.
- [57] I. Melian-Cabrera, M. Lopez Granados, P. Terreros, J.L.G. Fierro, Catal. Today., 45 (1998) pp. 251-256.
- [58] M. Saito, K. Murata, Catal. Surv. Asia., 8 (2004) pp. 285-294.
- [59] M.D. Rhodes, A.T. Bell, J. Catal., 233 (2005) pp. 198-209.
- [60] A. Gotti, R. Prins, J. Catal., 178 (1998) pp. 511-519.
- [61] T.P. Maniecki, P. Mierczynski, W.K. Jozwiak, Kinet. Catal., 51 (2010) pp. 843-848.
- [62] J. Ye, C. Liu, D. Mei, Q. Ge, ACS Catal., 3 (2013) pp. 1296-1306.
- [63] O. Martin, A.J. Martín, C. Mondelli, S. Mitchell, T.F. Segawa, R. Hauert, C. Drouilly, D. Curulla-Ferre, J. Perez-Ramirez, Angew. Chem. Int. Ed., 55 (2016) pp. 6261-6265.
- [64] J. Ye, C. J. Liu, D. Mei, Q. Ge, J. Catal., 317 (2014) pp. 44-53.
- [65] M. Behrens, D. Brennecke, F. Girgsdies, S. Kießner, A. Trunschke, N. Nasrudin, S. Zakaria, N.F. Idris, S.B.A. Hamid, B. Kniep, R. Fischer, W. Busser, M. Muhler, R. Schlögl, Appl. Catal., A, 392 (2011) pp. 93-102.
- [66] G.R. Sheffer, T.S. King, J. Catal., 115 (1989) pp. 376-387.
- [67] G.R. Sheffer, T.S. King, J. Catal., 116 (1989) pp. 488-497.
- [68] T. Fujitani, M. Saito, Y. Kanai, T. Kakumoto, T. Watanabe, J. Nakamura, T. Uchijima, Catal. Lett., 25 (1994) pp. 271-276.
- [69] G.J.J. Bartley, R. Burch, Appl. Catal., 43 (1988) pp. 141-153.
- [70] M.S. Spencer, Catal. Lett., 50 (1998) pp. 37-40.
- [71] R. Burch, S.E. Golunski, M.S. Spencer, J. Chem. Soc. Faraday Trans., 86 (1990) pp. 2683-2691.
- [72] G.C. Chinchen, K.C. Waugh, D.A. Whan, Appl. Catal., 25 (1986) pp. 101-107.
- [73] C.V. Ovesen, B.S. Clausen, J. Schiotz, P. Stoltze, H. Topsøe, J.K. Nørskov, J. Catal., 168 (1997) pp. 133-142.
- [74] R.A. Hadden, B. Sakakini, J. Tabatabaei, K.C. Waugh, Catal. Lett., 44 (1997) pp. 145-151.
- [75] N.Y. Topsøe, H. Topsøe, J. Mol. Catal. A: Chem., 141 (1999) pp. 95-105.
- [76] M.M. Gunter, T. Ressler, B. Bems, C. Büscher, T. Genger, O. Hinrichsen, M. Muhler, R. Schlögl, Catal Lett, 71 (2001) pp. 37-44.
- [77] B.L. Kniep, T. Ressler, A. Rabis, F. Girgsdies, M. Baenitz, F. Steglich, R. Schlögl, Angew. Chem. Int. Ed., 43 (2004) pp. 112-115.
- [78] T.L. Barr, J.J. Hackenberg, Appl. Surf. Sci., 10 (1982) pp. 523-545.
- [79] Y. Kanai, T. Watanabe, T. Fujitani, M. Saito, J. Nakamura, T. Uchijima, Catal Lett, 27 (1994) pp. 67-78.
- [80] Y.B. Kagan, A.Y. Rozovskij, L.G. Liberov, E.V. Slivinskij, G.I. Lin, S.M. Loktev, A.N. Bashkurov, Doklady Akademii Nauk SSSR, 224 (1975) pp. 1081-1084.
- [81] K. Klier, V. Chatikavanij, R.G. Herman, G.W. Simmons, J. Catal., 74 (1982) pp. 343-360.

- [82] G.C. Chinchen, P.J. Denny, D.G. Parker, M.S. Spencer, D.A. Whan, *Appl Catal.*, 30 (1987) pp. 333-338.
- [83] J. Weigel, R.A. Koepfel, A. Baiker, A. Wokaun, *Langmuir*, 12 (1996) pp. 5319-5329.
- [84] I.A. Fisher, A.T. Bell, *J. Catal.*, 172 (1997) pp. 222-237.
- [85] Y. Yang, C.A. Mims, D.H. Mei, C.H.F. Peden, C.T. Campbell, *J. Catal.*, 298 (2013) pp. 10-17.
- [86] Y. Wang, C. Woll, *Chem. Soc. Rev.*, 46 (2017) pp. 1875-1932.
- [87] Y. Zhang, R. Yang, N. Tsubaki, *Catal. Today*, 132 (2008) pp. 93-100.
- [88] R. Yang, Y. Zhang, N. Tsubaki, *Catal. Commun.*, 6 (2005) pp. 275-279.
- [89] J. Schumann, J. Krohnert, E. Frei, R. Schlogl, A. Trunschke, *Top. Catal.*, (2017).
- [90] J. Saussey, J.C. Lavalley, J. Lamotte, T. Rais, *J. Chem. Soc., Chem. Comm.*, (1982) pp. 278-279.
- [91] R.M. Agny, C.G. Takoudis, *Ind. Eng. Chem. Prod. Res. Dev.*, 24 (1985) pp. 50-55.
- [92] J. Saussey, J.C. Lavalley, *J Mol Catal.*, 50 (1989) pp. 343-353.
- [93] P.B. Rasmussen, P.M. Holmblad, T. Askgaard, C.V. Ovesen, P. Stoltze, J.K. Norskov, I. Chorkendorff, *Catal. Lett.*, 26 (1994) pp. 373-381.
- [94] P.A. Taylor, P.B. Rasmussen, C.V. Ovesen, P. Stoltze, I. Chorkendorff, *Surf. Sci.*, 261 (1992) pp. 191-206.
- [95] T. Fujitani, I. Nakamura, T. Uchijima, J. Nakamura, *Surf. Sci.*, 383 (1997) pp. 285-298.
- [96] G. J. Millar, C.H. Rochester, K.C. Waugh, *Catal. Lett.*, 14 (1992) pp. 289-295.
- [97] J. E. Bailie, C.H. Rochester, G.J. Millar, *Catal. Lett.*, 31 (1995) pp. 333-340.
- [98] P. J.A. Tijm, F.J. Waller, D.M. Brown, *Appl. Catal.*, A: General, 221 (2001) pp. 275-282.
- [99] E. Fiedler, G. Grossmann, D.B. Kersebohm, G. Weiss, C. Witte, *Methanol, Ullmann's Encyclopedia of Industrial Chemistry*, Wiley-VCH Verlag GmbH & Co. KGaA, 2000.
- [100] Lower, *General chemistry text book maps*, 2018.
- [101] J.G. van Bennekom, J.G.M. Winkelman, R.H. Venderbosch, S.D.G.B. Nieland, H.J. Heeres, *Ind. Eng. Chem. Res.*, 51 (2012) pp. 12233-12243.
- [102] G.H. Graaf, P.J.J.M. Sijtsema, E.J. Stamhuis, G.E.H. Joosten, *Chem. Eng. Sci.*, 41 (1986) pp. 2883-2890.
- [103] G.H. Graaf, J.G.M. Winkelman, *Ind. Eng. Chem. Res.*, 55 (2016) pp. 5854-5864.
- [104] J.G. van Bennekom, R.H. Venderbosch, J.G.M. Winkelman, E. Wilbers, D. Assink, K.P.J. Lemmens, H.J. Heeres, *Chem. Eng. Sci.*, 87 (2013) pp. 204-208.
- [105] R. Gaikwad, A. Bansode, A. Urakawa, *J. Catal.*, 343 (2016) pp. 127-132.
- [106] A. Alvarez, A. Bansode, A. Urakawa, A.V. Bavykina, T.A. Wezendonk, M. Makkee, J. Gascon, F. Kapteijn, *Chem. Rev.*, 117 (2017) pp. 9804-9838.
- [107] W.L. Luyben, *Ind. Eng. Chem. Res.*, 39 (2000) pp. 1529-1538.

Chapter 1

2. Materials and methods



Chapter 2

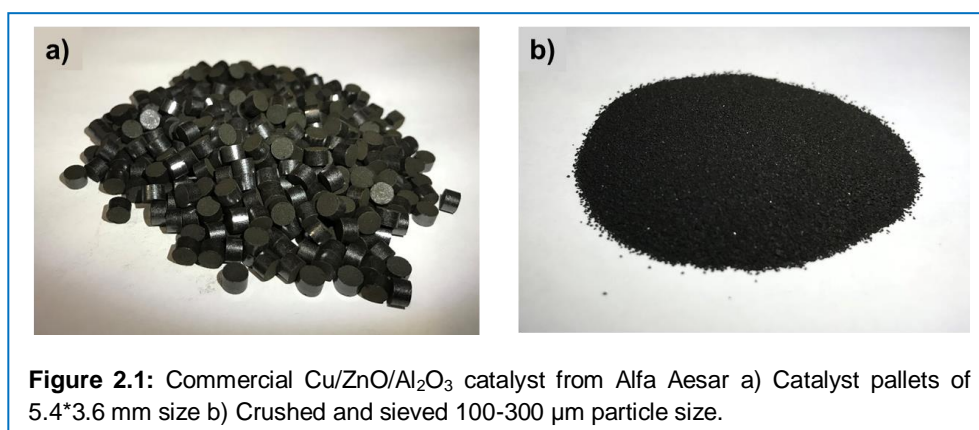
Scope

This chapter covers two topics, first, the synthesis procedures of Cu-ZnO nanomaterials by different synthesis approaches, and second the description of the high-pressure reactor set up for methanol synthesis as well as different reactor configurations for *operando* experimental studies (Chapter 4 and 5).

2.1 Catalysts synthesis

The main goal of the catalyst synthesis is to obtain an ideal catalyst which shows the high reactants conversion and an excellent desired product selectivity under the optimized reaction conditions over a long period of time. Many different types of copper-based catalysts and its preparation routes have been reported in the literature. The ideal catalyst should have a smaller copper particle size, high copper surface area and minimum copper agglomeration at high temperature. Although the role of ZnO in methanol synthesis catalyst is highly debated, it has been widely accepted that there exists Cu-ZnO synergy, in which ZnO acts as a spacer between the copper particles to avoid agglomeration [1, 2]. Addition of a high surface area aluminium oxide ($\gamma\text{-Al}_2\text{O}_3$) to Cu-ZnO not only provides the support, but also enhances the thermal stability at high temperature during the reaction. Various supports have been tested including ZrO_2 , SiO_2 , GaO_2 , TiO_2 , however, the direct role in the reaction apart from acting as a support has not been observed [4]. The catalyst synthesis method highly depends on its application and reaction process requirement. Coprecipitation, impregnation, sol-gel, hydrothermal, and nanomaterial synthesis are few among others which are widely used in laboratory scale synthesis, and even at industrial scale synthesis. The catalysts synthesized by coprecipitation are considered robust and contains homogeneous mixture of metal oxides. The ease of synthesis and high reproducibility even at a bigger scale made it widely applicable for the large-scale synthesis and employable for industrial chemical processes.

At present, most of the commercial methanol synthesis processes use the Cu/ZnO/Al₂O₃ based ternary catalyst which is generally synthesized by coprecipitation method. Johnson Matthey, Sudchemie, Haldor Topsoe, BASF are the major catalyst producer companies. The molar concentration of each component in Cu/ZnO/Al₂O₃ is in the range of CuO = 50-70%, ZnO = 20-50%, Al₂O₃ = 5-20% [5]. Various factors affect the catalytic properties during the synthesis process. For instance, the precursor mixing, precipitation and subsequent treatments like aging, washing, drying, calcination, and reduction can have an influence on the ultimate microstructure of Cu/ZnO/Al₂O₃ catalysts. [Figure 2.1](#) shows the commercial methanol synthesis catalysts pellets and particles. The catalyst was purchased from Alfa Aesar (Product ID: 45776). This catalyst was used for high-pressure methanol synthesis and mechanistic studies, explained in [Chapter 3](#) and [4](#), respectively.



A) Nanomaterial synthesis

The other class of catalyst synthesis is nanomaterial synthesis approach, in which controlled synthesis of metal oxide with specific size helps to obtain a uniform, size, and shape-controlled metal oxide in different morphology [6]. The particular reaction demand of small copper size to avail high surface area can be fulfilled by nanomaterials. With this nanomaterial synthesis approach, it is expected to achieve smaller particle size, more uniform morphology and higher surface area of metal oxide nanoparticles. In this study, Cu and ZnO or

Chapter 2

Al_2O_3 were synthesized using different synthesis approach to get smaller copper particles which are either coated or separated by ZnO or Al_2O_3 to avoid agglomeration of copper particles at a higher temperature.

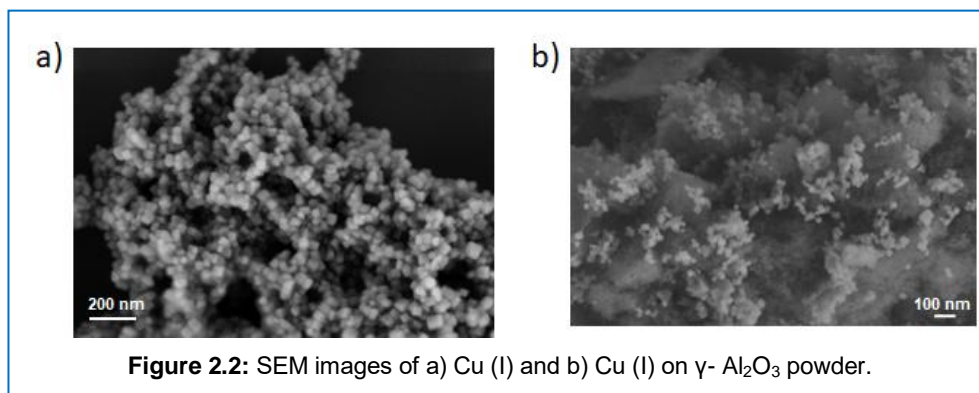
2.1.1 Chemicals and catalyst synthesis

All the chemical reagents were used as purchased from Sigma-Aldrich, Fluka, Alfa Aesar and Acros without further purification. Copper (II) acetylacetonate ($\text{Cu}(\text{acac})_2$, Acros, >98%), Copper methoxide ($\text{Cu}(\text{OMe})_2$, Sigma-Aldrich, 97%), Copper (I) acetate (Sigma-Aldrich, 97%), Aluminium oxide as catalyst support (Alfa Aesar, 1/8" pellet), Zinc acetate (Sigma-Aldrich, 99.99%), Benzyl alcohol (BnOH, Sigma-Aldrich, puriss), Acetophenone (AcPh, Sigma-Aldrich, puriss), Benzylamine (BnNH_2 , Fluka, $\geq 99.0\%$).

Based on the literature and material synthesis understanding, we chose following synthesis pathways to prepare copper with zinc or aluminium oxide nanomaterials.

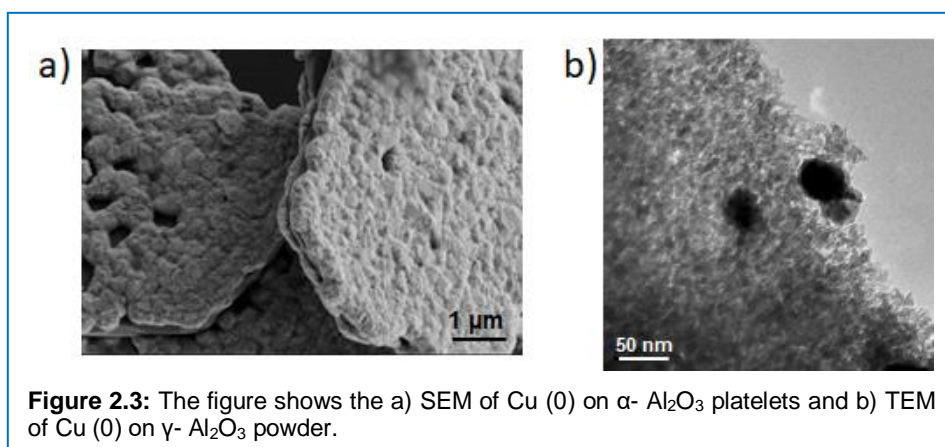
A) Scheme 1: Synthesis of Cu (I) on $\gamma\text{-Al}_2\text{O}_3$

Copper methoxide (0.2 g) was mixed with 15 mL acetophenone in 30 mL glass vial under argon and then heated in an oil bath at 120 °C for 12-24 h, with constant stirring. The final reaction solution of yellow precipitate was cooled, washed with ethanol, and centrifuged at 4000 rpm for 10 min. to remove the organic residue. The precipitate was dried in an oven at 60 °C overnight. The XRD pattern of the dried precipitate shows the formation of pure Cu_2O phase with the crystalline size of 21 nm determined by Scherrer equation. Similarly, another reaction was also carried out with an addition of $\gamma\text{-Al}_2\text{O}_3$ support into the reaction mixture. As shown in Figure 2.2b, the SEM image shows that the Cu_2O particles were completely dispersed into the $\gamma\text{-Al}_2\text{O}_3$ matrix. The synthesis process was optimized further to obtain the smaller and more uniform Cu_2O particles, as shown in Scheme 2.



B) Scheme 2: Synthesis of Cu^0 on α - and γ - Al_2O_3

In order to achieve smaller and well dispersed copper particles, the synthesis method reported by Kränzlin et al. was adopted for metallic copper synthesis [7]. The synthesis method was modified by addition of α - Al_2O_3 into the reaction mixture of copper acetylacetonate (7.6g) dissolved in 300 mL of benzyl alcohol in a 500 mL glass bottle. The bottle was heated up to 183 °C under constant stirring by using an overhead stirrer and was kept at that temperature for 3 to 15 h. Finally, the reaction mixture was cooled down, centrifuged at 4000 rpm for 10 min, and washed with ethanol and acetone. Then the obtained catalyst powder was dried overnight in an oven at 60 °C. The PXRD pattern confirmed the formation of pure Cu (0) phase. The SEM image (Figure 2.3a) also shows that the Cu (0) particles covered the α - Al_2O_3 platelets completely. A very dense thick layer of Cu (0) particles were

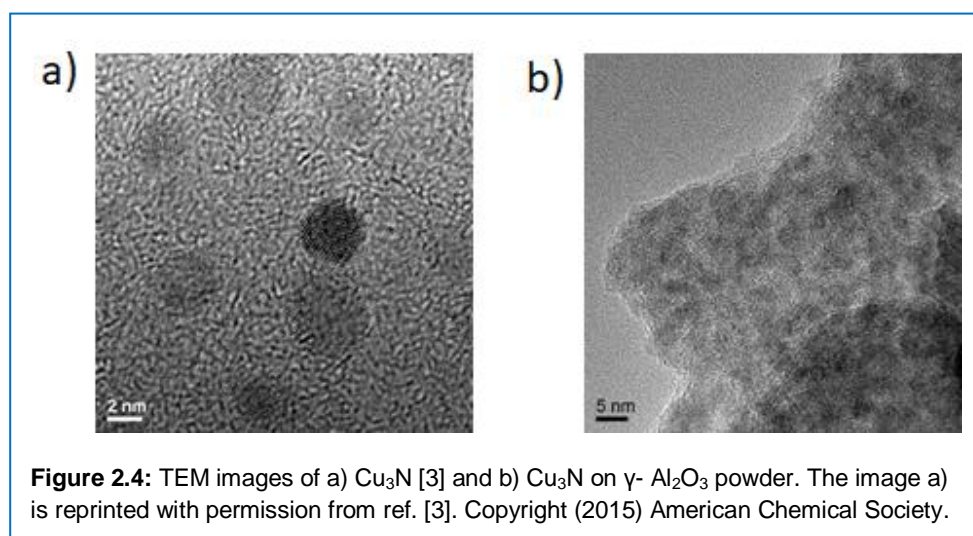


Chapter 2

observed, which probably possessed a low copper surface area. This catalyst might not represent the ideal catalyst for methanol synthesis. Therefore, the higher surface area γ - Al_2O_3 support was added in the reaction mixture instead of intrinsically low surface area α - Al_2O_3 support. The TEM image (Figure 2.3b) shows that the smaller particle size of Cu (0) dispersed γ - Al_2O_3 support can be achieved.

C) Scheme 3: Synthesis of Cu_3N on γ - Al_2O_3

It was reported that an ultra-small copper particle size can be synthesized by the copper nitride (Cu_3N) method developed by Deshmukh et al. This method yields Cu_3N particles with the size of 3-4 nm (Figure 2.4a), which can further decomposes to copper (II) oxide in air. In typical synthesis, 0.05 g of copper ethoxide was mixed with 5 mL of benzylamine in a 10 mL glass tube under argon atmosphere. The reaction mixture was then heated in an oil bath at 160 °C for 30 min. to produce Cu_3N precipitate. The precipitate was washed with pentane twice, and finally dried in an oven at 60 °C [3]. Using similar synthesis approach, the $\text{Cu}_3\text{N}/\gamma$ - Al_2O_3 catalyst was prepared by adding γ - Al_2O_3 support into the reaction mixture. As a result, the well-dispersed Cu_3N particles on γ - Al_2O_3 were achieved, as shown in the Figure 2.4b.



The Cu_3N supported on $\gamma\text{-Al}_2\text{O}_3$ was further decomposed to metallic copper Cu (0) at 250 °C in 5% H_2 in N_2 atmosphere. As a result, the copper particles agglomerated and increased the particle size to 42 nm.

D) Scheme 4: Cu_2O - ZnO core-shell morphology

The sol-gel method allows tailoring of size and shape of the resulting compounds by proper choice of metal precursor and reaction conditions [8]. Idalia et al. reported synthesis of metal oxide from metal acetate precursor using benzyl alcohol as an oxygen-containing mild surfactant to control the size and morphology of the metal oxide [9-11]. The catalyst was synthesized by mixing copper acetate (0.05g) with 5 mL of benzyl alcohol in a 10 mL glass tube under argon gas. The reaction mixture was then placed in a microwave oven with 300 W heating power and 2.45 GHz frequency operating at 160 °C for 3 min. under constant stirring. After microwave irradiation, the flask was removed from microwave oven and allowed to cool at room temperature. A reddish-brown product was obtained. The product was washed three times using ethanol and diethyl ether, centrifuged at 4000 rpm for 20 min. and dried in an oven at 60 °C.

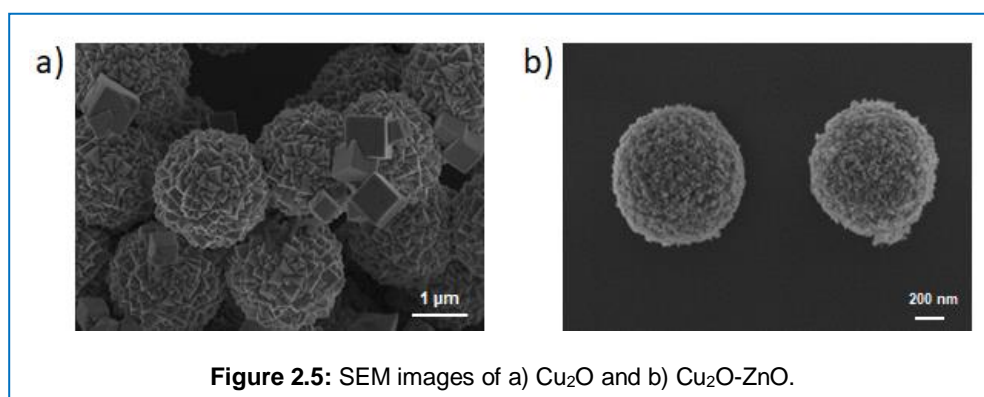
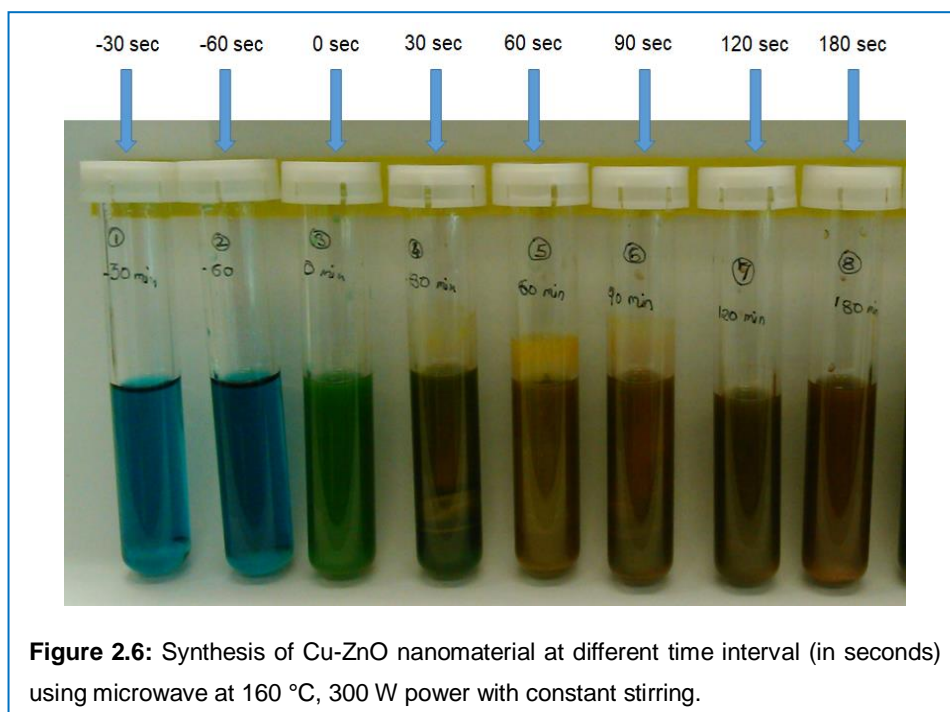


Figure 2.5: SEM images of a) Cu_2O and b) Cu_2O - ZnO .

Figure 2.5a shows the SEM image of the cuprous oxide sphere, probably formed by interlocking oxide cubes, which can be confirmed from the sharp edges of the sphere and also some isolated cubical structure of the oxide.

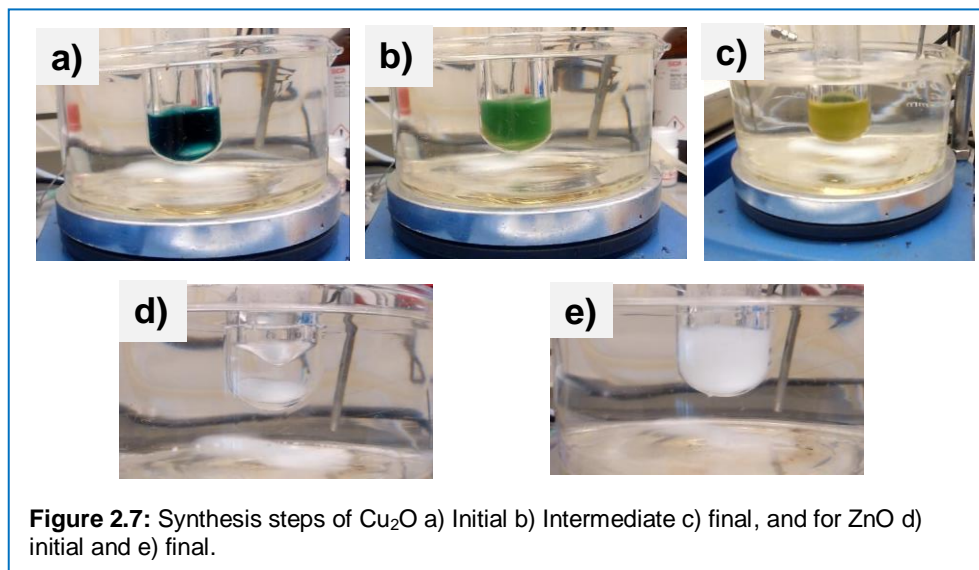
Chapter 2

XRD confirmed the formation of pure cuprous oxide phase. In the similar way, another synthesis was performed by mixing both copper acetate and zinc acetate with benzyl alcohol. [Figure 2.5b](#) shows the SEM image of the synthesized material, in which cuprous oxide formed a spherical core covered by small zinc oxide nanoparticles. The synthesis process was optimized for Cu₂O-ZnO core-shell nanomaterial by preparing material at different time intervals. The color of the solution was changed with time intervals from blue to reddish orange confirming the reaction completion and product formation, as shown in [Figure 2.6](#). The time -30 and -60 seconds (sec) shows the dissolution of metal precursor with increasing temperature. In order to reach the reaction temperature of 160 °C, approx. 60-80 sec of irradiation time were required at 300 W power. The zero second (0 sec) indicates that the temperature has reached the set point. The color of the solution was changed from blue to reddish orange as the reaction started from 0 to 180 seconds of continuous heating. The reaction was further performed at different temperature, 140, 150, 160, and 170 °C for 180 seconds. It was found that the



product formed at 160 °C shows a complete conversion and uniform material morphology.

The material synthesized using microwave as a heating source yielded very low quantity of the final product due to small volume. Hence, the synthesis method was changed from microwave heating to oil bath heating which facilitate higher quantity of final product due to larger synthesis volume. At the beginning, Cu_2O and ZnO were separately synthesized to optimize the synthesis time at 160 °C. [Figure 2.7](#) shows the different synthesis stages of Cu_2O and ZnO . After 25 min. of reaction, the solution changed to reddish orange for Cu_2O ([Figure 2.7a,b,c](#)) and white for ZnO ([Figure 2.7d,e](#)), which confirmed the completion of reaction. The phase purity and morphology of Cu_2O and ZnO was also confirmed by XRD and SEM analysis, respectively.



By using the optimized synthesis conditions, the Cu_2O and ZnO were prepared concurrently to obtain desired core-shell morphology. The copper and zinc acetate precursor were mixed together with benzyl alcohol and heated up to 160 °C using oil bath. [Figure 2.8](#) shows the color change during the synthesis of Cu_2O - ZnO nanomaterial in an oil bath.

Chapter 2

All the synthesized catalysts were characterized and tested for thermal stability by heating under nitrogen flow. The core-shell $\text{Cu}_2\text{O-ZnO}$ synthesized by non-aqueous sol-gel method showed good stability with minimum agglomeration. Hence, the catalyst synthesized by Scheme 4 using oil bath was used for experimental studies. The details of optimal synthesis conditions and experimental results are explained in [Chapter 4](#).

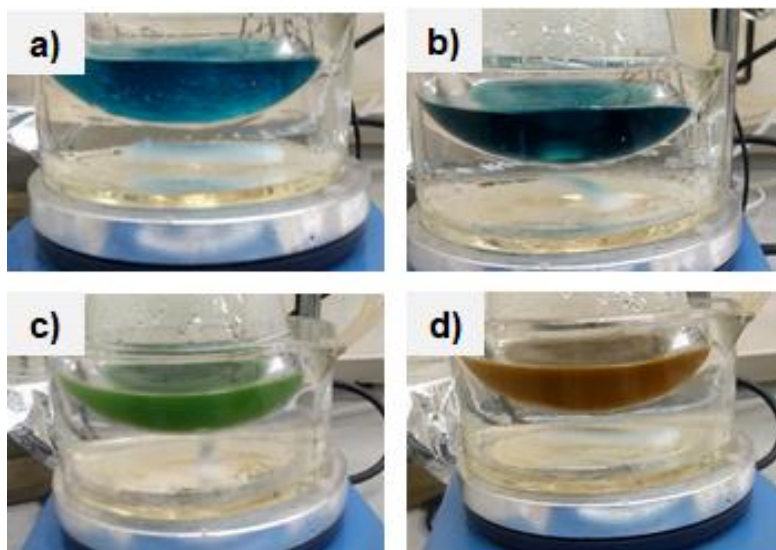


Figure 2.8: Synthesis steps of $\text{Cu}_2\text{O-ZnO}$ a) Initial b) and c) Intermediate d) final.

2.2 Experimental setup and catalytic tests

Continuous flow tubular reactor is a popular and widely accepted choice in heterogeneous catalysis. It enhances heat and mass transfer, provides

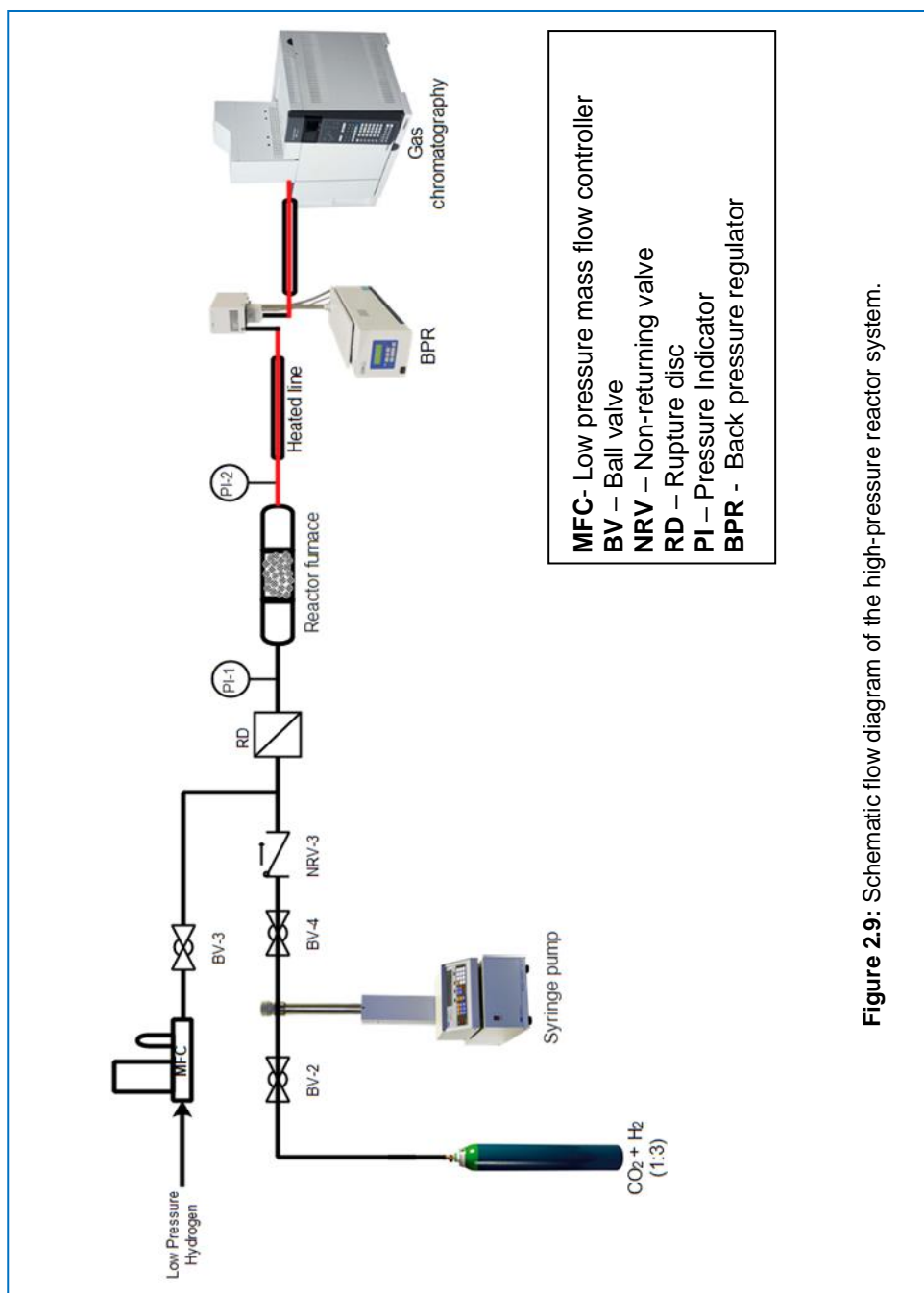


Figure 2.9: Schematic flow diagram of the high-pressure reactor system.

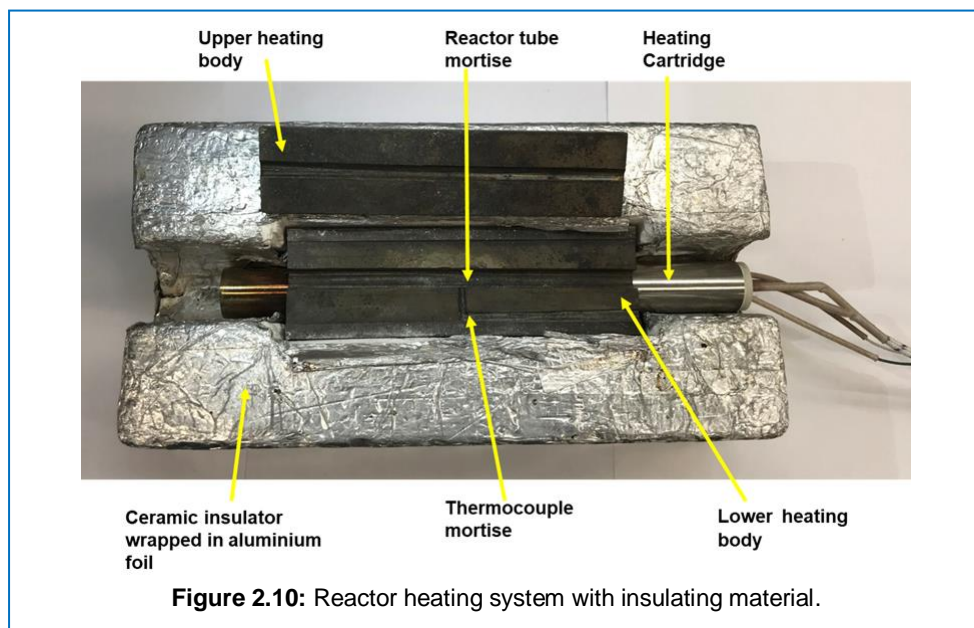
Chapter 2

precise residence time control, shortens overall process time, and improves safety, reproducibility, product quality and scalability [12, 13]. Such advantages are the main reasons for implementing flow reactors not only in academia, but also at an industrial scale. Lab-scale small catalytic tubular reactors vary in the range of micron to few millimeters, which provides the safety, due to low reaction volume. This safety is not only in the context of solvent or hazardous chemical synthesis but instead, small reactor volume provides minimum severity in case of accidents. The controlled feeding rate of reactants for exothermic reaction with fast kinetics suits as a perfect example for flow reactors due to high mass and heat transfer rate. Such advantages of tubular flow reactor make it the best candidate for high-pressure reactions over conventional reactors batch reactors [14]. [Figure 2.9](#) shows the schematic representation of high-pressure tubular reactor system used in this research work for CO₂ hydrogenation reaction.

2.2.1 Working principle of flow reactor

A tubular homemade fixed bed high-pressure reactor was designed and developed during the research work. It consists of a stainless steel (SS) reactor tube (Swagelok, Europe) with an inner diameter of 1.7 mm or 3.05 mm and length approx. 21 cm was placed in the temperature controlled oven along with a thermometer. The heating plates were made up of two stainless steel blocks, with a length approximately 15 cm. The lower SS heating block was heated by means of resistive heating cartridge with a capacity of 750 W (200 * 20 mm, Watlow), placed below the SS body as shown in [Figure 2.10](#). The complete assembly of SS heating body with heating cartridge was placed in a heat insulating ceramic block, to avoid heat loss. The thermocouple (K type, Watlow, 1.6* 150 mm) was placed along with axial direction of reactor tube with end in L shaped mortise, to make direct contact with the reactor and get more accurate temperature near catalyst bed. The reactor temperature was controlled using PID controller from Watlow (EZ-zone). The top SS plate covered with a ceramic block was placed from the top, to cover the reactor

tube. Both ceramic blocks were wrapped entirely in aluminium foil for better insulation and handling.



For the high-pressure system, two components play crucial role: first, a back pressure regulator (BPR) that regulates the overall system pressure and second, a syringe pump that delivers the stable and continuous feed. Identification of the BPR which can control low a flow rate (in few mL) at high pressure (up to 510) bar was significantly challenging. The Jasco BPR (BP-2080 Plus) provided an effective solution. The high-pressure syringe pump that delivers the premixed gas feed to the reactor is also an important part of pressure controlling system. Traditionally, the gas flow has been controlled using a mass flow controller (MFC) where gas cylinder pressure drives the flow through the MFC. It was challenging to avail a MFC which can dispense gas at pressures higher than 400 bar, hence, the high pressure syringe pump was the best solution. The Teledyne ISCO syringe pump was identified as the best possible choice to work with low flow rates and high pressures. These pumps are unique as they can work at constant pressure as well as constant flow mode.

Chapter 2

The feed gas was passed using high-pressure syringe pump (Teledyne ISCO, 260 D) to achieve the stable feed flow. The desired CO₂ and H₂ gas ratio was obtained by using premixed gas composition cylinder with fixed concentration with an internal standard for GC analysis. The premixed feed gas of CO₂:H₂ (1:3) with feed composition of 23% CO₂, 69% H₂ and 8% Ar was supplied by Abelló Linde (Spain). Since the density plays an important role at high pressure, and a change in the ambient temperature, changes the density of the composition, hence constant temperature was provided by jacket covering the syringe pump cylinder. The temperature of the pump cylinder was kept constant at 20 °C by water circulation. The outlet of the syringe pump was connected to a ball valve and further to the reactor. As depicted in [Figure 2.11](#) low-pressure H₂ mass flow controller (Bronkhorst, Hi-Tec) was used to pass hydrogen for catalyst reduction prior to the reaction. The outlet of H₂-MFC was connected to a needle valve before a tee-fitting that was connected with the syringe pump outlet. Furthermore, the tee outlet was connected to a rupture disc RD-1 (HiP) before the reactor inlet to avoid the excess pressure condition. The pressure drop across the catalyst bed was measured with two pressure transmitters PI-1 and PI-2 (STW, Germany) placed at inlet and outlet of the reactor. These pressure transmitters were connected to a digital pressure readout system (HaoYing, China). The total reaction pressure in the reactor system was controlled by a back pressure regulator (model BP-2080 Plus, Jasco, Japan), specially designed for supercritical fluids with minimum dead volume. The main components of BPR such as valve rod, needle, seal, and seat were kept at higher temperature (80 °C) to avoid condensation of liquefied products. At the outlet of the reactor, inline filter frit (10 μ) was placed inside the 1/16" union to avoid any trans-pass of catalyst particles to the BPR. The outlet of the BPR carrying product stream was fed directly to the gas chromatography through the transfer line heated at 150 °C to keep the products in the vapor phase. A flow meter was used (MesaLabs DryCal Definer 220) to measure the flow rate at the outlet of the GC.

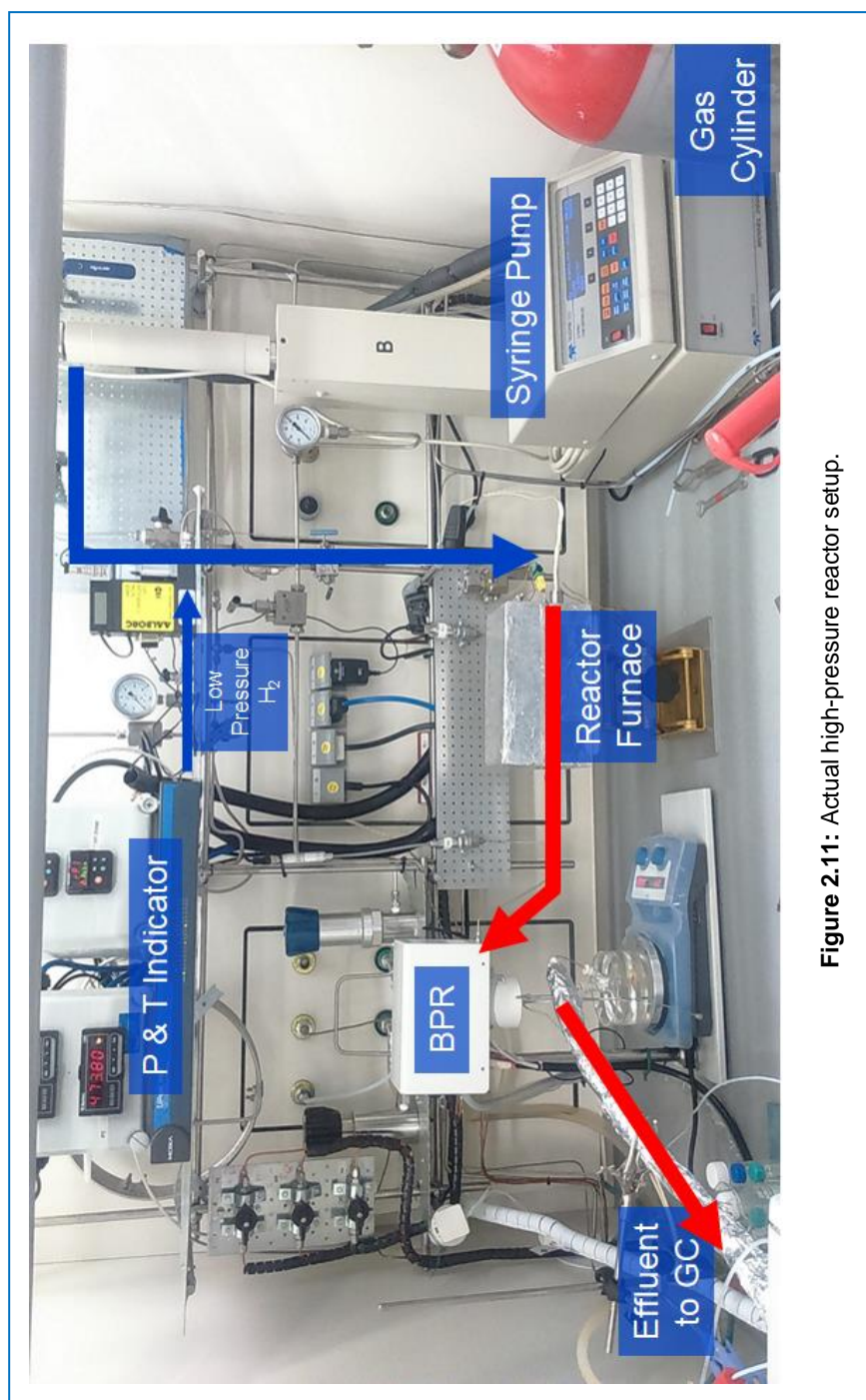


Figure 2.11: Actual high-pressure reactor setup.

Chapter 2

2.2.2 Analytical system

The concentration of reactant and products were analyzed by the gas chromatography (Bruker, GC 450) equipped with manual as well as online injection functionality. The GC method was developed to detect all possible products from CO₂ hydrogenation as well as Fischer-Tropsch reaction. The GC has been equipped with three 6-port valves. **Figure 2.12** is showing a schematic representation of the configuration of 6-port valves. The products were detected by TCD (Thermal Conductivity Detector) and FID (Flame Ionization Detector) operating in parallel mode. The valve compartment was heated at 150 °C to avoid condensation of any liquid products. Helium was used as a carrier gas on both the channels. The TCD channel was equipped with HayeSep-Q (0.5 m * 1/8" * 2 mm) and CP-Molsieve-13X (1.5 m * 1/8" * 2 mm) packed column connected in series. Two independent 6-port valves were used for the injection of the sample from a 10 µl and 250 µl sample loop on TCD and FID channels respectively. The HayeSep-Q column on TCD channel pre-splits the product mixture into permanent gases (O₂, H₂, N₂, CO, CH₄) and other components like CO₂, methanol, dimethyl ether, and hydrocarbons. Then the permanent gases were passed to the CP-Molsieve column using a 6-port valve. To the FID channel, a CP-WAX 52CB (25 m x 0.53 mm, df= 2µm)

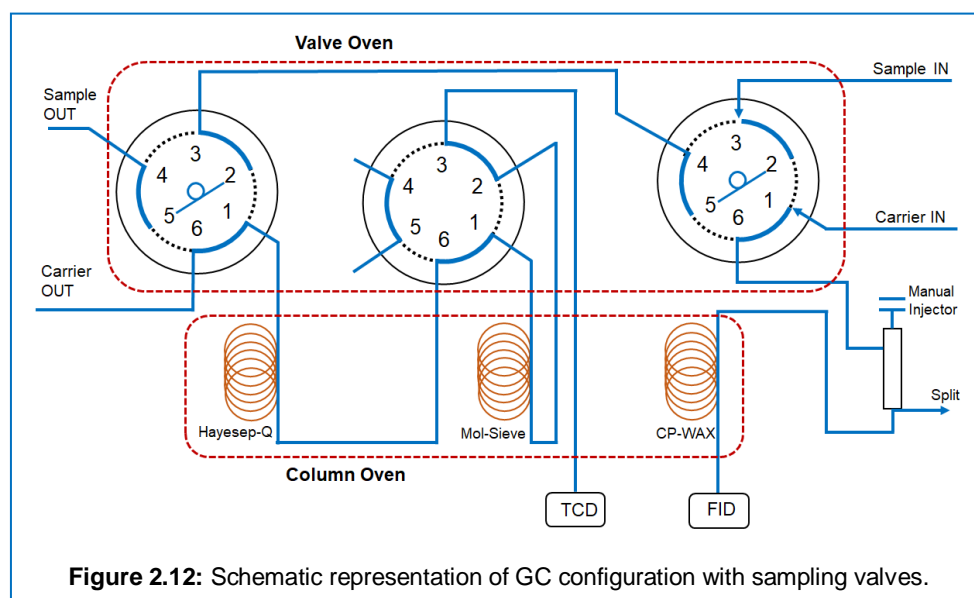


Figure 2.12: Schematic representation of GC configuration with sampling valves.

capillary column was connected to separate compounds such as alcohols, aldehydes, acetates. The injector of FID channel was operated in a split mode with split ratio of 1:10. The column oven was kept at a constant temperature at 45 °C for 3.50 min. to allow better separation of permanent gases. Followed by increasing the oven temperature to 150 °C at the rate of 15 °C min⁻¹. The total analysis time was 12 min. including the 0.50 min. for the stabilization of oven. A 4-port valve (not shown) was used as stream shut off valve during the online injection of sample.

The data acquisition and analysis were performed by Varian Galaxie software. The calibration of the detected components was carried out using the external standard method. The known gas composition mixture was injected to obtain calibration curve in the acquisition software. In case of liquid phase products like methanol, methyl formate, a 1.5 L tedler bag was used to make liquid components mixture in a certain ratio. Typically, the known volume of the N₂ gas used to fill in the bag using MFC to keep the calibration liquid in vapor form. Highly pure known amount of liquid used to inject in the tedler bag through the septa using an appropriate syringe. The tedler bag with injected liquid mixture was kept for some time to make sure that the liquid vaporized and equilibrated. After confirmation that no liquid droplets observed inside the bag, the outlet of the tedler bag was connected to the inlet of the GC and followed the usual procedure for the injection and analysis.

2.2.3 Reactor automation

LabVIEW software (National Instruments) was used to control the reaction parameters. [Figure 2.13](#) shows the screenshot of the LabVIEW program which was used to control and monitor the high-pressure reactor remotely. The programme was able to communicate with a syringe pump, temperature controllers, pressure indicators and a back pressure regulator. The communication between various components and computer was achieved using serial port communication. An 16-port RS232 communication hub (MOXA Uport 1610-16) was connected to the computer using USB 2.0

Chapter 2

connection. To this hub, all the instruments were connected using the DB9 RS-232 connector. To carry out reactions in highly safe manner, the programme was equipped with an alarm system which keeps a record of all the process values within the configured limits. Deviation of any process parameter from the desired value activates an emergency shutdown procedure. The shutdown procedure sets all the flow controllers to zero and turns off the heating system while displaying blinking alarms on the LabView control panel. The inlet and outlet pressure of the reactor were monitored continuously, and the corresponding pressure drop across the catalyst bed is displayed on the screen. If the value of pressure drop across the catalyst bed increases above the desired set value, the emergency shutdown procedure gets activated. Any overshoot of temperature and/or flow also activates the emergency shutdown procedure. Together with LabVIEW based safety system, all the devices have its own internal alarm facility which was configured carefully to ensure the safe operation of the reactor system. To test the catalyst at different temperatures and flow conditions, the respective program recipe was developed. The pump flow and temperature controllers can be operated in auto or manual mode. In auto mode, the values from the temperature program recipe were sent to the instrument while in manual mode it was possible to enter the set points directly. The temperature control section also shows the heater power applied to the heating system together with the PID parameters. All the process parameters values which are displayed and can be controlled from the software were logged in a file along with the real time.

2.2.4 Safety

The hydrogenation reaction was performed at elevated temperature and pressure, which could pose a risk that must be eliminated to work in a safe

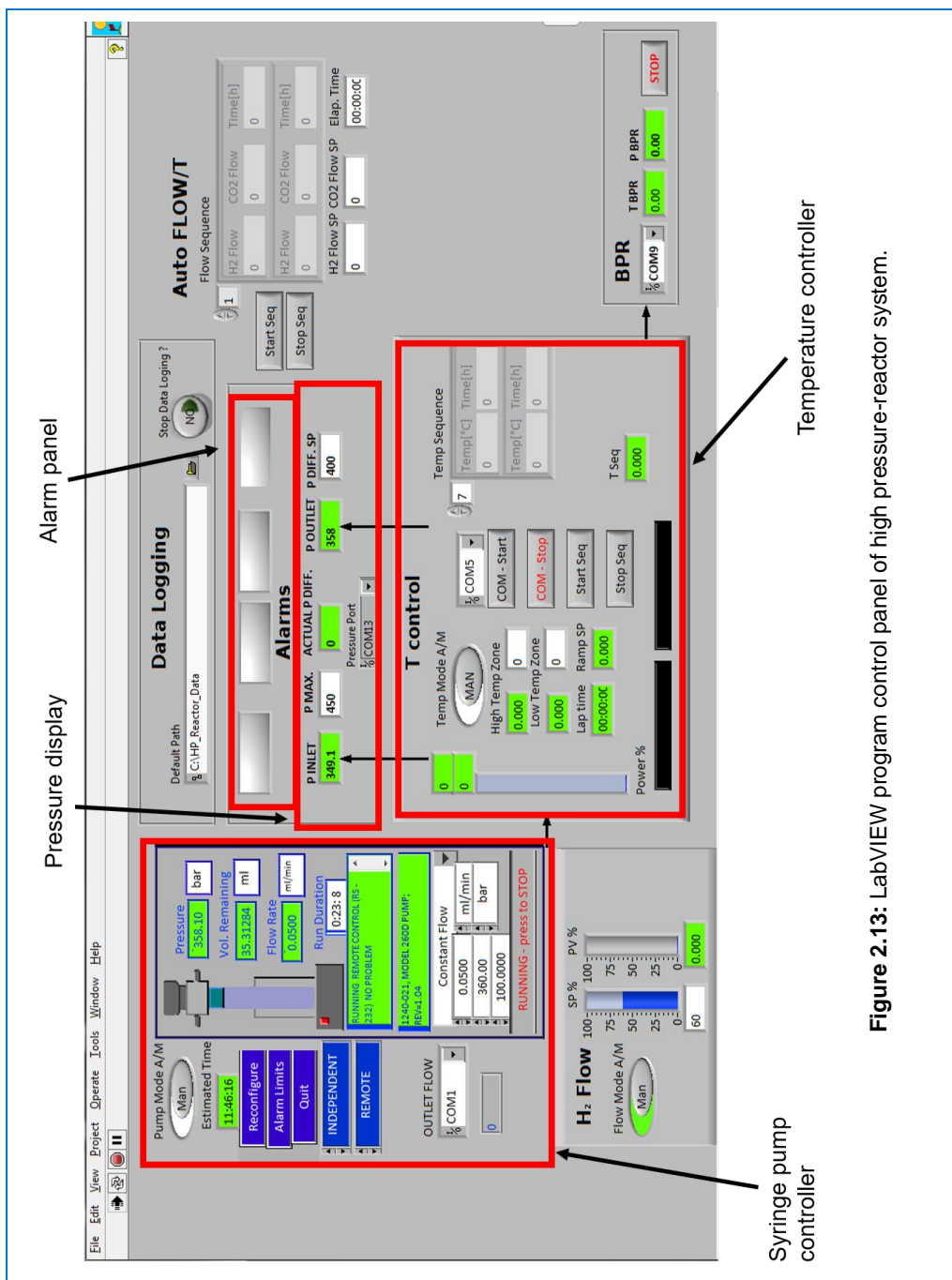


Figure 2.13: LabVIEW program control panel of high pressure-reactor system.

Chapter 2

environment. The reaction using fixed bed reactor in SS tube helps to perform the reaction even at high pressure up to 1034 bar due to an enhanced thickness of the tube, but increasing temperature lowers the maximum working pressure. Besides building a complete robust system for harsh reaction conditions, special care has been taken for safety, by implementing several safety features.

- A) A rupture disc was placed after the feed pump, inline with room temperature gas feed before the hot reactor zone, which is standard protocol in high-pressure setup. It consists of a thin rupture disc which is always in contact with pressurized fluid on one side and ambient air on other side. It constitutes purposely created weakest point of the reactor system with maximum pressure limit (bursting limit) 515-535 bar, and in case of overpressure emergency, the disc breaks and directs the contents of reactor to a safe vent.
- B) The syringe pump automatically stops in case of overpressure which exceeds limits defined by the user gets detected. This system is also connected to LabVIEW programme which triggers the alarm condition and shuts down the overall operation of reactor.
- C) The overall system pressure is controlled by BPR, thanks to Jasco BPR which has its own internal safety features. A user can define the maximum pressure limits for BPR and in case of over pressure the BPR releases the pressure from the outlet.

Prior to commissioning a shake-down was performed to verify the system integrity. The pressure was increased by steps of 50 bar up to 510 bar and leak test was performed using soap solution. The inlet and outlet of the system were closed at 510 bar and left overnight to observe any small pressure drop due to a minor leak in the system. After confirmation of leak-proof system, the reactor was heated with ramp rate of $2\text{ }^{\circ}\text{C min}^{-1}$ at 510 bar and at each $50\text{ }^{\circ}\text{C}$ the system was checked for the, no leaks were observed and confirmed

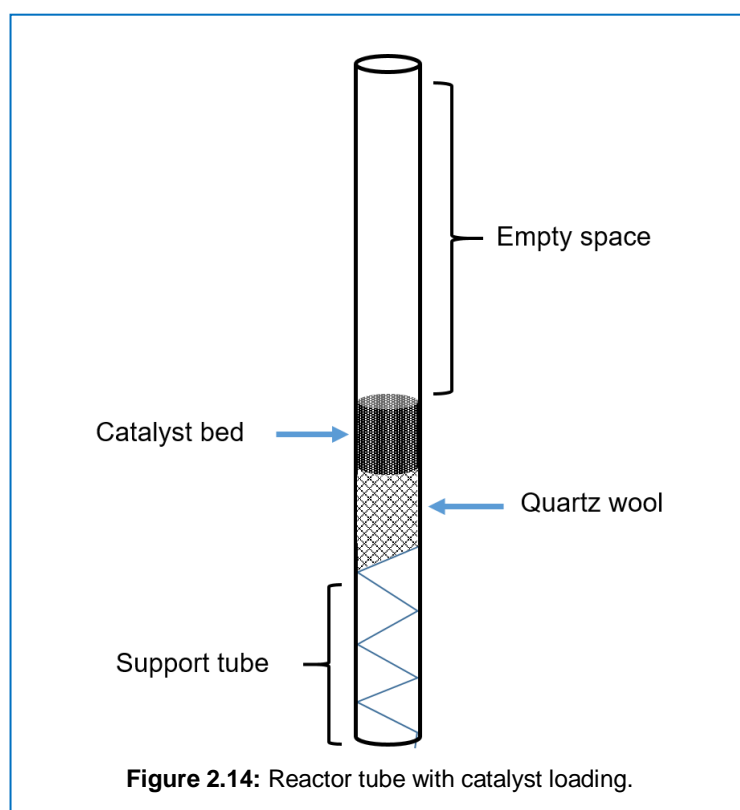
successful shake-down process. Similar protocol was followed in case of any major changes or spare parts replacement in the reactor system.

2.3 Working with the reactor

A standard operating procedure was developed for catalysts loading in the reactor and pressurizing the system, as these are the important steps during routine operation. Improper loading of catalyst in the reactor tube could sweep away the catalysts particles and/or create higher pressure drop across the catalyst bed making operation impossible.

2.3.1 Catalyst loading

The loading of the catalyst particles in the reactor is the crucial part of the reactor system. Initially, the catalyst powder was finely grounded and then pressed in the pellet die with 5 ton of pressure to form a pellet. Later the pellet was crushed using mortar and pestle and sieved using 100-300 μm and 10-20



Chapter 2

μm mesh. Before loading the catalyst into the 1/8" or 1/4" tube reactor, a small piece of a zig-zag tube was placed from the bottom of the reactor around 3-4 cm length as shown in [Figure 2.14](#). This tube acts as a support for the catalyst and prevents the catalyst bed movement due to pressure or the gas flow. A small portion of this tube was left outside of the reactor to allow its easy withdrawal from reactor tube after the reaction. Quartz wool was placed above this tube into the reactor from the top; care needs to be taken while inserting quartz wool to avoid it forming small fine particles that can block the reactor and increase the pressure drop. The total length of the inserted tube and quartz wool was around 4-6 cm. The sieved catalyst particles were carefully added into the reactor from the top.

The reactor is tilted and tapped gently to allow the catalyst particles to flow through the reactor and settle on the quartz wool. The procedure followed 2-3 times to make sure that the catalyst bed is uniformly packed. The total catalyst bed length was varied from 2-10 cm depending on the density of the catalysts, reactor tube size and desired space velocity. The top portion of the catalyst bed left open inside the reactor for easy and complete catalyst recovery.

2.3.2 Reactor operation

A reactor tube prepared as mentioned in [section 2.3.1](#) was then placed into the furnace and was connected to the system using 1/8" or 1/4" compression fittings. The furnace was kept horizontally on the moving stage which allows the up and down movement of the furnace. The reactor was pressurized to a desired reaction pressure to find any leaks into the reactor compression fittings prior to any catalyst treatment. The reactor was depressurized and made ready for the catalyst reduction before the reaction. The 10% H_2 in Ar was used to reduce the catalyst at 330 °C for 2 h at atmospheric pressure. The heating ramp was kept 2 or 10 °C min^{-1} . After reduction, the heating was turned off to cool down the reactor. In order to cool down faster, the heating furnace was lowered, so the reactor tube was directly

exposed to the atmospheric temperature under steady state flow of H₂/Ar. Then the gas flow turned off and hydrogen was flushed out using CO₂/H₂ composition mixture from the syringe pump at 20 bar several times, to make sure that no excess of H₂/Ar left in the reactor or in the system. The BPR was set to the desired pressure and the reactor was pressurized using CO₂:H₂ (1:3) premixed gas composition using syringe pump operating in a constant pressure mode. After attending the desired pressure, the syringe pump's constant pressure mode was switched to the constant flow rate mode to establish steady flow through the reactor. The flow rate at the outlet of the BPR was measured with a volumetric flow meter to estimate the corresponding GHSV. The outlet of the BPR was connected to a water condenser which prevents water from entering into GC column. After water removal, the feed goes to the GC for identification and quantification of the reactant and products from the reactor outlet. The reactor was kept at the ambient temperature to get steady state desired feed gas composition.

Once the steady state feed composition was ensured by the GC, the heating furnace was then raised up, to place the reactor into the furnace and covered with insulating material. The reaction was carried out at different temperatures ranging from 160 to 340 °C. The LabVIEW temperature programme was used to scan the various temperatures at desired time span. The CO₂ conversion was determined directly from the CO₂ molar concentration measured by the TCD detector. The detection limits for methanol and CO were 10 and 200 ppm, respectively, based on the signal to noise (S/N) of the chromatograms. This ensures the accuracy of CO₂ conversion, better than 0.1 %. The conversion and selectivity values were calculated by averaging over several injections after stabilization of product concentrations. In an experiment, during reaction, each temperature and pressure were kept for 3 h and analyzed the outlet gases after each 12 min. using GC. The tendency and accuracy of the catalytic performance were

Chapter 2

ensured by minimum two runs carried out on different days. The standard deviations for CO₂ conversion and product selectivities were < 2.2 %.

2.4 Conclusions

A high-pressure lab scale micro-reactor setup for the continuous catalytic hydrogenation of CO₂ at pressures up to 510 bar was successfully constructed. The stable feed gas flow was achieved by using syringe pump whereas a high pressure BPR was used to control overall reaction pressure. The product analysis was carried out by using online GC system equipped with two parallel detection channels. The GC method for product separation was successfully developed. Premixed feed gas composition brings the advantage of less feed stabilization time at high reaction pressure and low flow rate. It also ensures the constant feed composition gas flow through the syringe pump. The LabVIEW program facilitated the automation of the reactor to monitor and control the critical parameters of the system remotely. The temperature and flow program feature in LabVIEW program allowed to scan various temperatures and flows automatically for the given catalyst. Furthermore, the emergency shutdown function enabled unmanned and safe operation of the reactor during the nights and over the weekend.

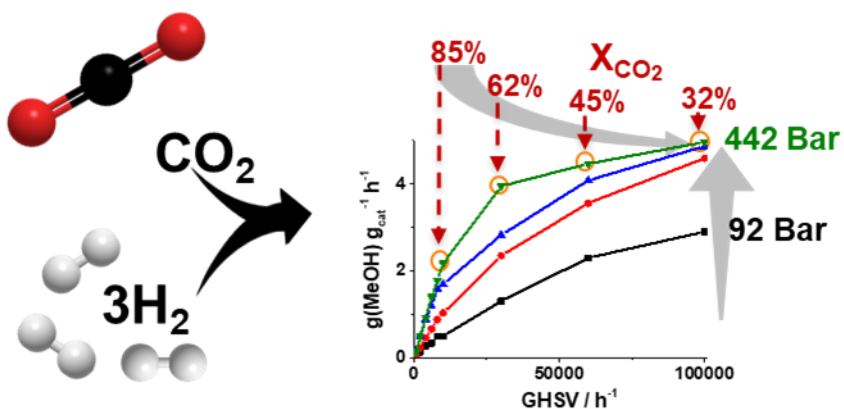
Bibliography

- [1] R. Burch, S.E. Golunski, M.S. Spencer, *J. Chem. Soc. Faraday Trans*, 86 (1990) pp. 2683-2691.
- [2] A. Le Valant, C. Comminges, C. Tisseraud, C. Canaff, L. Pinard, Y. Pouilloux, *J. Catal.*, 324 (2015) pp. 41-49.
- [3] R. Deshmukh, G. Zeng, E. Tervoort, M. Staniuk, D. Wood, M. Niederberger, *Chem. Mater.*, 27 (2015) pp. 8282-8288.
- [4] A. Gotti, R. Prins, *J. Catal.*, 178 (1998) pp. 511-519.
- [5] A. Álvarez, A. Bansode, A. Urakawa, A.V. Bavykina, T.A. Wezendonk, M. Makkee, J. Gascon, F. Kapteijn, *Chem. Rev.*, 117 (2017) pp. 9804-9838.
- [6] M.B. Gawande, A. Goswami, F. X. Felpin, T. Asefa, X. Huang, R. Silva, X. Zou, R. Zboril, R.S. Varma, *Chem. Rev.*, 116 (2016) pp. 3722-3811.
- [7] N. Kränzlin, S. Ellenbroek, D. Duran-Martín, M. Niederberger, *Angew. Chem. Int. Ed.*, 51 (2012) pp. 4743-4746.
- [8] P. Tamizhdurai, S. Sakthinathan, S.-M. Chen, K. Shanthi, S. Sivasanker, P. Sangeetha, *Sci. Rep.*, 7 (2017) pp. 46372-46385.
- [9] I. Bilecka, L. Luo, I. Djerdj, M.D. Rossell, M. Jagodič, Z. Jaglicic, Y. Masubuchi, S. Kikkawa, M. Niederberger, *J. Phys. Chem. C*, 115 (2011) pp. 1484-1495.
- [10] A. Nel, T. Xia, L. Mädler, N. Li, *Science*, 311 (2006) pp. 622-627.
- [11] M. Niederberger, G. Garnweitner, *Chem. Eur. J*, 12 (2006) pp. 7282-7302.
- [12] R.M. Machado, K.R. Heier, R.R. Broekhuis, *Curr. Opin. Drug Discov. Devel.*, 4 (2001) pp. 745-755.
- [13] I. Rossetti, M. Compagnoni, *Chem. Eng.*, 296 (2016) pp. 56-70.
- [14] D.K.B. Mohamed, X. Yu, J. Li, J. Wu, *Tetrahedron Lett.*, 57 (2016) pp. 3965-3977.

Chapter 2

3.

High pressure advantages in stoichiometric hydrogenation of CO₂ to methanol



Chapter 3

3.1 Introduction

The high-pressure conditions in the synthesis of methanol from syngas (CO and H₂ mixture typically containing some fraction of CO₂) have been known over the last 90 years [1]. Since 1966, the trend has shifted to lower pressure methanol synthesis (<100 bar) using highly active Cu-ZnO based catalysts [3]. Using these Cu-ZnO based catalysts which are most common for methanol synthesis nowadays, high-pressure advantages in methanol synthesis by the hydrogenation of CO and particularly CO₂ had not been explored and documented for a long time, except the excellent work reported by Ipatieff and Monroe in 1945 for Cu-based catalysts [4]. Recently, we reported a range of high-pressure reaction conditions, yielding remarkable almost-full one-pass conversion of CO₂ to methanol with high selectivity using Cu/ZnO/Al₂O₃ catalysts and also to methanol-derived products such as dimethyl ether (DME) by co-presence of an acidic zeolite [5]. The elevated H₂ partial pressure (molar ratio, CO₂:H₂=1:>10), higher than the stoichiometric one (CO₂:H₂=1:3), was found kinetically as well as thermodynamically beneficial for methanol synthesis as described in [Chapter 1](#). Employing the reaction pressure of 360 bar (reactants pressure of 331 bar due to the presence of Ar for GC analysis), outstanding CO₂ conversion (>95%) and methanol selectivity (>98%) were achieved at 260 °C at relatively high GHSV of ca. 10000 h⁻¹ using commercial Cu-ZnO based methanol synthesis catalyst. In addition, exceptionally high methanol yield of 7.7 g_{MeOH} g_{cat}⁻¹ h⁻¹ was attained at the expense of lower CO₂ conversion (65.8%) and methanol selectivity (77.3%).

Despite the exceptionally high CO₂ conversion and methanol selectivity under high-pressure conditions and high process viability concerning costs and methanol productivity, the reported reaction condition requires recycling or further conversion of unreacted H₂ feed in excess. In addition, CO produced by RWGS should be recycled if methanol selectivity is not sufficiently high. Recycling of H₂ can only be avoided by achieving its full conversion. In other words, the challenge in this respect is to achieve complete conversion of both

High pressure advantages in stoichiometric hydrogenation of CO₂ to methanol

CO₂ and H₂ with high methanol productivity. This goal naturally requires the operation of the reaction at the stoichiometric CO₂ to H₂ ratio (1:3).

This chapter presents a thorough examination of high-pressure reaction conditions (100-480 bar; in reactants pressure of 92-442 bar considering 8% Ar in the feed as an internal standard) at 220-300 °C for stoichiometric CO₂ hydrogenation. The main aim is to identify reaction conditions to maximize CO₂ and H₂ conversions with high methanol selectivity and/or productivity. A commercial Cu/ZnO/Al₂O₃ catalyst, optimized for the conversion of syngas to methanol, was employed as catalyst due to its high activity in CO₂ hydrogenation to methanol [5]. Tendency and effects of kinetic and thermodynamic controls over the reaction performance are discussed along with the trends in theoretical thermodynamic equilibria to critically evaluate what is achievable with the optimized Cu/ZnO/Al₂O₃ catalyst are discussed. The possibility of mass transfer limitation of the catalysts due to dense feed composition at higher pressure was investigated by changing catalyst particle size and quantitatively evaluated by means of Thiele modulus, effectiveness factor, and Weisz-Prater criterion.

3.2 Experimental

The details of high-pressure fixed-bed reactor setup and the gas chromatography used to conduct the CO₂ hydrogenation reaction to methanol at wide pressure range is already explained in [Chapter 2](#). Specifically, in this work, tubular reactor made up of stainless steel was used with an outer diameter of 1/8" or 1/4" with the inner diameter of 0.07" or 0.12", respectively. A commercial methanol synthesis catalysts Cu/ZnO/Al₂O₃ was purchased from Alfa Aesar. The catalysts pellet of 5.4 mm * 3.6 mm size was crushed, sieved to a particle size of 100-300 μm, and charged to the reactor with approximate catalyst bed length of 100-20 mm depending on the amount of catalysts defined by the desired reaction conditions. Prior to the reaction, the catalyst was reduced in hydrogen stream (H₂:Ar=90:10) at 20 ml min⁻¹ for 2 h at 330 °C and atmospheric pressure. The CO₂:H₂ (1:3) reactant gas premixed composition

Chapter 3

was precisely dispensed through a syringe pump. For GHSV of 650 h^{-1} , the 1/4" reactor tube with 1.0 g of the catalyst was used, while for higher GHSV conditions ($2000\text{-}8000 \text{ h}^{-1}$ and $10000\text{-}100000 \text{ h}^{-1}$) the 1/8" reactor tube with 400 and 50 mg of the catalyst was used. The catalyst for methanol synthesis was tested at five different pressure conditions of 50, 100, 200, 360, 480 bar (actual total pressure of CO_2 and H_2 was 46, 92, 184, 331, and 442 bar, respectively). In this work, GHSV is defined by the volumetric flow rate of inlet stream at normal pressure divided by the reactor volume where the catalyst is packed (including the catalyst volume). A wide range of GHSV conditions ($650\text{-}100000 \text{ h}^{-1}$) were examined. GHSV is also shown in catalyst-mass-normalized unit, in which the value ranges $0.37\text{-}49.85 \text{ NL g}_{\text{cat}}^{-1} \text{ h}^{-1}$. For the GHSV calculations in both units, the total flow rate at normal pressure including Ar was used. The vaporized outlet stream was injected to GC every ca. 12 min for 3 h at each reaction condition of temperature, pressure and GHSV and averaged values was taken.

3.3 Thermodynamic calculations

Methanol synthesis is an exothermic reaction and proceeds with volume contraction thus as stated in [Chapter 1](#) high pressure and low temperature are favorable for high methanol yield. At these high pressure conditions, the product can condense to form a liquid phase in the reactor [6-10]. Prior to high pressure reactions, the equilibrium data have been calculated using commercial simulation tool Aspen HYSYS V8.6. The SRK EOS has been extensively used for calculations of phase and equilibria. The modified SRK-EOS binary interaction parameters for CO , CO_2 , H_2 , methanol and water were taken from the optimized values reported by Heeres and co-workers for methanol synthesis [11] ([Appendix A, Table A3.7](#)). The equilibrium CO_2 conversion and methanol selectivity at 46, 92, 184, 331, 442 bar and temperature range of 150 to $340 \text{ }^\circ\text{C}$ is shown in [Appendix A, Figure A3.1](#) and [A3.2](#) respectively.

High pressure advantages in stoichiometric hydrogenation of CO₂ to methanol

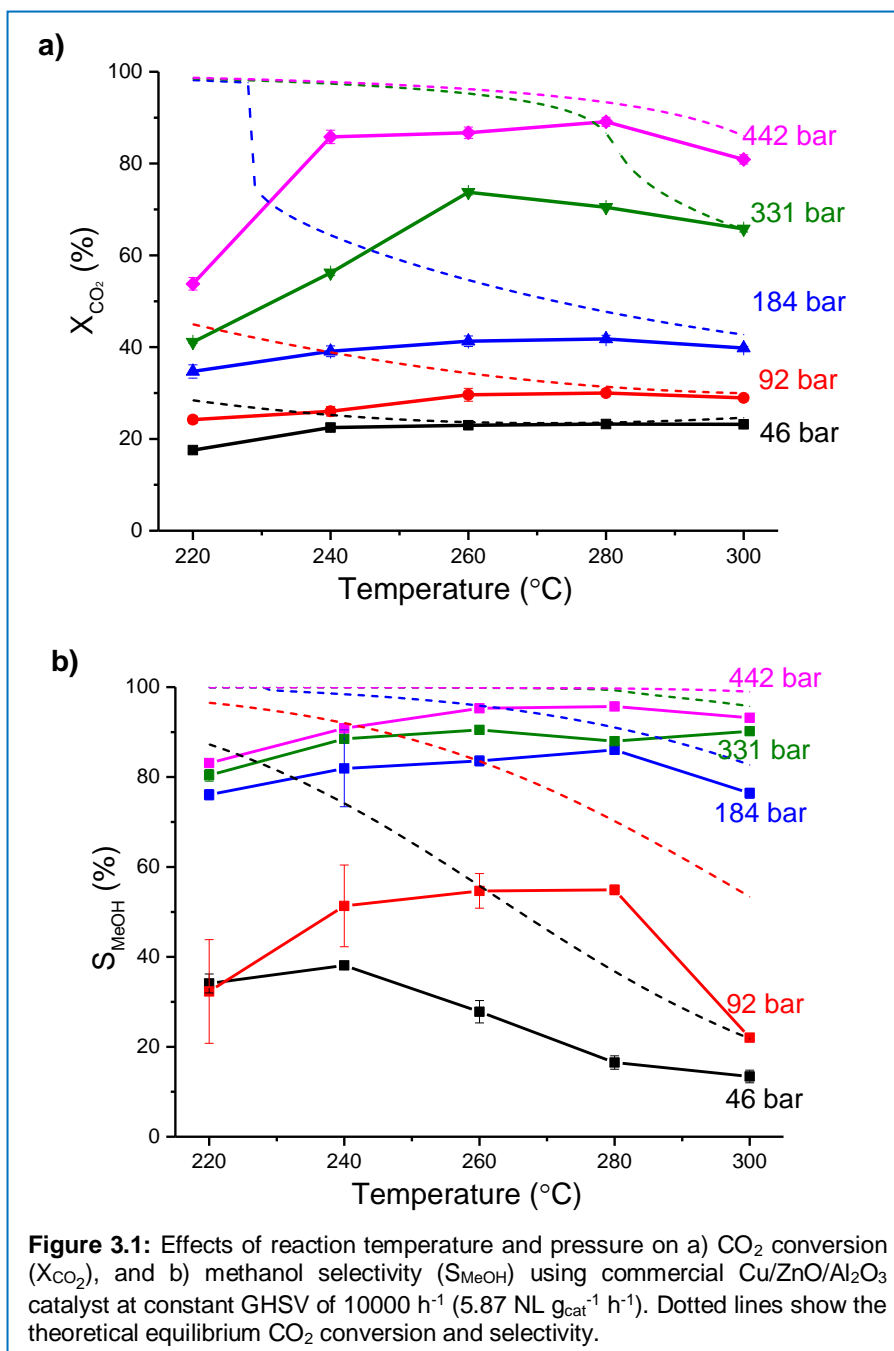
3.4 Results and discussion

3.4.1 Effect of temperature under high pressure conditions

The [Figure 3.1](#) shows effects of temperature on CO₂ conversion and methanol selectivity were examined at the reactants pressure of 92, 184, 331, and 442 bar. The catalytic tests were performed at a constant GHSV of 10000 h⁻¹, although, as discussed in [Section 3.4.2](#), this reaction parameter can directly influence the residence time of the reactants in the reactor and thus catalytic performance. CO₂ conversion and methanol selectivity are presented in comparison with the thermodynamic equilibrium values. Advantages of high-pressure conditions are obvious according to the thermodynamic calculations ([Figure 3.1](#), dotted lines). At 92 bar, CO₂ conversion varies from roughly 50% (220 °C) to 30% (300 °C) with very good to moderate methanol selectivity (96.5% at 220 °C and 53.4% at 300 °C), whereas at the highest examined pressure of 442 bar, theoretically CO₂ can be effectively converted to methanol (98.7% at 220 °C and 86.1% at 300 °C) with very high selectivity for the entire temperature range (>99.9% at 220 °C and 99.0% at 300 °C). At the intermediate pressures examined (184 and 331 bar), there was a sudden change in CO₂ equilibrium conversion at ca. 230 and 280 °C, respectively (this change also takes place at 92 bar but at a much lower temperature (ca. 160 °C), shown in [Appendix A Figure A3.1](#)). This is due to enhanced CO₂ conversion induced by the phase transition and separation (formation of liquid phase) associated with the condensation of the products when the reaction temperature is lower than the transition point. Such phase separation allows CO₂ conversion to methanol beyond one-phase equilibrium, as precisely described and demonstrated by Heeres and coworkers [8]. The positive impact of such phase separation on CO₂ conversion becomes less prominent at higher pressures as noticeable from the equilibrium CO₂ conversion curves of 184 and 331 bar. At 442 bar the impact becomes even unnoticeable. This tendency is attributed to the highly dense reactant/product mixture whose density only slightly differs from that of the liquid products and/or it indicates that they are simply miscible at the high pressure

Chapter 3

conditions. Experimentally, the general advantages of high-pressure conditions in CO₂ conversion, methanol selectivity, and thus methanol yield were confirmed with a better catalytic performance at higher pressures (Figure 3.1). Besides methanol, CO was found as the only major product arising from RWGS



High pressure advantages in stoichiometric hydrogenation of CO₂ to methanol

reaction. Another product observed was methane with a minor quantity (<0.8%). In comparison to the theoretical equilibrium, larger deviations were observed at lower temperatures for both CO₂ conversion and methanol selectivity. These two key indicators of reaction performance showed the maxima at 260-280 °C, except methanol selectivity at 331 bar, and then decreased at higher temperatures.

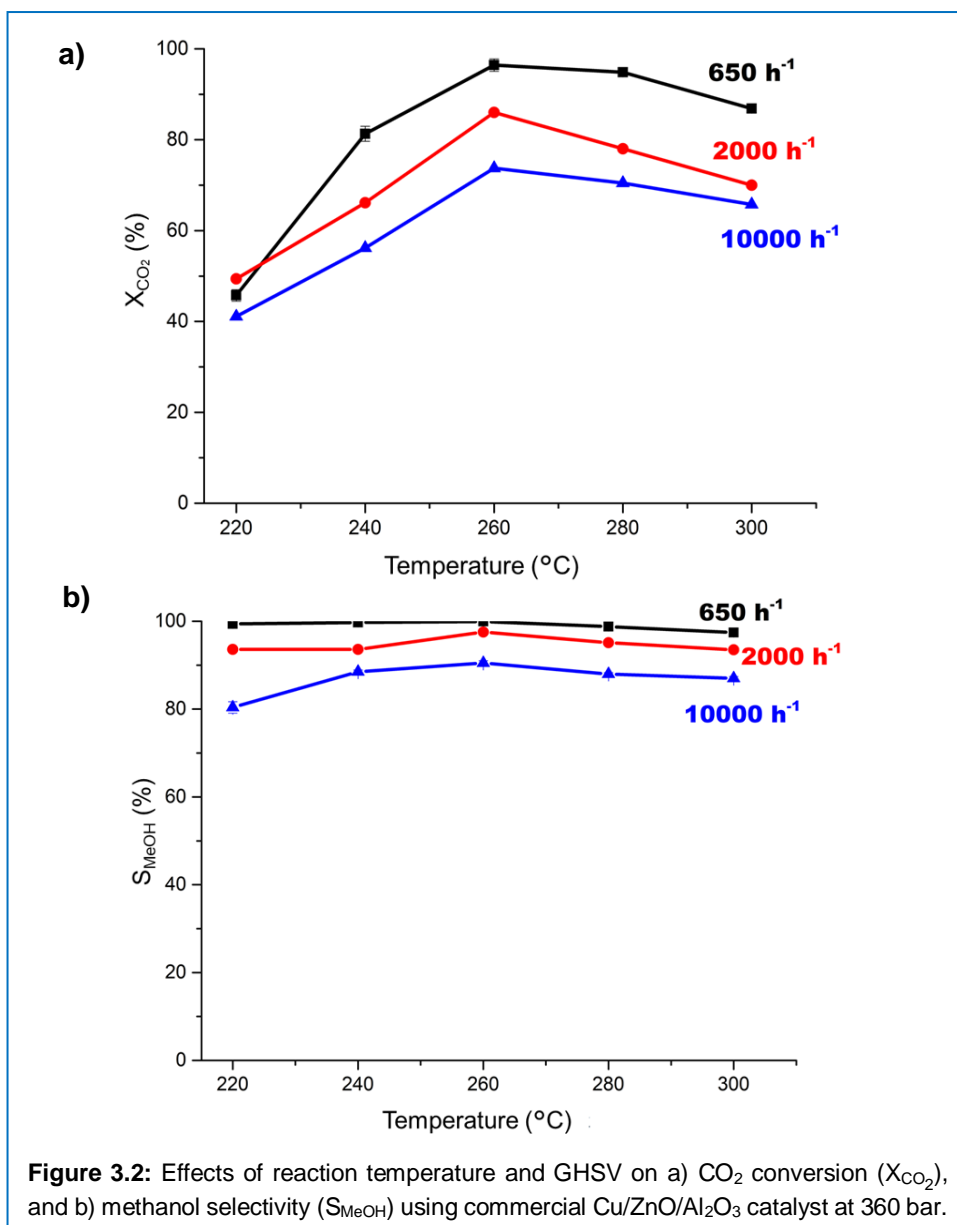
The performance deterioration above the optimum temperature of 260-280 °C is in accordance with the trend expected by the theoretical equilibrium. In the range of 220-300 °C, there were smaller deviations between experimental and theoretical CO₂ conversion and methanol selectivity above the optimum temperature, whereas larger deviations were found below the optimum temperature. This implies that thermodynamic equilibrium has been reached or, at least, has significant effects at the temperatures higher than the optimum temperature at each pressure condition. In other words, at the temperatures below the maxima in catalytic performance, the reaction is kinetically controlled due to poor reaction rates determined by the catalyst at the low temperatures. Theoretically, CO₂ conversion can be drastically boosted below 230 °C at 184 bar. However, such performance enhancement was not observed, and a very poor value was obtained at 220 °C. This is a clear indication that the reaction is kinetically controlled at the temperature. To fully benefit from the phase separation, the reaction has to be performed at lower GHSV to achieve high reaction rates at low temperatures. Also, it is important to remark that the advantageous phase separation is expected to take place theoretically at higher temperatures under higher pressure conditions. Therefore, high-pressure conditions can be greatly beneficial in this respect to achieve phase separation under kinetically favorable high-temperature conditions.

The best catalytic performance in terms of CO₂ conversion and methanol selectivity was obtained at 260 °C at 331 bar and at 280 °C at 92, 184, and 442 bar. Maximally performing reaction temperatures were examined at higher and lower GHSV conditions at 331 bar. Interestingly, it was found that the optimum

Chapter 3

temperature remained the same irrespective of different GHSV conditions shown in Figure 3.2.

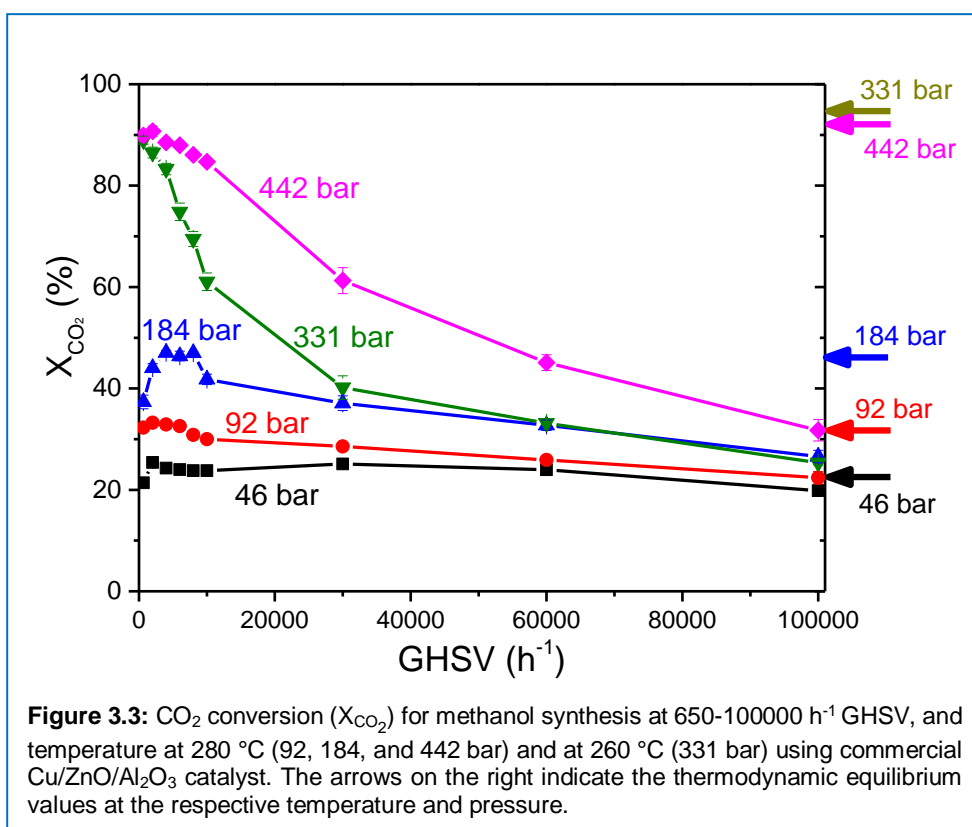
Therefore, we have taken the optimum temperatures at the respective pressures for the following study where the influence of GHSV on catalytic performance is investigated.



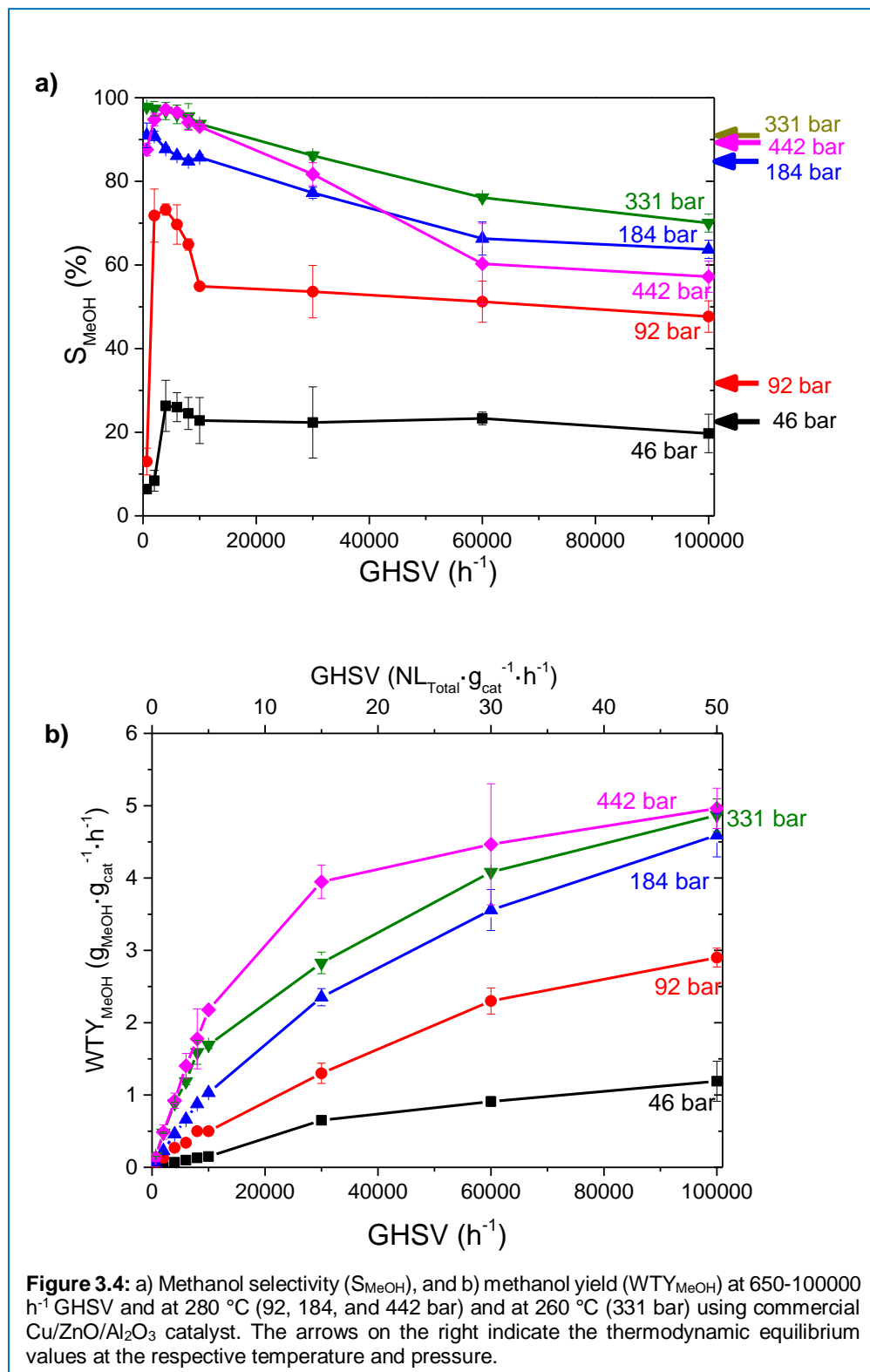
High pressure advantages in stoichiometric hydrogenation of CO₂ to methanol

3.4.2 Effects of GHSV under high pressure conditions

The reaction performance under the high-pressure conditions at the optimum temperature was further evaluated in a wide range of GHSV (650-100000 h⁻¹, equivalent to 0.37-49.85 NL g_{cat}⁻¹ h⁻¹) Figure 3.3 and 3.4a presents CO₂ conversion and methanol selectivity as a function of GHSV at 46, 92, 184, 331, and 442 bar, and Figure 3.4b shows corresponding methanol productivity in terms of weight time yield (WTY) expressed in the unit of g_{MeOH} g_{cat}⁻¹ h⁻¹. In the Figure 3.3 and 3.4a, equilibrium CO₂ conversion and methanol selectivity values are indicated by the arrows on the right side of the graph.



Chapter 3



High pressure advantages in stoichiometric hydrogenation of CO₂ to methanol

Clearly, the catalytic performance approaches the thermodynamic limit at the low range of GHSV (i.e. longer residence time). It is, however, not beneficial to over-reducing GHSV as the catalytic performance, especially methanol selectivity, becomes worse. This is mainly due to the formation of side products like methane and ethanol (Appendix 3A, Tables A3.1-3.5). Also, under the very low GHSV conditions, methanol yield is consequently very low. Thus, such reaction conditions are not practically relevant for large-scale industrial operations. The decreased CO₂ conversion towards the lowest examined GHSV at 184 bar may be due to the additional chemical equilibria involving methane and ethanol, but no clear understanding is available.

What is striking from the dependence of methanol WTY on GHSV (Figure 3.4b) is that there are reaction conditions giving high CO₂ conversion and methanol selectivity with methanol WTY close to 1.0 g_{MeOH} g_{cat}⁻¹ h⁻¹, which is generally considered as an excellent one. At 442 bar, the WTY reached the value of 0.92 g_{MeOH} g_{cat}⁻¹ h⁻¹ at 4000 h⁻¹ with 88.5% CO₂ conversion and 97.2% methanol selectivity (Appendix 3A, Table A3.1). 0.89 g_{MeOH} g_{cat}⁻¹ h⁻¹ was obtained at 331 bar also at 4000 h⁻¹ with 83.3% CO₂ conversion and 96.8% methanol selectivity (Appendix 3A, Table A3.2).

Similar methanol WTY can be attained at lower pressure, but this requires increasing GHSV due to lower CO₂ conversion and methanol selectivity. For example, at 184 bar 0.88 g_{MeOH} g_{cat}⁻¹ h⁻¹ was obtained at 8000 h⁻¹ with 47.0% CO₂ conversion and 84.8% methanol selectivity (Appendix 3A, Table A3.3). At 92 and 46 bar (Appendix A, Tables A3.4 and A3.5 respectively), high GHSVs (30000 or 100000 h⁻¹) was necessary to achieve >1.0 g_{MeOH} g_{cat}⁻¹ h⁻¹ with poor CO₂ conversion (28.6 or 20.2%, respectively) and moderate-poor methanol selectivity (53.6 or 19.7%, respectively).

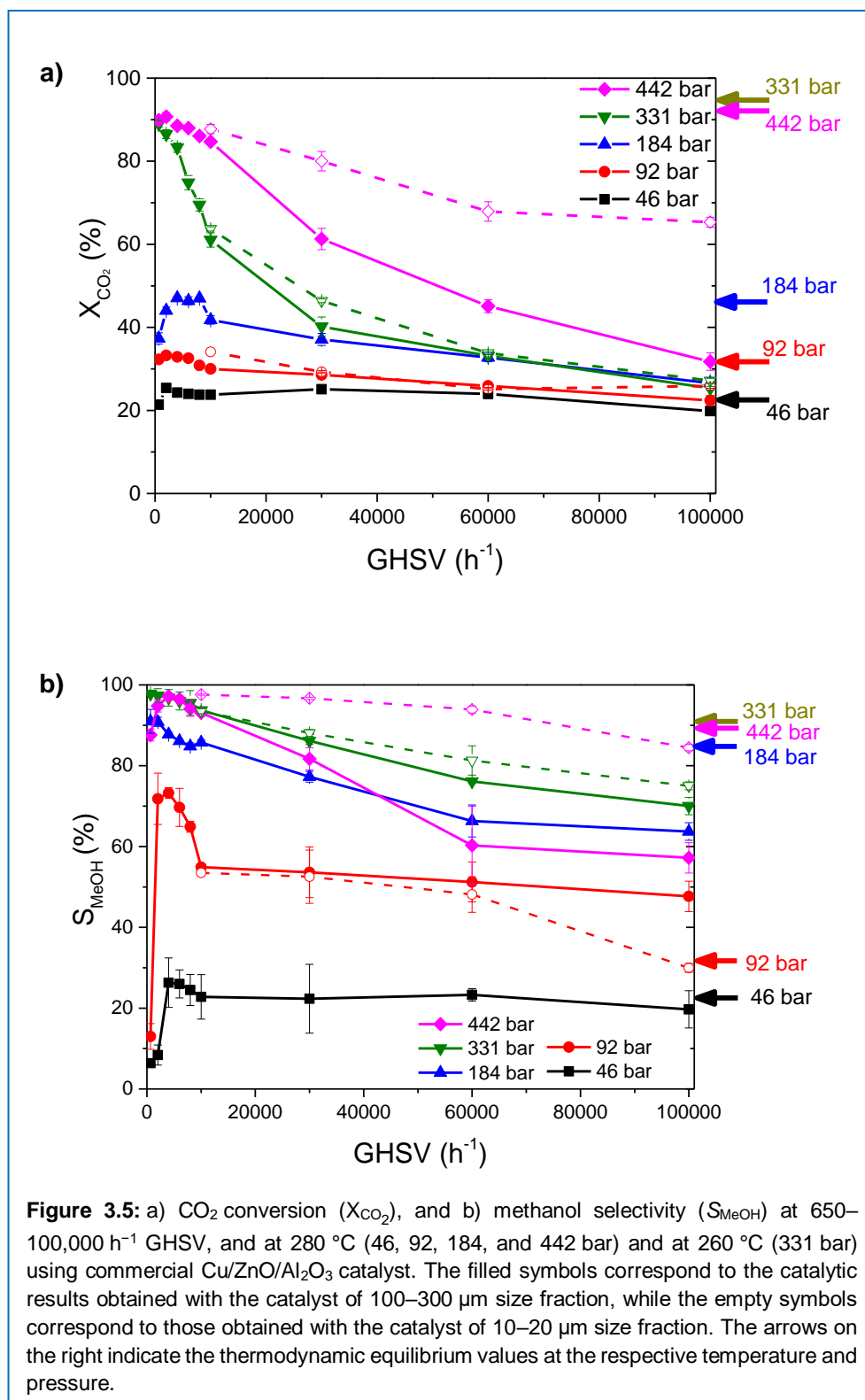
In practice, high CO₂ conversion and high methanol selectivity may not be the most critical performance indicator when unreacted CO₂, CO, and H₂ can be efficiently recycled. Although larger molar and thus volumetric flow (i.e. high GHSV) demands higher energetic requirement for the recycling process due to

Chapter 3

low CO₂ conversion, such conditions can greatly improve methanol WTY as discussed above. This was clearly demonstrated under the high GHSV conditions of this work (Figure 3.4b). At 100000 h⁻¹ even at the moderate pressure of 92 bar, a very high WTY of ca. 3 g_{MeOH} g_{cat}⁻¹ h⁻¹ was achieved and overall excellent WTYs above 4.5 g_{MeOH} g_{cat}⁻¹ h⁻¹ could be attained above 184 bar. Interestingly, the high-pressure benefit in CO₂ conversion was less pronounced at high GHSV, and the conversion values converged to roughly 20-30% at 100000 h⁻¹ for all examined pressure conditions. In contrast, high-pressure advantage in methanol selectivity remained (70.0% at 331 bar, 47.7% at 92 bar, 19.7% at 46 bar) although methanol selectivity decreased remarkably at higher GHSV at 442.

Furthermore, there were clear differences of the GHSV dependency of CO₂ conversion at the different pressures. The drop in CO₂ conversion was more prominent at higher pressure conditions (331 and 442 bar) upon increasing GHSV, whereas methanol selectivity was not affected by the GHSV variation as much except methanol selectivity at 442 bar. According to the thermodynamic calculation (Figure 3.1, dotted lines and Appendix A Figure A3.1 and 3.2), only under the two high-pressure conditions (331 and 442 bar) product condensation and phase separation (or formation of highly dense phase of the reactants and products at 442 bar due to the rather smooth and continuously changing CO₂ conversion profile with increasing temperature) are expected to occur at the reaction temperatures examined. The more significant drop in CO₂ conversion at higher GHSVs may be related to the phase behavior. For example, a more severe mass transfer limitation may be induced at higher GHSV conditions, resulting in /liquid hindered diffusion of the reactants and products through the catalyst body by the dense phase formation.

High pressure advantages in stoichiometric hydrogenation of CO₂ to methanol

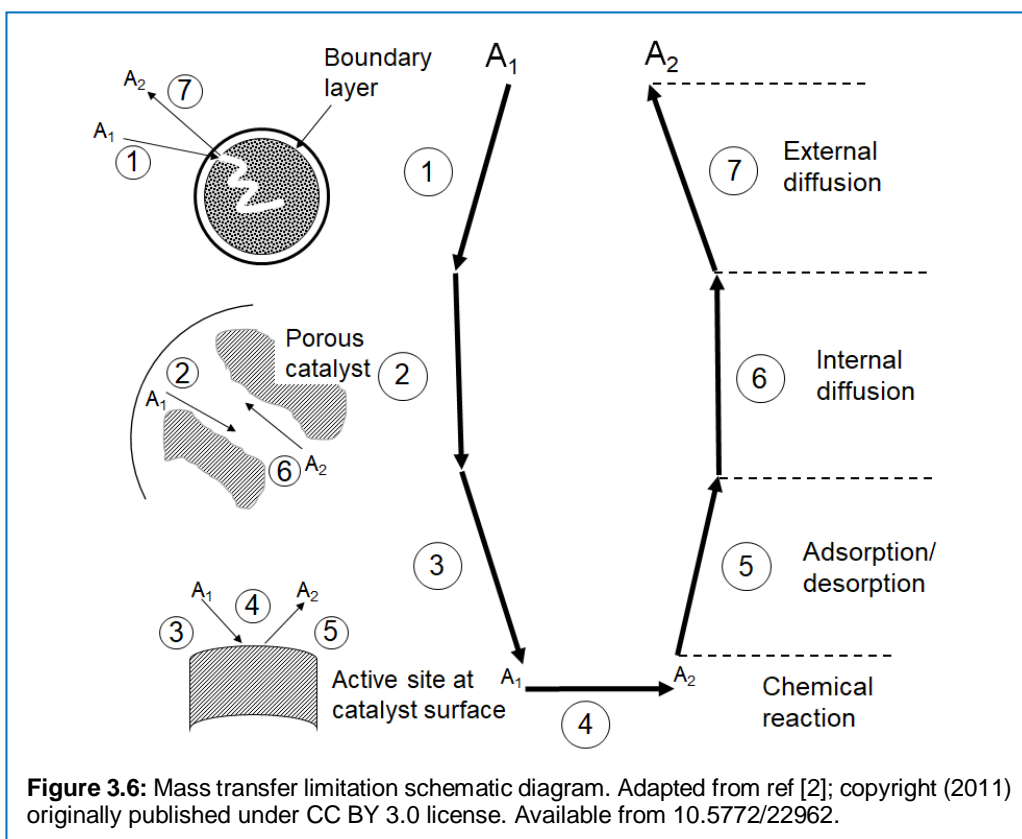


Chapter 3

At high pressure the formation of dense/liquid phase can significantly limit the reaction rate and productivity of the process. Due to high pressure the external mass transfer limitation or the transfer of reactant gas phase to catalyst surface hindrance is negligible (Figure 3.6). While internal mass transfer or intra particle dense phase gas transfer limitation within the catalyst pores, can reduce the reaction rate. Since overall reaction rate of methanol synthesis could strongly affect by the mass transfer limitations, hence their verification and minimization are utmost important for process optimization.

In order to verify if there is internal mass transfer limitation or not, we have performed the reaction using the catalyst with the particle size one order of magnitude smaller (10-20 μm) than those screened and reported above (100-300 μm) at representative pressure (92, 331, and 442 bar) and GHSV (10000-100000 h^{-1}) conditions. External mass transfer limitation was neglected because the drop in catalytic performance occurs at high GHSV conditions which are favorable for external mass transfer. Figure 3.5 and 3.7 present the effects of catalyst particle size on the catalytic performance and WTY obtained at different GHSVs with smaller catalyst particles (empty symbols and dotted lines) and by larger catalyst particles (filled symbols and solid lines). The reaction performance using the smaller catalyst particles was almost identical to that of the larger ones at 92 and 331 bar, but there was a remarkable enhancement of CO_2 conversion and methanol selectivity observed at 442 bar. Even at the highest examined GHSV (100000 h^{-1}) high CO_2 conversion (65.3%) and methanol selectivity (91.9%) were achieved, giving outstanding WTY of 15.2 $\text{g}_{\text{MeOH}} \text{g}_{\text{cat}}^{-1} \text{h}^{-1}$.

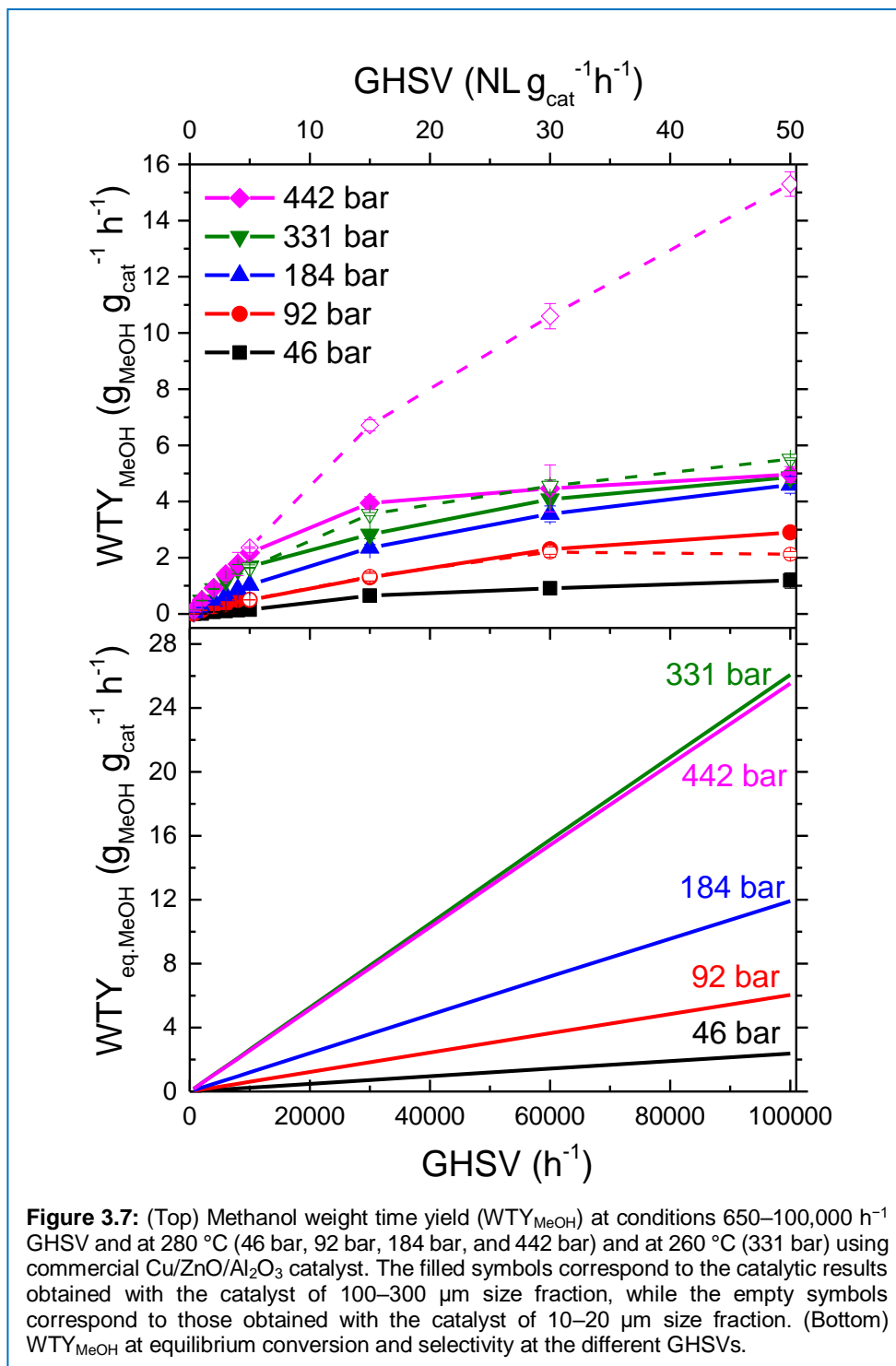
High pressure advantages in stoichiometric hydrogenation of CO₂ to methanol



At lower GHSV of 30000 h⁻¹, CO₂ conversion was 80.0% with 96.7% methanol selectivity, giving WTY of 6.7 g_{MeOH} g_{cat}⁻¹ h⁻¹. Compared to the theoretical WTY limit (7.7 g_{MeOH} g_{cat}⁻¹ h⁻¹) defined by the equilibrium conversion and selectivity, the value is very high. At 10000 h⁻¹, WTY of 2.4 g_{MeOH} g_{cat}⁻¹ h⁻¹ was almost the same as the theoretical value 2.6 g_{MeOH} g_{cat}⁻¹ h⁻¹.

These large effects of particle size on the catalytic performance clearly prove that there was a severe internal mass transfer limitation, especially at 442 bar as hinted by the great decrease in CO₂ conversion at higher GSHVs using the larger catalyst particles. The degree of internal mass transfer was quantitatively evaluated by means of Thiele modulus, effectiveness factor, and Weisz-Prater criterion (Tables 3.1, 3.2 and Figure 3.8).

Chapter 3



High pressure advantages in stoichiometric hydrogenation of CO₂ to methanol

3.4.3 Evaluation of internal mass transfer limitation

The results to evaluate the particle size effects on catalytic activity shown in Figure 3.5 and 3.7 were used to calculate Thiele modulus and the effectiveness factor at different GHSV and pressure conditions according to the method shown in the literature based on two experimental results obtained using two different particle sizes [12].

The relationship between Weisz-Prater criterion (C_{WP}), Thiele modulus (ϕ_1) and effectiveness factor (η), and their relation to the observed reaction rate r_A (A is CO₂ here) can be expressed by,

$$C_{WP} = \eta\phi_1^2 = \frac{r_A \rho R^2}{D_{eff} C_{surf}} = 3(\phi_1 \coth\phi_1 - 1) \quad (\text{Eq. 3.1})$$

where ρ is the catalyst density, R is the catalyst particle size, D_{eff} is the effective diffusion coefficient and C_{surf} the concentration of A at the outer surface of the catalyst. Now, if two catalytic runs (with the subscript 1 and 2) are performed using two different catalyst particle sizes, in which only the particle size of the catalyst is varied, the ratio of the two equations yields the following equation.

$$\frac{r_{A2} R_2^2}{r_{A1} R_1^2} = \frac{\phi_{12} \coth \phi_{12} - 1}{\phi_{11} \coth \phi_{11} - 1} \quad (\text{Eq. 3.2})$$

In this case, the terms C_{surf} , ρ , and D_{eff} cancel out because they can be assumed to be identical since all the reaction conditions are the same except particle size.

Also, let us assume that Thiele modulus can be expressed in the following form,

$$\phi_1 = R \sqrt{\frac{-r'_{AS} \rho}{D_{eff} C_{surf}}} \quad (\text{Eq. 3.3})$$

where r'_{AS} is the intrinsic rate of the surface reaction of A .

Thus, by taking the ratio of the Thiele moduli for the two experiments, we obtain the following relation.

Chapter 3

$$\phi_{11} = \frac{R_1}{R_2} \phi_{12} \quad (\text{Eq. 3.4})$$

Substituting Eq. 3.4 into Eq. 3.2 results in Eq. 3.5.

$$\frac{r_{A2} R_2^2}{r_{A1} R_1^2} = \frac{\phi_{12} \coth \phi_{12} - 1}{\frac{R_1}{R_2} \phi_{12} \coth \frac{R_1}{R_2} \phi_{12} - 1} \quad (\text{Eq. 3.5})$$

For R_1 and R_2 , representative values of 200 and 20 μm , respectively, were taken. By substituting these values in Eq. 3.5, we obtain

$$\frac{r_{A2} * 20^2}{r_{A1} * 200^2} = \frac{\phi_{12} \coth \phi_{12} - 1}{10 \phi_{12} \coth(10 \phi_{12} - 1)} \quad (\text{Eq. 3.6})$$

The Eq. 3.6 can be numerically solved to obtain the Thiele moduli ϕ_{11} and ϕ_{12} . The effectiveness factor η and C_{WP} can be conveniently calculated using Eq. 1.

Table 3.1: Effect of particle size effects at 442 bar at 280 °C. Run no.1 corresponds to the experiments with 200 μm catalyst (actual size 100-300 μm) and Run no. 2 corresponds to the experiments with 20 μm catalyst (actual size 10-20 μm).

GHSV (h ⁻¹)	Run no.	CO ₂ conversion (%)	Methanol Selectivity (%)	WTY of MeOH (g _{MeOH} g _{cat} ⁻¹ h ⁻¹)	Rate of reaction (mol _{MeOH} g _{cat} ⁻¹ s ⁻¹) *10 ⁵	Thiele modulus (ϕ)	Effectiveness factor (η)	C _{WP}
10000	1	84.7	93.1	2.9	1.89	1.15	0.92	1.22
	2	87.7	97.6	2.4	2.01	0.12	0.99	0.01
30000	1	61.3	81.7	3.9	3.42	3.78	0.58	8.37
	2	80.0	96.7	6.7	5.82	0.38	0.99	0.14
60000	1	45.1	60.3	4.5	3.88	6.01	0.41	15.3
	2	67.9	93.9	10.6	9.19	0.61	0.98	0.36
100000	1	31.8	57.2	5.0	4.3	9.05	0.3	24.17
	2	64.5	89.9	15.9	13.8	0.91	0.95	0.78

The Weisz-Prater criterion clearly shows the values much larger than 1 at higher GHSVs at 442 bar with the larger catalyst particles (Table 3.1). This indicates severe internal mass transfer limitation at 442 bar. The effectiveness factor was 0.3 at 100000 h⁻¹ at 442 bar, showing the poor utilization of catalyst surfaces within the particle.

The effectiveness of catalyst utilization improves at the lowest space velocity (10000 h⁻¹) of the study, and the value of 0.92 was obtained with the

High pressure advantages in stoichiometric hydrogenation of CO₂ to methanol

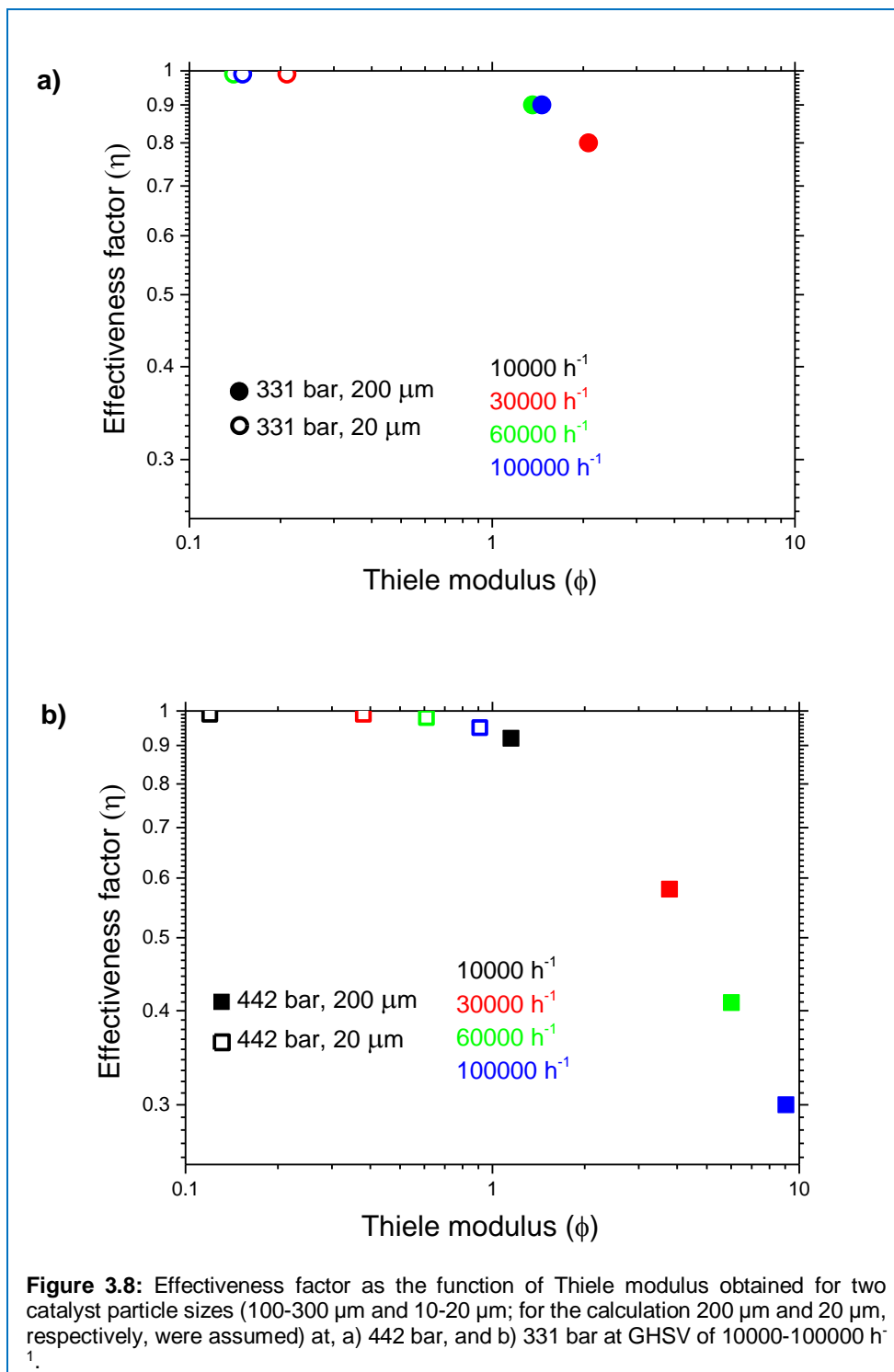
catalyst of the larger size. When the smaller size catalyst was used, much smaller values of the Weisz-Prater criterion and high value (above 0.95) of the effectiveness factor were obtained, evidencing the effective use of the whole catalyst body for the reaction when the size is reduced by one order of magnitude.

At 331 bar, the availability of the catalytic sites is improved as shown by lower values of the Weisz-Prater criterion and by the high values of effectiveness factor (Table 3.2). These results strongly suggest that condensation of reactants/products takes place within the catalyst body at the very high-pressure conditions examined, inducing the mass transfer limitation. As demonstrated by the extraordinary WTY above 15 g_{MeOH} g_{cat}⁻¹ h⁻¹, this product condensation can be extremely beneficial when mass transfer limitation is can be overcome and/or absent.

Table 3.2: Effect of particle size effects at 331 bar at 260 °C. Run no. 1 corresponds to the experiments with 200 µm catalyst (actual size 100-300 µm) and Run no. 2 corresponds to the experiments with 20 µm catalyst (actual size 10-20 µm).

GHSV (h ⁻¹)	Run no.	CO ₂ conversion (%)	Methanol Selectivity (%)	WTY of MeOH (g _{MeOH} g _{cat} ⁻¹ h ⁻¹)	Rate of reaction (mol _{MeOH} g _{cat} ⁻¹ s ⁻¹) *10 ⁵	Thiele modulus (φ)	Effectiveness factor (η)	C _{WP}
10000	1	61.0	93.7	1.7	1.47	-	-	-
	2	63.7	93.5	1.6	1.42	-	-	-
30000	1	40.2	86.2	2.8	2.45	2.08	0.80	3.43
	2	46.4	88.1	3.6	3.08	0.21	0.99	0.04
60000	1	33.2	76.1	4.1	3.54	1.36	0.90	1.65
	2	33.8	81.3	4.6	3.94	0.13	0.99	0.02
100000	1	25.3	70.0	4.9	4.22	1.46	0.88	1.88
	2	27.2	75.0	5.5	4.78	0.15	0.99	0.02

Chapter 3



High pressure advantages in stoichiometric hydrogenation of CO₂ to methanol

The reaction mechanisms of methanol synthesis via CO₂ hydrogenation, namely via CO₂ or CO, are widely debated [13], although a recent study as represented by Studt and coworkers concluded that the major carbon source of methanol is CO₂, promoted by the synergetic functions of Cu and ZnO [14]. In this study, CO selectivity increased consistently at higher GHSV (Figure 3.5b and Appendix 3A, Tables A3.1-3.5). A detailed mechanistic discussion is out of the scope of this work, but the results indicate that longer residence time enhances methanol selectivity, and that methanol synthesis proceeds via CO produced by RWGS. The same conclusion had been drawn in over-stoichiometric CO₂ hydrogenation where excess hydrogen was used (CO₂:H₂=1:10) [5]. Still, there is one point which has not been discussed widely, which is the exothermicity of methanol synthesis which can create local hot spots and temperature gradients along the axial and radial directions of the catalyst bed. The reactor we have used has a high surface to volume ratio as a kind of microreactor, and in principle, the geometry is well suited for heat management. However, the generated heat may not be sufficiently removed when WTY of methanol is very high, and thus a large heat is generated within the reactor and large temperature increase may be created close to the inlet of the reactor. The enhanced reaction under such conditions would be endothermic RWGS, thus CO formation could be pronounced in such cases. The trend is indeed what we observed; the higher the GHSV, i.e. higher the WTY consequently in most cases, the higher the CO selectivity. These aspects will be investigated further, but this may be a possible explanation of apparent reaction path of methanol synthesis via CO produced by RWGS under high-pressure conditions because of the existence of local hot spots, besides the scenario that CO₂ hydrogenation indeed proceeds via CO at high-pressures.

3.5 Conclusions

Relationship among reaction temperature, pressure, and GHSV in stoichiometric CO₂ hydrogenation to methanol over a well-established commercial Cu/ZnO/Al₂O₃ catalyst were systematically investigated in the aim

Chapter 3

to understand the advantages given by high-pressure reaction conditions (46-442 bar) and to achieve as high CO₂ conversion and methanol selectivity with high methanol productivity towards full conversion to methanol. A strong interplay between kinetics and thermodynamics in the reaction performance was evidenced. At kinetically favorable high temperature (>260 °C) especially at lower GHSV, it was possible to enter the regime where thermodynamic equilibrium plays dominant roles in determining the catalytic activity. In this regime, high-pressure advantages can be conveniently predicted based on the equilibrium conversion and selectivity. A good WTY of 0.92 g_{MeOH} g_{cat}⁻¹ h⁻¹ could be achieved at 442 bar with 88.5% CO₂ conversion and 97.2% methanol selectivity using our standard, larger size of catalyst particles (100-300 μm). At high pressure conditions above 331 bar, the dense phase formation by product condensation limits the overall reaction rate by internal mass transfer. When smaller catalyst particles (10-20 μm) are used instead, the limitation can be effectively removed. Thus-obtained catalytic performance fully benefits from the high-pressure advantages of high reaction rate (kinetics), high equilibrium conversion (thermodynamics) and enhanced conversion (phase separation). Under these conditions of negligible mass transfer limitations, at 442 bar a very good WTY of 2.4 g_{MeOH} g_{cat}⁻¹ h⁻¹ could be observed with 87.7% CO₂ conversion and 97.6% methanol selectivity. At a very high GHSV (100000 h⁻¹), an extraordinary WTY of 15.2 g_{MeOH} g_{cat}⁻¹ h⁻¹ could be achieved.

This work clearly shows favorable reaction conditions towards full one-pass conversion in stoichiometric CO₂ hydrogenation to methanol. Development of highly active, new generation catalysts is mandatory to reach this goal by entering to the thermodynamically controlled regime at lower temperature. Another practically important operation condition identified was high GHSV. Even at lowered pressure of 184 bar, a remarkable WTY of 4.5 g_{MeOH} g_{cat}⁻¹ h⁻¹ could be obtained. Hence, high GHSV conditions at relatively high-pressure were found also beneficial in practice for high-yield methanol synthesis when unreacted CO₂, H₂ and formed CO are recycled. In summary, this work has

High pressure advantages in stoichiometric hydrogenation of CO₂ to methanol

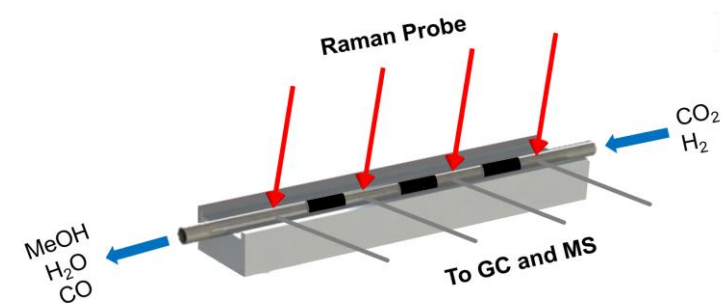
demonstrated that both kinetic and thermodynamic factors play decisive roles in methanol synthesis and also that thermodynamically favorable high-pressure conditions allow reaching the reactivity in the thermodynamically controlled regime and/or with outstanding methanol productivity.

Chapter 3

Bibliography

- [1] BASF, German Patents 415 686, 441 433, 462 837, 1923.
- [2] R. Klaewkla, M. Arend, W.F. Hoelderich, A Review of Mass Transfer Controlling the Reaction Rate in Heterogeneous Catalytic Systems, Mass Transfer - Advanced Aspects, in: D.H. Nakajima (Ed.) Mass Transfer-Advanced Aspects, Intech, 2011.
- [3] J.B. Hansen, P.E. Hojlund Nielsen, Methanol Synthesis: Handbook of Heterogeneous Catalysis, Wiley-VCH Verlag GmbH & Co. KGaA, (2008).
- [4] V.N. Ipatieff, G.S. Monroe J. Am. Chem. Soc., 67 (1945), pp. 2168-2171.
- [5] A. Bansode, A. Urakawa J. Catal., 309 (2014), pp. 66-70.
- [6] E.L. Sorensen, J. Perregaard, Condensing methanol synthesis and ATR- the technology choice for large-scale methanol production, in: X. Bao, Y. Xu (Eds.) Studies in Surface Science and Catalysis, Elsevier, 2004, pp. 7-12.
- [7] T. Chang, R.W. Rousseau, P.K. Kilpatrick, Ind. Eng. Chem. Process Des. Dev., 25 (1986), pp. 477-481.
- [8] J.G. van Bennekom, R.H. Venderbosch, J.G.M. Winkelman, E. Wilbers, D. Assink, K.P.J. Lemmens, H.J. Heeres, Chem. Eng. Sci., 87 (2013), pp. 204-208.
- [9] M. Castier, P. Rasmussen, A. Fredenslund, Chem. Eng. Sci., 44 (1989) 237-248.
- [10] J.B. Hansen, F. Joensen, High Conversion of Synthesis Gas into Oxygenates: A. Holmen, K.J. Jens, S. Kolboe (Eds.) Studies in Surface Science and Catalysis, Elsevier, 1991, pp. 457-467.
- [11] J.G.v. Bennekom, J.G.M. Winkelman, R.H. Venderbosch, S.D.G.B. Nieland, H.J. Heeres, Ind. Eng. Chem. Res., 51 (2012) pp. 12233-12243.
- [12] H.S. Fogler, Elements of Chemical Reaction Engineering, Prentice Hall PTR, 2006.
- [13] E.L. Kunkes, F. Studt, F. Abild-Pedersen, R. Schlögl, M. Behrens, J. Catal., 328 (2015), pp. 43-48.
- [14] F. Studt, M. Behrens, E.L. Kunkes, N. Thomas, S. Zander, A. Tarasov, J. Schumann, E. Frei, J.B. Varley, F. Abild-Pedersen, J.K. Nørskov, R. Schlögl, ChemCatChem, 7 (2015), pp. 1105-1111.

4. Space-resolved gas analysis of high-pressure CO₂ hydrogenation to methanol



Chapter 4

4.1 Introduction

In CO₂ hydrogenation to methanol, one of the most lively debates concerns the path to methanol, namely via direct hydrogenation of CO₂ or via CO first formed by RWGS [1-4]. This information can be in principle obtained by detailed studies of the reaction at different space velocities. However, for this reaction it is particularly challenging to gain conclusive insights because the final catalytic results are largely influenced by not only the reaction kinetics but also the thermodynamics accompanying phase condensation (Chapters 3 and 5). In this respect, it is highly valuable to directly obtain information about the gas concentration gradients along the catalyst bed under realistic conditions to understand the active reaction paths. Such gas phase profiling along the axial direction of the catalyst bed is of general challenge in heterogeneous catalysis and the challenge is even greater for reactions operated at high pressure and temperature as targeted in this thesis.

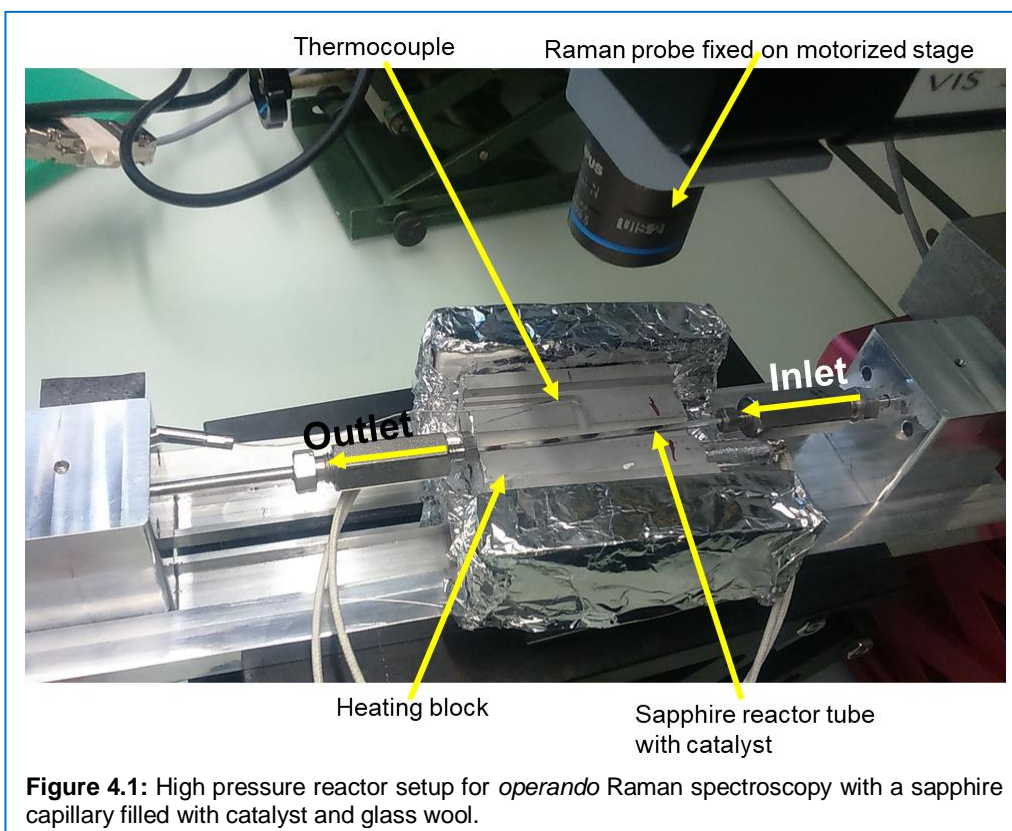
In this work, spatially resolved gas sampling/analysis techniques, using GC/MS and Raman spectroscopy, were developed and employed to gain information about the gradient of gaseous chemical species to gain insights into the reaction pathways of high-pressure methanol synthesis by stoichiometric CO₂ hydrogenation. The developed analytical techniques were used to understand the effects of reaction temperature and pressure on the reaction pathways using the commercial Cu/ZnO/Al₂O₃ catalyst. The results are discussed in the light of thermodynamic equilibrium conversion and selectivity.

Space-resolved gas analysis of high-pressure CO₂ hydrogenation to methanol

4.2 Experimental

4.2.1 High pressure reactor for *operando* Raman spectroscopy

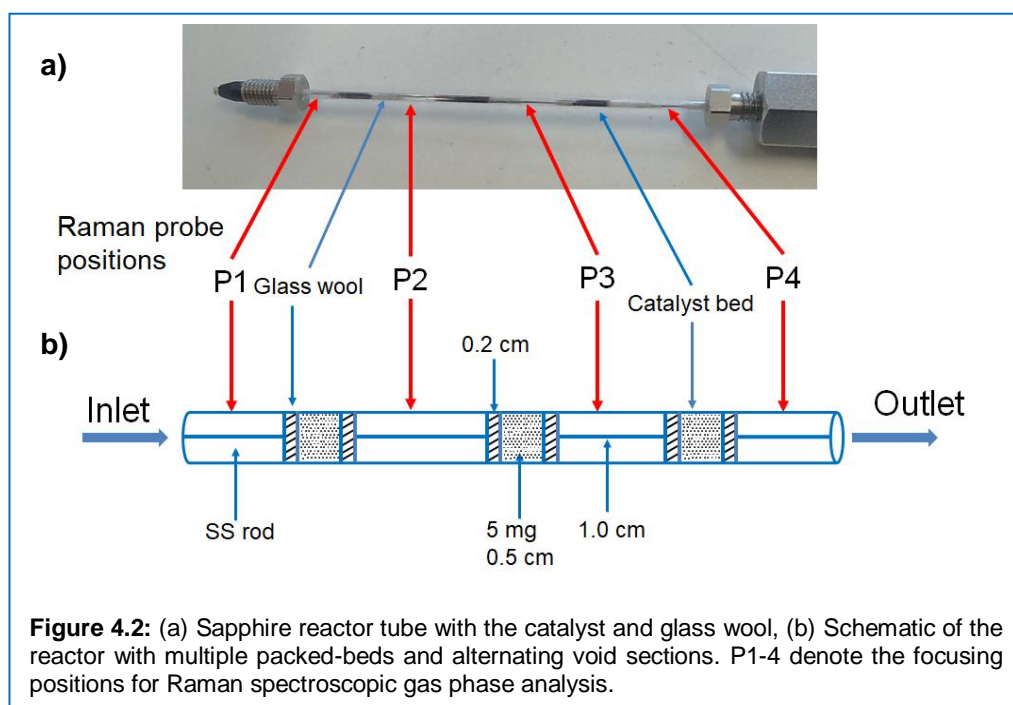
The detailed high-pressure reactor setup is explained elsewhere [5]. Briefly, Teledyne ISCO syringe pump was used to dispense high-pressure CO₂, while H₂ was pressurized using a gas booster and its flow rate was controlled by a high-pressure MFC. The two gases were mixed and passed to the reactor as shown in [Figure 4.1](#). Reaction pressure was controlled by back pressure regulator placed after the outlet of the reactor. Two pressure indicators placed before and after the reactor were used to measure pressure drop over the catalyst bed, which was negligible (<2 bar) in all cases.



To hold the very high pressure, the reactor tube (OD = 1.5 mm, ID = 1 mm, L = 100 mm) made of sapphire was used and it was filled with the Cu/ZnO/Al₂O₃ commercial methanol synthesis catalyst ([Chapter 3](#)). Leak-tight

Chapter 4

sealing between the sapphire tube with the stainless steel fittings were achieved by coating the ends of the tube with a thin layer of polyimide and using graphite reinforced polyimide ferrule so that the adhesion to the sapphire surface was enhanced. The catalyst pellets were crushed and sieved to 63-80 μm particle size. 15 mg of catalyst was loaded in the sapphire tube arranged in three separate packed beds (each ca. 5 mg and 5 mm) segregated by void sections (10-12 mm) as depicted in Figure 4.2. The alternating sections of void and catalyst were segregated by means of dense plugs made of quartz wool. To prevent the quartz wool plugs from sliding and combining under pressure, a stainless steel rod (0.6 mm OD) was inserted in each void section to support the plugs at its extremities.



The composition of the reactor outlet stream was analyzed online by GC, while the four void sections enabled the analysis of the intermediate/product stream at discrete positions by Raman microscopy (Renishaw, InVia, $\lambda=532$ nm, details in [6]). Mounted on a motorized linear actuator, a fiber-coupled Raman probe was positioned along the axial reactor axis to focus on one of

Space-resolved gas analysis of high-pressure CO₂ hydrogenation to methanol

the positions marked as P1-4 in [Figure 4.2](#). Position 1 (P1) allowed the gas analysis of the unreacted feed, while the Raman study at P2, P3 and P4 (outlet) yielded the gas composition at the respective positions. In addition, a white-light camera implemented in the remote probe enabled the observation of phases present in each void partition.

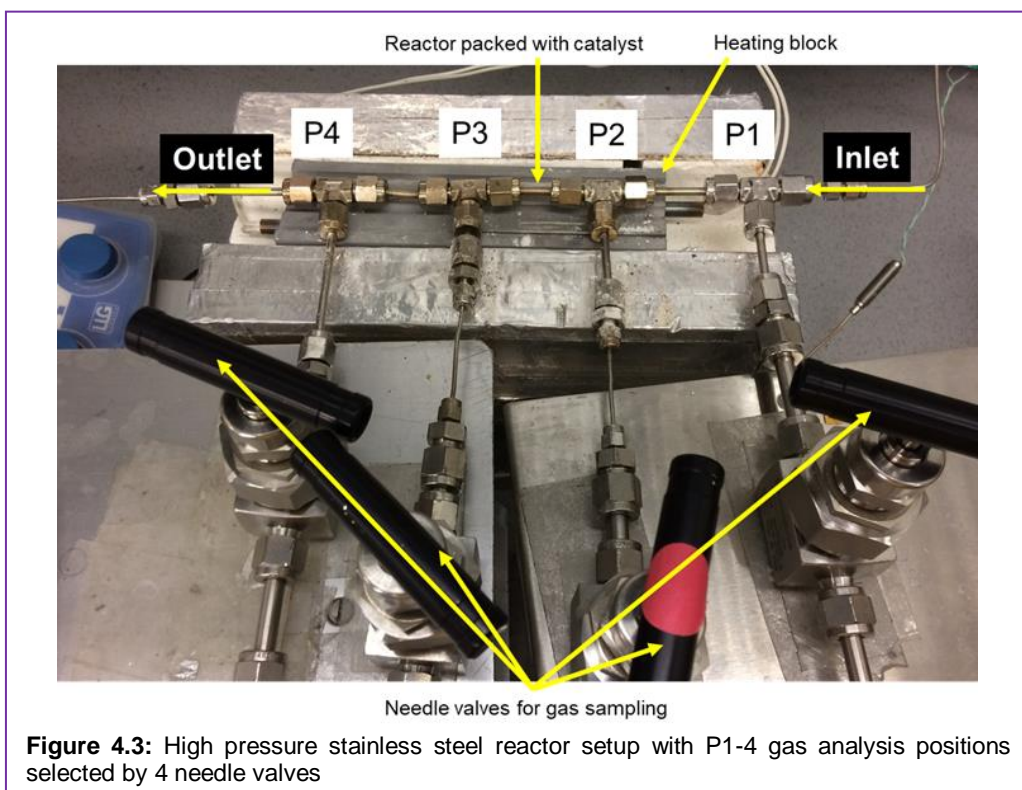
The catalyst was reduced at 330 °C for 30 min in a flow of 90% H₂ in He prior to each reaction. The reactor was subsequently cooled down to room temperature and pressurized to reaction pressure by feed gas. Reactions were carried out at 184 bar and at 180 and 260 °C. The total flow rate of 16 NmL/min corresponded to GHSV of 80,000 h⁻¹. A feed composition of H₂:CO₂ = 2.5:1 was used in order to increase the density of the reacting stream and improve the quality of the Raman spectra. Indeed, the higher density improved the signal-to-baseline ratio in comparison to a stoichiometric feed ratio of 3:1. Complicated light-matter interaction arose from intense refraction and reflection caused by the circular cross-section of the cylindrical sapphire tube, decreasing the signal intensity collected by the remote probe in backscattering mode. However, the light-collection efficiency loss, caused by light transmittance through the transparent reactor, was lessened by the higher stream density.

4.2.2 Space-resolved gas analysis using SS reactor

The space-resolved gas analysis was performed using the high-pressure reaction system explained in [Chapter 2](#). The commercial Cu/ZnO/Al₂O₃ catalyst was packed in a 1/8" SS tube reactor. The catalyst was packed in a similar way as explained earlier for sapphire tube. 180 mg of 100-300 μm particle size catalyst was packed in three separate catalyst beds (60 mg each). The catalyst was supported on 10 μm frit to avoid catalyst sliding under high-pressure gas flow. The equidistant void was maintained between the catalyst beds for gas sampling analysis. Continuous gas sampling from the high-pressure reactor was achieved by means of needle valve connected to the reactor. The sampling gas flow rate was adjusted by the needle valve to be

Chapter 4

ca. 2 mL min^{-1} . The composition of feed and products was analyzed online by GC and MS. The four void sections connected to the needle valve enabled analysis of the reactant and product mixture before/between the catalyst packed beds. The gas analysis was performed in such a way that overall pressure and flow pattern change within the reactor by the gas sampling does not affect the catalytic performance significantly. Figure 4.3 shows the image of the SS reactor system with gas sampling needle valve.



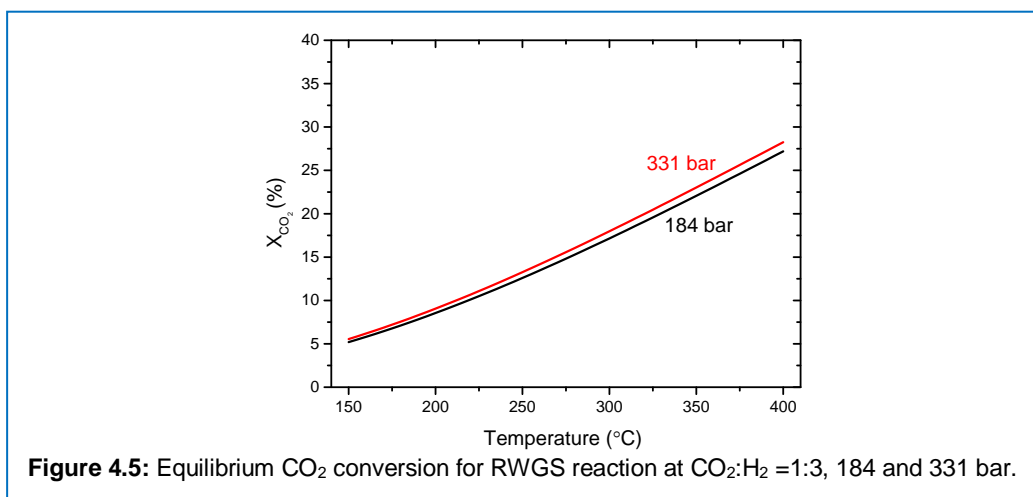
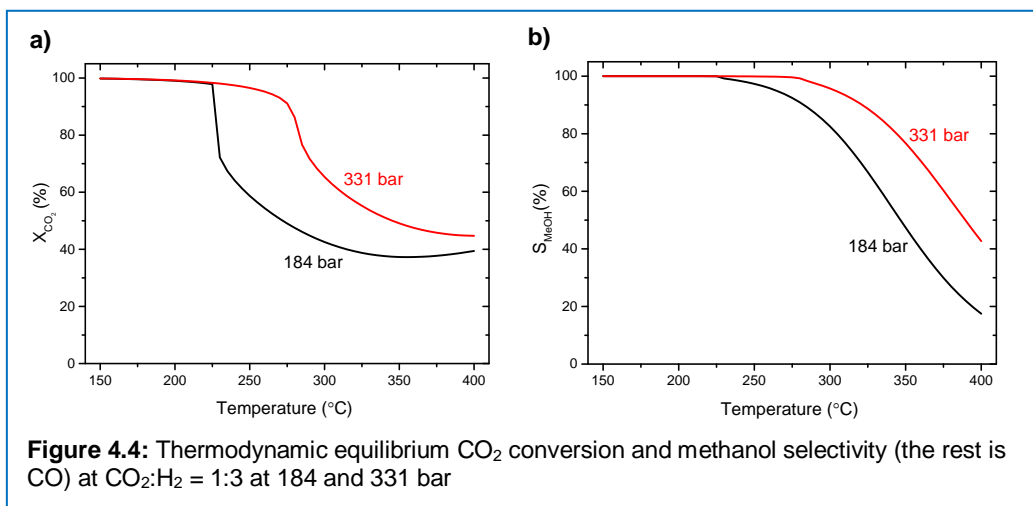
The catalyst was packed in the reactor with three beds (B1, B2 and B3), and gas samples were analyzed at 4 different places, viz. P1, P2, P3 and P4. The P1 position is before the catalyst bed 1 (B1), thus the gas composition is the same as feed gas composition. The following positions P2, P3 and P4 represent the gas composition after passing over catalyst bed B1, B2 and B3 respectively.

Space-resolved gas analysis of high-pressure CO₂ hydrogenation to methanol

4.3 Results and discussion

4.3.1 Equilibrium conversion and selectivity

To facilitate interpretation and discussion of the results, thermodynamic equilibrium CO₂ conversion and product selectivity of stoichiometric methanol synthesis from CO₂ and H₂ (Chapter 1 - Eq. 1.2, Figure 4.4) and also RWGS (Chapter 1 – Eq. 1.3 but at CO₂:H₂=1:3, Figure 4.5) were calculated for two pressure conditions (184 and 331 bar) in the temperature range of 150-400 °C using Aspen HYSYS following the same procedure as explained in Chapter 3. The thermodynamic behavior of the former reaction has been discussed in Chapter 3. It is interesting to confirm that the latter equilibrium is almost



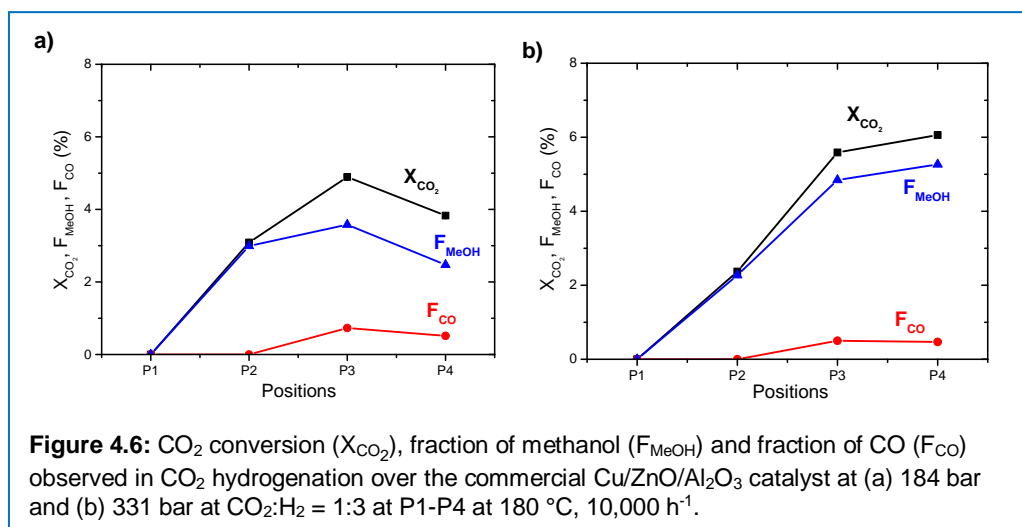
Chapter 4

pressure-independent while it is highly temperature-dependent as expected by Le Châtelier's principle (Chapter 1).

4.3.2 Space-resolved gas analysis by GC

The reaction products formed in the gas phase over the Cu/ZnO/Al₂O₃ commercial methanol synthesis catalyst were first investigated by GC sampling at different positions of the reactor (Figure 4.3). CO₂ conversion and carbon-based mole fractions, which are defined as CO₂ conversion scaled by respective product selectivity (i.e. $F_{\text{MeOH}} + F_{\text{CO}} = X_{\text{CO}_2}$), were used to understand in a facile fashion how much CO₂ is converted and to which product.

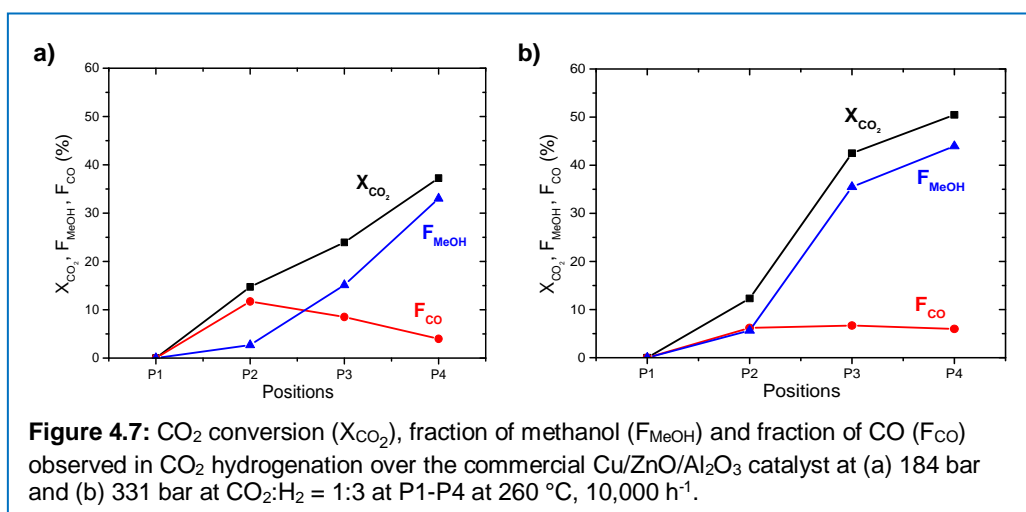
Figure 4.6a shows the catalytic performance at 180 °C at 184 bar, while that at 331 bar is shown in Figure 4.6b. Generally, at this low reaction temperature we observe low CO₂ conversion but high methanol selectivity, thus high fraction of methanol. What is striking is the profile of CO₂ conversion and also consequent product fractions. At this low conversion, virtually the partial pressure of the reactants (CO₂ and H₂) is unaltered throughout the catalyst bed and generally one expects little change in the reaction rate and product selectivity at different positions of the catalyst bed. However, Figure 4.6 shows that this is not the case and the deviation is more prominent at the lower pressure investigated (184 bar, Figure 4.6a) where CO₂ conversion



Space-resolved gas analysis of high-pressure CO₂ hydrogenation to methanol

does not linearly increase and it even drops between P3-P4. Also, when the rate of CO₂ conversion is decreased, fraction of CO increases. Assuming that the intrinsic reaction selectivity at this temperature is almost 100% towards methanol (judging from the values at P2) and that CO₂ conversion rate does not change along the catalyst bed, only explanation for these CO₂ conversion drop and CO formation is methanol decomposition, forming CO as well as CO₂. Base on the profiles of CO₂ conversion and product fractions at 331 bar (Figure 4.6b), this methanol decomposition to CO/CO₂ also takes place but significantly lesser extent. This is likely due to the pressure effects affecting to shift the equilibrium towards the product (methanol) side, showing a unique advantage of high-pressure reaction conditions [7].

The same experiment was performed at two higher temperatures (260 and 340 °C) and the results obtained at 260 °C are summarized in Figure 4.7. First, the CO₂ conversion values are about one order of magnitude higher than those of 180 °C. Also, at both examined pressures, relatively high CO selectivity was observed. At 184 bar (Figure 4.7a), CO was the major product, but then the fraction of CO decreased towards the outlet position. This is indicative of CO conversion to methanol, although there is a possibility of water-gas shift reaction forming CO₂ and H₂ from CO and H₂O. However, methanol fraction drastically increased as CO fraction dropped towards the

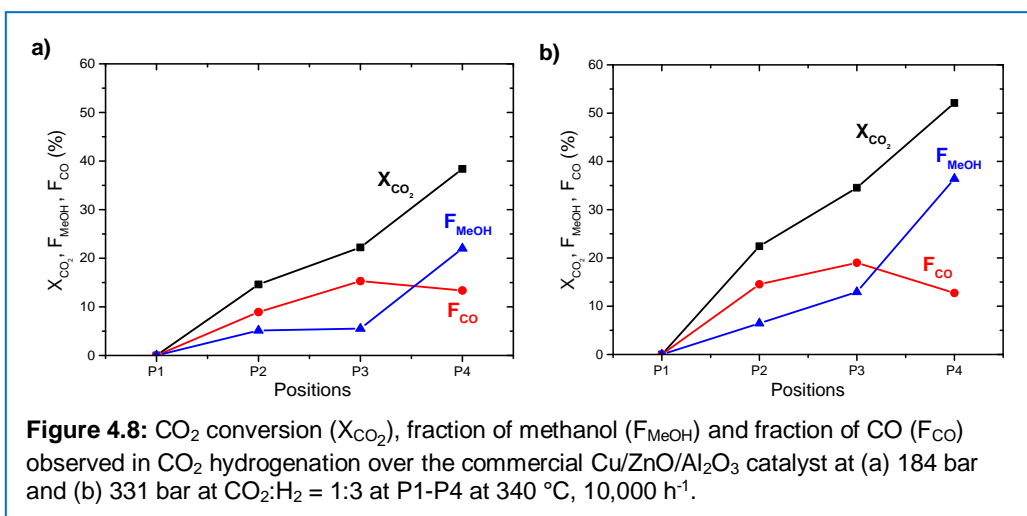


Chapter 4

outlet direction, and thus the former reaction (i.e. CO hydrogenation to methanol, Eq. 1.4) is likely the active path under the reaction condition, although there may be some portion of methanol produced from the direct conversion of CO₂ (Eq. 1.2). At 331 bar (Figure. 4.7b) CO fraction remained relatively constant, whereas methanol fraction increased drastically along with CO₂ conversion between P2 and P3. At 184 bar (Figure. 4.7a) CO₂ conversion linearly increased and did not drop as observed at 180 °C. These results indicate three important insights: (i) methanol formation is faster than decomposition, (ii) CO₂ is constantly converted to methanol or CO as the intermediate at 184 bar and (iii) there is another factor boosting CO₂ conversion at 331 bar. Regarding the point (ii), at 184 bar at P2, very high CO selectivity was observed and its continuous decrease and drastic increase in methanol production implies that CO₂ is converted to CO at almost constant rate and then CO is further converted to methanol. In this case, the latter reaction rate would mainly determine the fraction of methanol and CO in the reactor. The point (iii) indicates interesting and important effects of reaction pressure. According to Figure 4.4a, at 260 °C, we expect phase condensation at 331 bar but not at 184 bar. This can explain the sudden boost in CO₂ conversion between P2-P3; the CO₂ conversion was sufficiently high to reach the dew point of the condensable products (methanol and water) at this position in the reactor, positively impacting on the reaction rate or shifting the equilibrium towards methanol.

Furthermore, the results obtained at the highest examined temperature (340 °C) are presented in Figure 4.8. As in the case of 260 °C, a large amount of CO was observed with decrease in its fraction with respect to methanol towards the reactor outlet. On the other hand, CO₂ conversion increased almost linearly. These two observations indicate that RWGS is the first step of CO₂ hydrogenation at an almost constant reaction rate and thus-produced CO reacts with H₂ to produce methanol.

Space-resolved gas analysis of high-pressure CO₂ hydrogenation to methanol



It is also interesting to note the boosted methanol formation between P3-P4. The similar observation at 260 °C was interpreted to be caused by phase condensation. At this temperature, however, we do not expect such phase condensation to take place (Figure 4.4a). One possibility may be a dense phase formation, like surface wetting, in the pore of catalyst which is virtually identical to phase condensation. Despite the high temperature, such dense liquid-like layer over catalyst surface may be present. Besides, it is worth highlighting the maximum CO fraction observed in the reactor at 260 and 340 °C. According to the thermodynamic calculation (Figure 4.4a), the equilibrium CO₂ conversions for RWGS at CO₂:H₂=1:3 are about 14% and 21% at 260 and 340 °C, respectively. A careful look in Figure 4.8 shows that the CO fraction is close to the equilibrium CO₂ conversion in the middle of the reactor (since the fraction is the percentage of CO₂ converted to methanol; therefore these numbers can be directly compared). Still the CO fraction decreases accompanying the increase of methanol fraction close to the outlet of the reactor, and this implies that methanol synthesis rate gets boosted at the position. It is speculated that the dense phase formation over the catalyst accelerate CO hydrogenation to methanol. Besides, methanol decomposition may take place, but it is not possible to gain information about this point from the data obtained at this high temperature. Nevertheless, it is certain that the

Chapter 4

consumption rate of CO and CO₂ to form methanol is much greater than methanol decomposition rate under these conditions.

Based on the above studies, we can conclude that the pressure effects on the reaction paths are relatively minor than the temperature effects, although higher pressure is advantageous in enhancing CO₂ conversion likely due to the kinetic advantages (i.e. more dense medium thus more collisions necessary for reaction) and favored thermodynamics. Interestingly, at 260 °C often we find optimum catalytic performance and at this temperature, phase condensation seems indeed boosting the reactivity of CO₂ to methanol by the concerted kinetic and thermodynamic advantages.

4.3.3 Space-resolved gas analysis by Raman spectroscopy

Similar space-resolved gas sampling experiments were performed using Raman spectroscopy instead of using GC and MS (MS data are not presented here due to large data fluctuation and accurate data quantification). The major advantage of this spectroscopic approach is that the reaction and flow-patterns are not disturbed in contrast to the case of GC/MS analyses where a part of the flow of the reaction mixture has to be sampled.

Figure 4.9 shows a typical Raman spectrum of the reaction stream obtained at 260 °C at the outlet (P4). The rotational transitions of H₂ (355, 587, 812, 1033, 1246, 1447 cm⁻¹) as well as the Fermi dyad of CO₂ and satellite bands (1265, 1286, 1387, 1408 cm⁻¹) were clearly identified. Because of the small Raman scattering cross section of CO, its characteristic feature at 2140 cm⁻¹ was not sufficient for quantitative analysis and only its formation could be confirmed at high CO concentration. The features at 2840 and 2945 cm⁻¹ are attributed to methanol, showing too weak signal for quantitative analysis. For these reasons, the most intense bands of H₂ and CO₂, 587 and 1387 cm⁻¹, respectively, were considered for quantitative composition analysis to gain mechanistic insights. The band areas were calculated and the changes in the band area ratio H₂/CO₂ along the reactor was used to understand the reaction

Space-resolved gas analysis of high-pressure CO₂ hydrogenation to methanol

path based on the stoichiometry of the two major reactions, *viz.* CO₂:H₂=1:3 for methanol synthesis and CO₂:H₂=1:1 for RWGS.

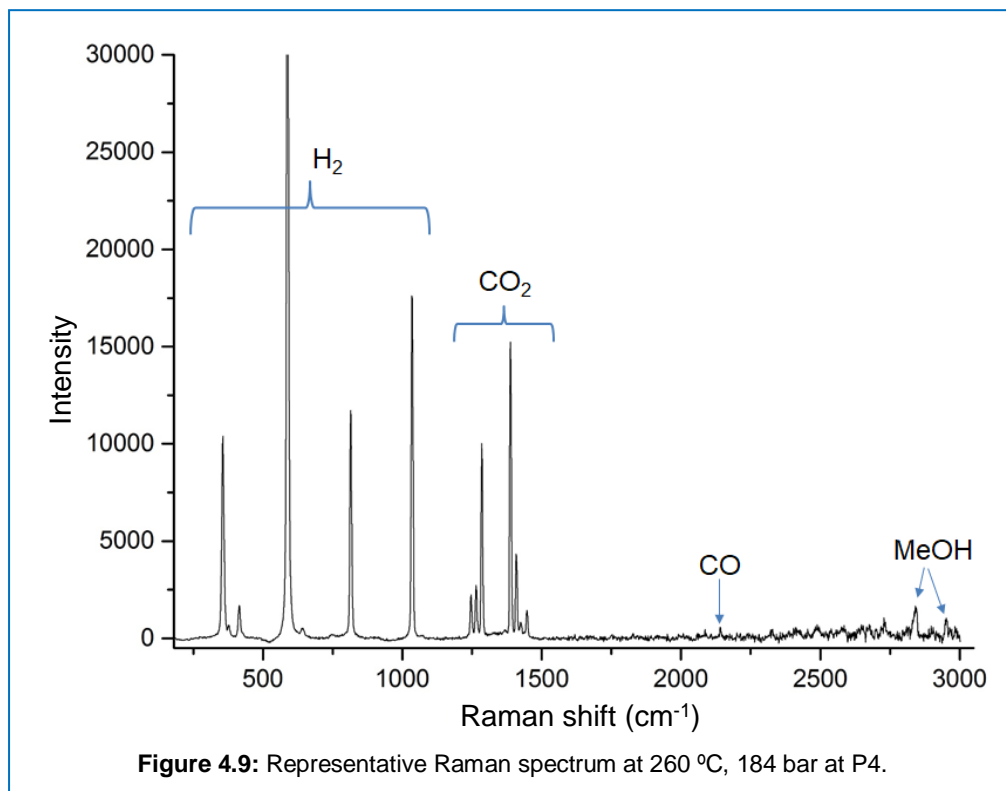
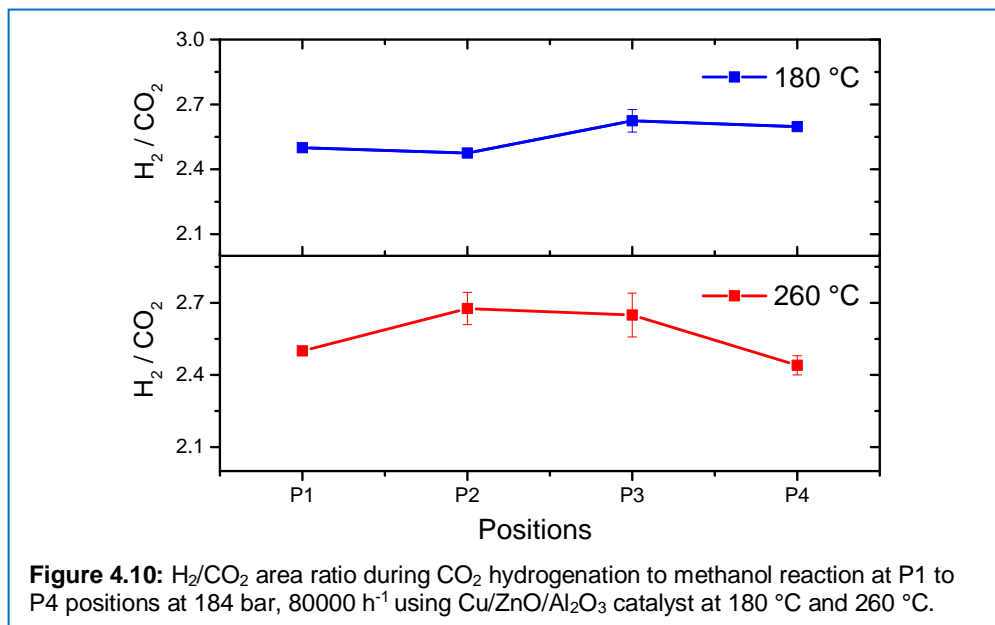


Figure 4.10 shows the H₂/CO₂ ratio of the band areas at different void positions at 180 °C and 260 °C at 184 bar. The initial area ratio at P1 was scaled to 2.5 to represent the molar ratio of unreacted feed confirmed by GC measurements. The reaction at 180 °C showed a slight decrease in the ratio from P1 to P2, before increasing towards P3, and no major change was observed moving from P3 to P4.

In the case of direct methanol synthesis from CO₂ as in Eq. 1.2, 3 moles of H₂ would be consumed per mole of CO₂ for the production of methanol, making H₂ the limiting reactant in our experimental condition (feed H₂/CO₂ = 2.5). On the other hand, if CO₂ is consumed to form CO via RWGS (Eq. 1.3), CO₂ would become limiting reactant. Therefore, a decrease in H₂/CO₂ ratio would signify an excessive H₂ consumption as in the former case of direct

Chapter 4



methanol synthesis, whereas an increase in the ratio would be a sign of a gradual CO₂ shortage by RWGS. In case methanol is a secondary product obtained from the subsequent hydrogenation of CO, as a net, the ratio is expected to decrease as an equivalent amount of H₂ is required whichever the CO_x (x=1 or 2) is the source of methanol. The initial slight decrease of the ratio at P1-P2 at 180 °C implies direct methanol synthesis reaction. Then at P2-P3, the ratio increases, which is indicative of RWGS. However, as discussed above, this is most likely due to the decomposition of methanol since such drastic selectivity change is unlikely at the low CO₂ conversion level. The increase in the ratio is therefore attributed to methanol decomposition, which can have the same net stoichiometry as RWGS (i.e. CO₂ + 3H₂ → MeOH + H₂O; MeOH → CO + H₂; as the net CO₂ + H₂ → CO + H₂O). In other words, methanol decomposition would increase the ratio, which is fully consistent with the observation and the previous results (Figure 4.6). In this Raman study, however, the ratio did not increase further as expected from the results in Figure 4.6. This may be due to the higher space velocity of this Raman study compared to the study by GC and consequent less pronounced change in the ratio.

Space-resolved gas analysis of high-pressure CO₂ hydrogenation to methanol

At 260 °C there was a clear initial increase of the ratio and then decrease towards the outlet (Figure 4.10). The increasing ratio indicates clearly the increase in the amount of CO in the reactor and then subsequent decrease indicates the increase in the amount of methanol, no matter which reaction paths are taken. This profile is in full accordance with the results presented in Figure 4.7a obtained in a comparable reaction condition where initially CO was produced and then CO was hydrogenated to methanol.

Furthermore, the sharp drop in the ratio at 260 °C coincided with the observation of condensation as liquid droplets at the rear end of the packed-bed at P4 (Figure 4.11). As discussed above, the condensation is believed to have enhanced methanol synthesis via CO or CO₂, by *in situ* separation of the less volatile components, namely water and methanol. Indeed, when focusing the Raman laser spot on the dense phase, more intense methanol peak was observed and the H₂/CO₂ ratio dropped to even lower values, suggesting the higher miscibility of CO₂ than H₂ in the condensed phase. According to the thermodynamic expectations at CO₂:H₂=1:3 (Figure 4.4a), liquid phase condensation is not expected at 184 bar, 260 °C, but it is likely facilitated by the excess of dense CO₂ used in this study in comparison to the stoichiometric ratio.

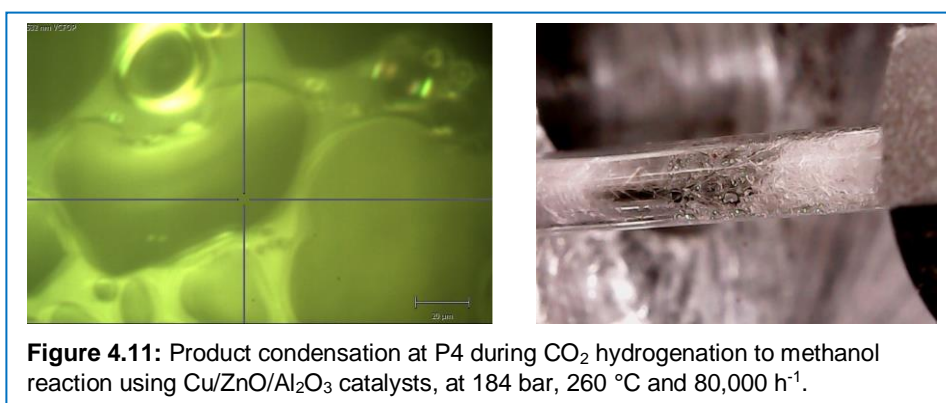


Figure 4.11: Product condensation at P4 during CO₂ hydrogenation to methanol reaction using Cu/ZnO/Al₂O₃ catalysts, at 184 bar, 260 °C and 80,000 h⁻¹.

Chapter 4

4.4 Conclusions

The present study employed two different approaches, one by GC/MS and the other by Raman spectroscopy, to gain compositional information of the gas phase at different axial positions of the catalytic reactor operated under high-pressure conditions of methanol synthesis from CO₂ and H₂. The first approach needs to sample gas from the reactor and thus the reaction may be disturbed to a small extent; however, the space-resolved gas sampling was successfully performed with the advantage of accurate quantification of all evolved gases by GC. The other approach using Raman spectroscopy with the pressure-resistant sapphire tube as the catalytic reactor could gain compositional information of the dense gas phase or even liquid phase without disturbing the reaction. Although the detection sensitivity did not allow quantification of all products, the important ones to extract information about the reaction paths, CO₂ and H₂, could be measured with high accuracy.

These studies showed that at 180 °C methanol is directly produced from the hydrogenation of CO₂ and the temperature seems too low for RWGS reaction. However, some of the formed methanol can decompose, producing CO and also CO₂. This decomposition was effectively suppressed at higher pressure, evidencing another advantage of high-pressure reaction condition. In contrast, at higher temperature (260 and 340 °C) endothermic RWGS reaction rate surpasses that of the exothermic direct methanol synthesis reaction, followed by CO hydrogenation to methanol. These results clearly pointed out that CO hydrogenation is the main source of methanol under the high-pressure conditions. Furthermore, at 260 °C at 331 bar, phase condensation was indicated to take place boosting further CO₂ conversion and methanol selectivity, showing kinetic and thermodynamic advantages of the specific reaction condition.

Space-resolved gas analysis of high-pressure CO₂ hydrogenation to methanol

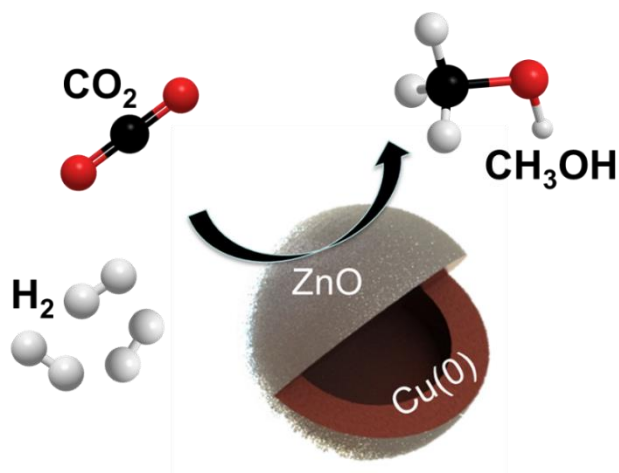
Bibliography

- [1] K. Klier, V. Chatikavanij, R.G. Herman, G.W. Simmons, *J. Catal.*, 74 (1982) pp. 343-360.
- [2] K. Klier, *Methanol Synthesis*, D.D. Eley, H. Pines, P.B. Weisz (Eds.) *Adv. Catal.*, Academic Press, 1982, pp. 243-313.
- [3] G.C. Chinchen, K.C. Waugh, D.A. Whan, *Appl. Catal.*, 25 (1986) pp. 101-107.
- [4] A.Y. Rozovskii, G.I. Lin, *Topics in Catalysis*, 22 (2003) pp. 137-150.
- [5] B. Tidona, C. Koppold, A. Bansode, A. Urakawa, P. Rudolf von Rohr, *J Supercrit Fluids.*, 78 (2013) pp. 70-77.
- [6] H. Reymond, P.R.v. Rohr, *Rev. Sci. Instrum.*, 88 (2017) pp. 1141031-6.
- [7] R. Sahki, O. Benlounes, O. Cherifi, R. Thouvenot, M.M. Bettahar, S. Hocine, *React. Kinet. Mech. Cat.*, 103 (2011) pp. 391-403.

Chapter 4

5.

Cu-ZnO core-shell catalysts prepared by non-aqueous sol-gel method



Chapter 5

5.1 Introduction

As reported and discussed in the previous chapters, Cu-based catalysts, especially promoted with ZnO, are the most common ones to exhibit high catalytic activity in the conversion of carbon oxides to methanol via hydrogenation [1, 2]. These catalysts are generally prepared by co-precipitation or impregnation methods and contains multiple components including structural promoters. These material synthesis methods are advantageous for their simplicity and scale-up; however, it is neither straightforward nor facile to control the morphology of the resulting materials and they often suffer from thermal instability, leading to sintering and thus catalyst deactivation. ZnO is known to act as spacer preventing Cu sintering and to function as hydrogen reservoir of atomic hydrogen promoting H spill-over to Cu [3]. The synergetic functions of Cu and ZnO, especially at the Cu-ZnO interfaces possibly by forming an alloy phase, are also widely reported to provide unique reactivity in methanol synthesis [4-13]. In this respect, the Cu-ZnO core-shell morphology could provide well-controlled metal-oxide interface and interaction by protecting the Cu core against sintering [14].

In this chapter, a novel, simple, facile synthesis route for Cu-ZnO core-shell nano-structured materials using so-called non-aqueous sol-gel synthesis method was developed and the resulting materials were tested for methanol synthesis reaction by CO₂ hydrogenation. The major advantages of the non-aqueous sol-gel synthesis method are high purity, high tunability of nanostructures, homogenous product quality and synthesis at relatively low temperature [15, 16]. In this work, benzyl alcohol was chosen as reducing agent [17-21] and strategies to form Cu-ZnO core-shell particles were developed. The obtained core-shell materials were evaluated for CO₂ hydrogenation to methanol under high pressure conditions. Unique phase changes on the shell (Zn component) was clarified and their role in the reaction was investigated by high-pressure *operando* XRD.

5.2 Experimental section

5.2.1 Chemicals

Copper (I) acetate (Sigma-Aldrich, 97%), zinc acetate (Sigma-Aldrich, 99.99%), benzyl alcohol (Sigma-Aldrich, puriss) were used as received. The reactant gas mixture ($\text{CO}_2:\text{H}_2:\text{Ar}=23:69:8$) was purchased from Abelló Linde (Spain).

5.2.2 Catalyst synthesis

Zinc acetate and copper acetate were dissolved in benzyl alcohol in an inert atmosphere using standard Schenk line and flask. In a typical synthesis, 5.7 mmol of zinc acetate was first dissolved in 30 mL benzyl alcohol and afterward 2.5 mmol of copper acetate was added into the solution under constant stirring under N_2 flow. The reaction vessel was purged with N_2 , sealed, and the solution was further stirred for 5 min. Later, the vessel was dipped into an oil bath preheated at 160 °C under stirring for 30 min. Precipitates were separated from the liquid phase by centrifugation and washed three times with ethanol. Pure Cu_2O and ZnO were also synthesized separately using the identical procedure but using only one of the precursors. The final dried powders of Cu_2O and ZnO were mixed and this is called “physical mixture”. Also, in order to evaluate the effects of stirring on the resulting material, Cu-ZnO material was prepared by the same protocol but without stirring. Finally, these materials were dried in an oven at 80 °C, pressed, crushed and sieved to particle size fraction (100-300 μm) for catalytic activity tests.

5.2.3 Catalyst characterization

A) *Ex situ* X-ray diffraction (XRD)

XRD patterns were recorded on Bruker AXS D8 advance diffractometer equipped with a Cu tube, a Ge (111) incident beam monochromator (1.54184 Å), and Vantec-1 PSD operated in transmission mode. Signal was recorded in 20-80° 2 θ with a step size of 0.02° and counting time of 4 seconds per step.

Chapter 5

Crystal phases were confirmed using Bruker X'Pert Pro software and JCPDS database. The phase quantification was done using Maud software and X'Pert High-score Plus software.

B) *In situ* XRD

In situ XRD measurements were performed to follow the crystallographic phases of selected materials under a H₂ reduction condition using a Bruker-AXS D8-Discover diffractometer equipped with parallel incident beam (Göbel mirror), vertical θ - θ goniometer, XYZ motorized stage and with a GADDS (General Area Detector Diffraction System). The X-ray diffractometer was operated at 40 kV and 40 mA to generate Cu K α radiation (1.54184 Å). 2D XRD patterns were collected covering 25-59° 2 θ at a detector-sample distance of 15 cm. The sample temperature was controlled with a MRI BTS-Basic high temperature sample stage. A sample was placed in a capillary made of fused silica with diameter 0.5 mm. The capillary was mounted in a "U" shaped stainless steel frame that provided a firm support to the capillary. The frame was fixed in the MRI chamber of the Bruker D8 Advance diffractometer. The two ends of the capillary are connected to SS 316, 1/16" tubes for gas inlet and outlet connections as shown in [Appendix Figure B5.1](#). 5% H₂ in N₂ gas was passed through the capillary at 1 bar. XRD patterns were collected from 150 °C up to 450 °C at $\Delta T=20$ °C at a heating rate of 5 °C min⁻¹.

C) *Operando* XRD

Powder X-ray diffraction patterns were acquired using a Bruker Apex DUO equipped with an APEX 2 4K CCD area detector and Mo K α radiation (1.71073 Å, 50 kV and 0.60 mA). The diffraction rings were collected, acquiring for 120 s. The obtained two dimensional powder diffraction images were integrated over the 4-40° 2 θ range and converted to standard XRD patterns. Programs used: Data collection with APEX II version v2009.1-02, Bruker (2007) Bruker AXS Inc., Madison, Wisconsin, USA and data processing with Pilot XRD² Eval implemented in APEX II. The final evaluation and processing of the XRD

Cu-ZnO core-shell catalysts prepared by non-aqueous sol-gel method

patterns at different temperatures was performed with EVA V.14.0.0.0 (Bruker-AXS 1996-2007).

A capillary was used as the reactor and it was a polyimide coated fused silica tube (Molex) with 662 μm outer diameter (OD), 150 μm inner diameter (ID) and 3 cm length. Polyimide coating gives inherent strength, thermal stability and flexibility to the capillary. A catalyst material was pressed into the pellet and crushed and sieved to 40-60 μm particle size, and typically 1.5 mg of the material was charged into the capillary held in the custom-made sample holder. The end connections of the capillary reactor were connected to the inlet and outlet of the reactor. The sample was heated using a hot air blower having a nozzle of 10 mm OD. The nozzle of the hot air blower was kept as close as possible to the sample, taking special attention to avoid disturbance of the nozzle tip with the X-ray beam path as shown in [Appendix Figure B5.2](#). The temperature of the capillary near the sample was measured during heating using a portable temperature sensor to ensure the sample temperature. The two ends of the reactor were connected to the syringe pump and BPR respectively. Prior to *operando* XRD, the catalyst was reduced in 5% H_2 in N_2 at 330 $^\circ\text{C}$. Due to the small inner diameter of the capillary and the catalyst packed inside, the reactor developed a pressure drop of ca. 150 bar. After the reduction for 20 min, the temperature was lowered to 30 $^\circ\text{C}$ and a compressed $\text{CO}_2:\text{H}_2$ (1:3) gas was passed through the capillary reactor and the effluent stream was continuously analyzed by mass spectrometer (MS). Once a desired catalyst temperature was reached, XRD patterns were taken every 3 min. with 120 seconds scan time.

D) N_2 physisorption

N_2 isotherms at 77 K were measured on a Quantachrome Autosorb 1-MP analyzer to obtain BET surface area. Prior to analysis, sample was degassed in vacuum at 250 $^\circ\text{C}$ for 12h.

Chapter 5

E) Temperature programmed reduction (TPR)

H₂-TPR of as-prepared catalyst was carried out on a Thermo TPDRO 1100 equipment with a TCD detector. The samples were heated from 25 to 400 °C at the rate of 2 °C min⁻¹ under a stream of 5% H₂ in N₂ at 20 mL min⁻¹. A soda lime (CaO+Na₂O) trap was used to adsorb mainly H₂O and CO₂.

F) N₂O chemisorption

Pulse chemisorption was used to measure the copper surface area and dispersion using nitrous oxide reported by Evans et al. [45]. The samples were reduced before analysis in the stream of 5% H₂ in He at 330 °C for 3 h after the ramp at 2 °C min⁻¹. The samples were cooled down to 90 °C under He flow. Then, a known volume of N₂O was injected as pulse using a six port valve. The N₂O was converted to N₂ when it oxidizes Cu surface. The unconverted N₂O was trapped in a container kept at liquid Ar temperature, whereas N₂ directly passed to a TCD detector for quantification. Copper surface areas were calculated assuming 1.46 x 10¹⁹ copper atoms per m² [45].

G) Electron microscopy

High resolution transmission electron microscopy (HR-TEM) images were recorded on a JEOL JEM-2200FS microscope operated at 200 kV. EDX analyses were carried out on a FEI Talos F200X microscope operated at 200kV in STEM mode. The samples for TEM analyses were dispersed in ethanol and drop-casted onto nickel coated copper and nickel grid and measured by JEOL 1011. In case of SEM analysis, the samples were ultrasonicated in ethanol for 10 min prior to measurement using JEOL 6400.

5.2.4 Catalytic test

Carbon dioxide hydrogenation to methanol was studied in a high-pressure continuous flow fixed-bed stainless steel reactor (1.8 mm ID). Detailed high-pressure fixed-bed reactor and analytical system are described in [Chapter 2](#). Briefly, 50 mg of the sieved catalyst pellets of 100-300 µm particle size were charged into the reactor. Then the catalyst was reduced before the reaction in

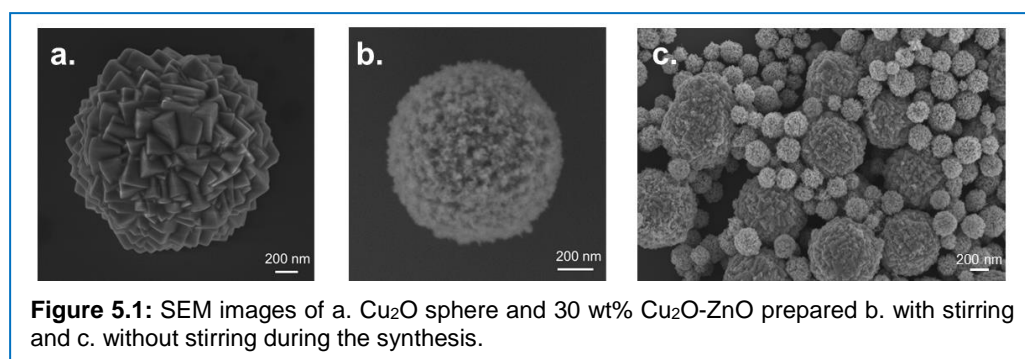
Cu-ZnO core-shell catalysts prepared by non-aqueous sol-gel method

the hydrogen stream at 20 mL min^{-1} for 2 h at $330 \text{ }^\circ\text{C}$, at atmospheric pressure. Later, the catalyst bed was pressurized using the pre-mixed reactant gas mixture ($\text{CO}_2:\text{H}_2:\text{Ar} = 23:69:8$) to a desired reaction pressure. The effluent stream was analyzed by on-line GC.

5.3 Results and discussion

5.3.1 Material structure

Figure 5.1 shows the SEM images of the materials synthesized by the different protocols of the non-aqueous sol-gel method. Figure 5.1a presents the material synthesized with of the Cu precursor only. The spherical cuprous oxide (identified by XRD) was formed by the cubes which was indicated by the sharp right angle edges of Cu_2O . Figures 5.1b and 5.1c show the material synthesized with both Cu and Zn precursors under stirring and without stirring, respectively,

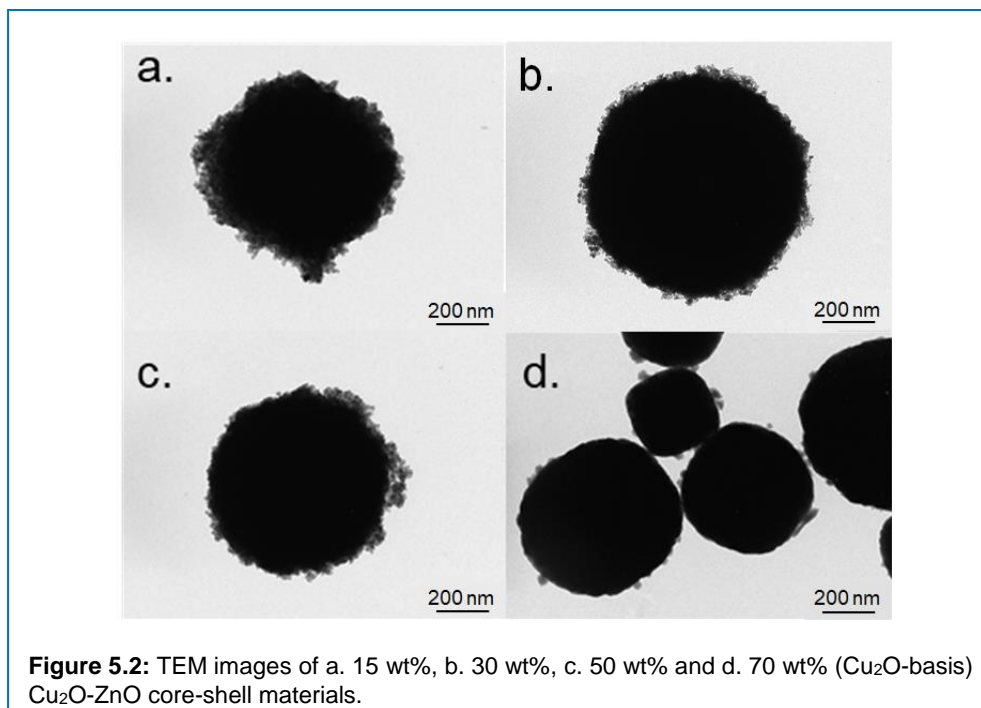


at a nominal targeted weight ratio of 3:7 ($\text{Cu}_2\text{O}:\text{ZnO}$). The influence of the solution stirring during the synthesis on the resulting material structure is clear. The stirring condition yields a material where ZnO nanoparticles cover the Cu_2O spherical core homogenously, whereas Cu_2O and ZnO particles are formed separately without stirring.

Figure 5.2 shows the TEM images of the nanomaterials synthesized by varying the relative Cu amount at 15 wt% (Figure 5.2a), 30 wt% (Figure 5.2b), 50 wt% (Figure 5.2c) and 70 wt% (Figure 5.2d) under the stirring condition. In all cases, Cu_2O core was covered by ZnO nanoparticles to different extent

Chapter 5

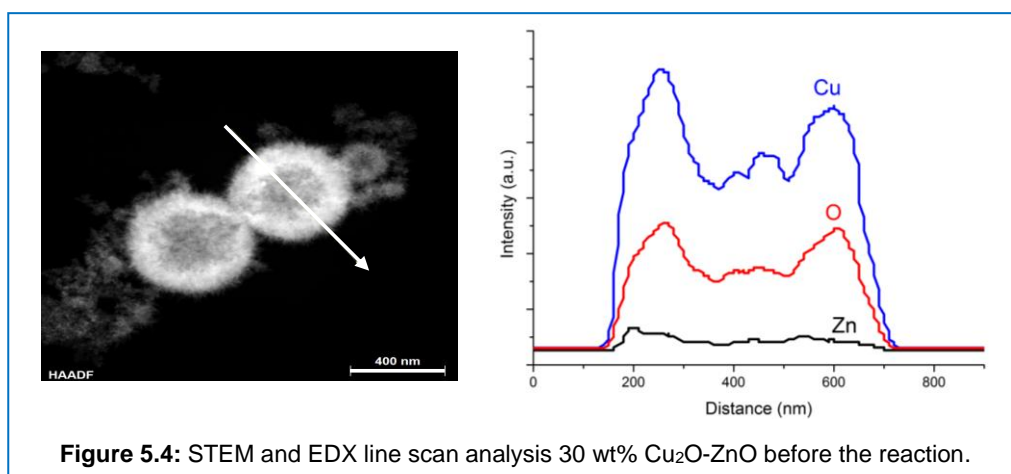
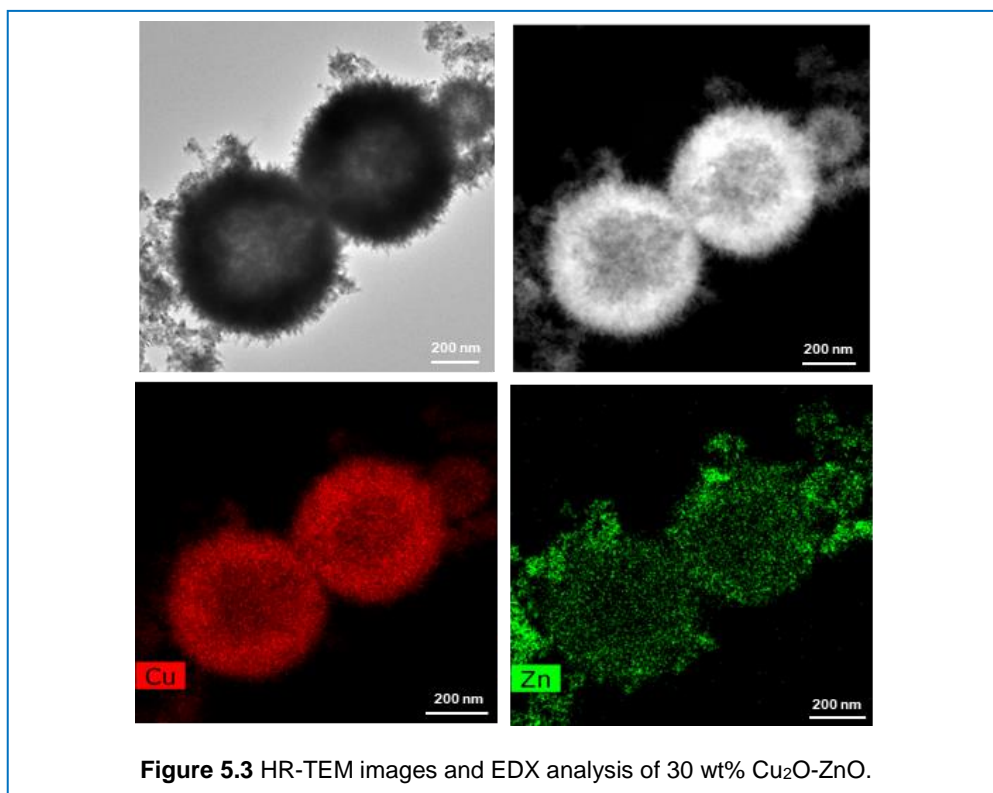
depending on the weight ratio of Cu_2O and ZnO . The spherical shaped nanomaterials have a diameter in the range of 500-800 nm.



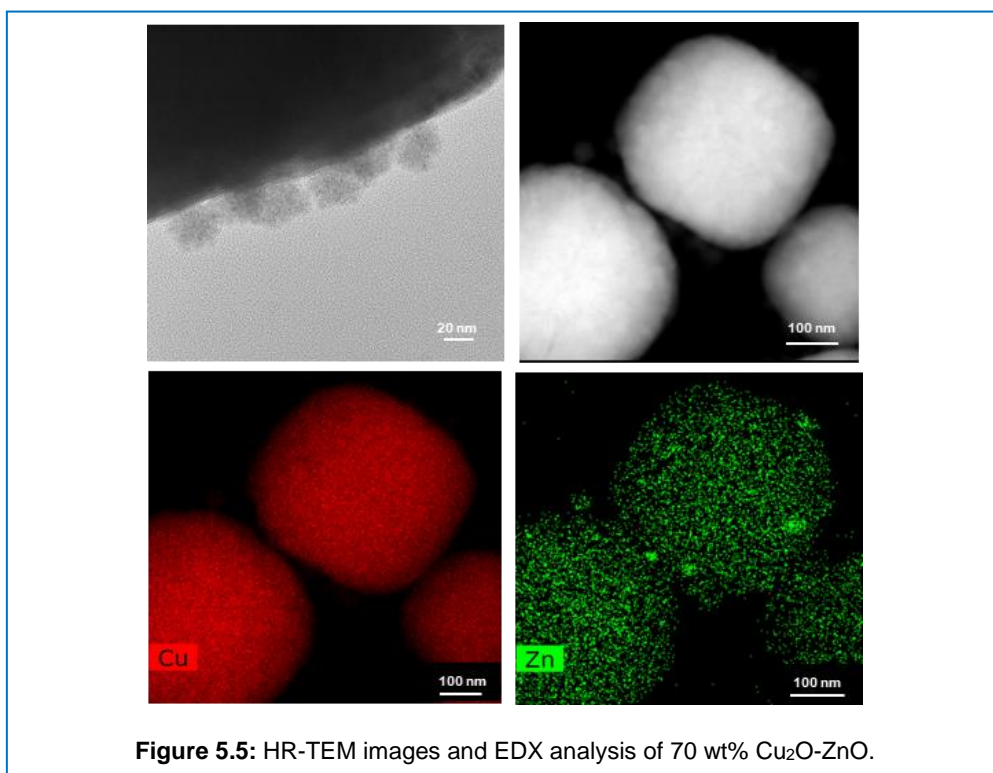
As the Cu_2O - ZnO weight ratio decreased, these small ZnO nanoparticles aggregated and formed thicker layers of ZnO on Cu_2O core (Figure 5.2). On the contrary, at lower relative Zn amount, thin and uneven coating of ZnO on the Cu_2O surface was observed (Figure 5.2d). In order to elucidate the Cu_2O - ZnO core-shell interface, 30 and 70 wt% Cu_2O - ZnO core-shell materials were studied by HR-TEM and EDX analyses (Figures 5.3 and 5.5), revealing that the core and shell mainly contain Cu and Zn , respectively.

Figure 5.3 indicates a hollow sphere structure and EDX line scan of 30 wt% Cu_2O - ZnO was performed to gain more precise elemental distribution (Figure 5.4). Cu_2O core is incompletely or partially filled, while Zn is homogeneously distributed over the core as evident from the Zn mapping (Figure 5.3). In contrast, when the Cu precursor content is higher in the synthesis (70 wt% Cu_2O - ZnO), the Cu_2O core of the material is completely filled (Figure 5.5).

Cu-ZnO core-shell catalysts prepared by non-aqueous sol-gel method



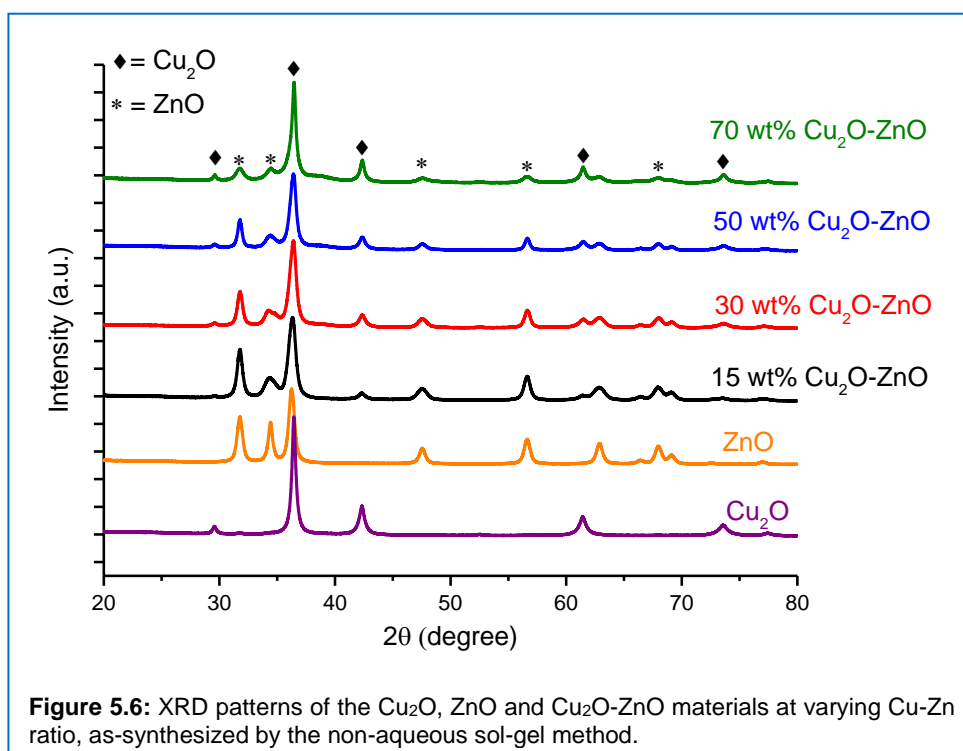
Chapter 5



5.3.2 *Ex situ* XRD

Figure 5.6 shows the XRD patterns of the materials synthesized by the non-aqueous sol-gel method. There were two crystallite phases identified: Cu₂O (29.6, 36.5, 42.4, 61.5, 73.6°, JCPDS: 01-078-2076) and ZnO (31.8, 34.4, 36.2, 47.5, 56.6°, JCPDS: 00-036-1451). Noticeably, the diffraction peaks of Cu₂O became stronger and sharper at higher Cu₂O/ZnO ratio and opposite trend was observed for ZnO. The Cu₂O crystallite sizes of these materials were 21 nm (Cu₂O), 12 nm (15 wt%), 11 nm (30 wt%), 19 nm (50 wt%), 23 nm (70 wt% Cu₂O-ZnO), while those of ZnO were 14 nm (ZnO), 15 nm (15 wt%), 16 nm (30 wt%), 19 nm (50 wt%), 13 nm (70 wt% Cu₂O-ZnO), showing generally higher crystallinity of Cu₂O ZnO when the Cu content is higher, while ZnO crystallinity does not affect much with change in Zn content. The XRD results confirm the phase purity of Cu₂O and ZnO in these materials.

Cu-ZnO core-shell catalysts prepared by non-aqueous sol-gel method

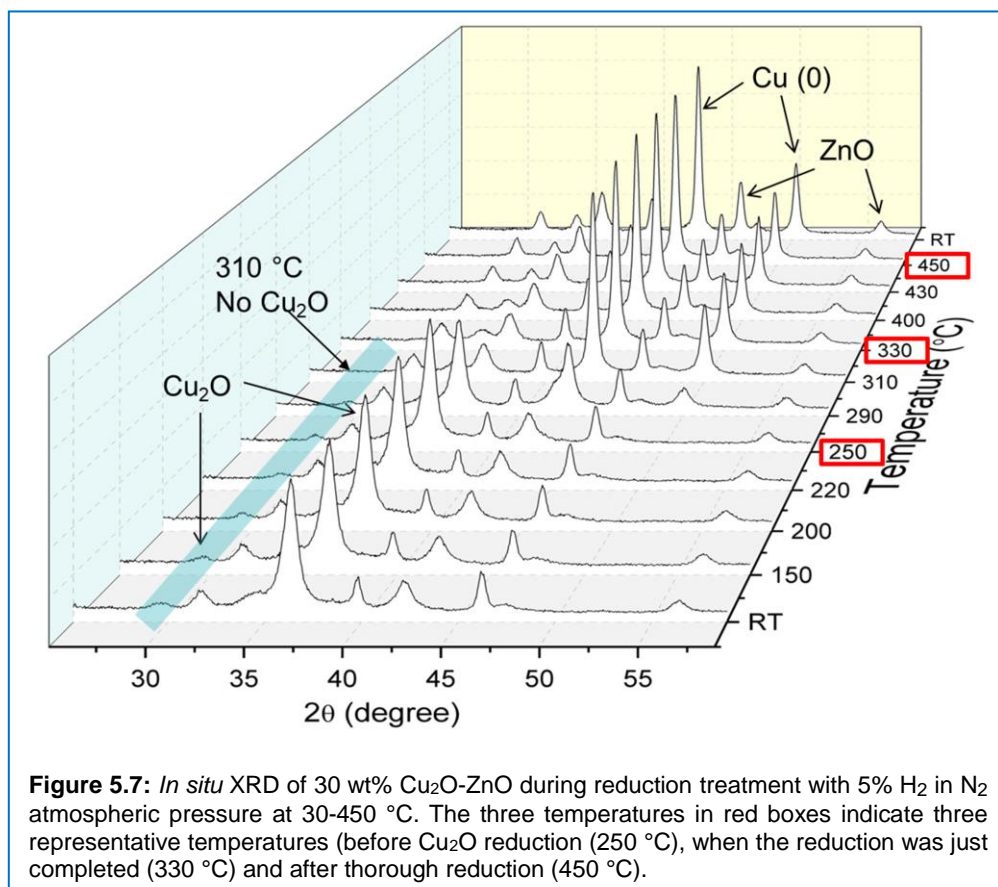


5.3.3 *In situ* XRD during thermal pretreatment in H₂

Copper is structurally one of the most temperature-sensitive metals among widely used catalytically active elements, and thus Cu particles tend to agglomerate at high temperature, reducing active copper surface area. Hence it is important to investigate at which temperature the core-shell materials are reduced from Cu₂O to Cu (0) and their thermal stability. Figure 5.7 shows XRD patterns of 30 wt% Cu₂O-ZnO as a function of temperature (30-450 °C) under the flow of 5% H₂ in N₂ at atmospheric pressure. Only this material is shown due to its high catalytic activity as discussed later. The reduction of the material was initiated at ca. 260 °C, and the catalyst was completely reduced Cu (0) at ca. 300 °C. According to the Scherrer equation, the crystallite size of the Cu component increased from 12 nm (as-synthesized, Cu₂O) to 21 nm (Cu (0), after reduction at 330 °C). Further temperature increase led to increase of the

Chapter 5

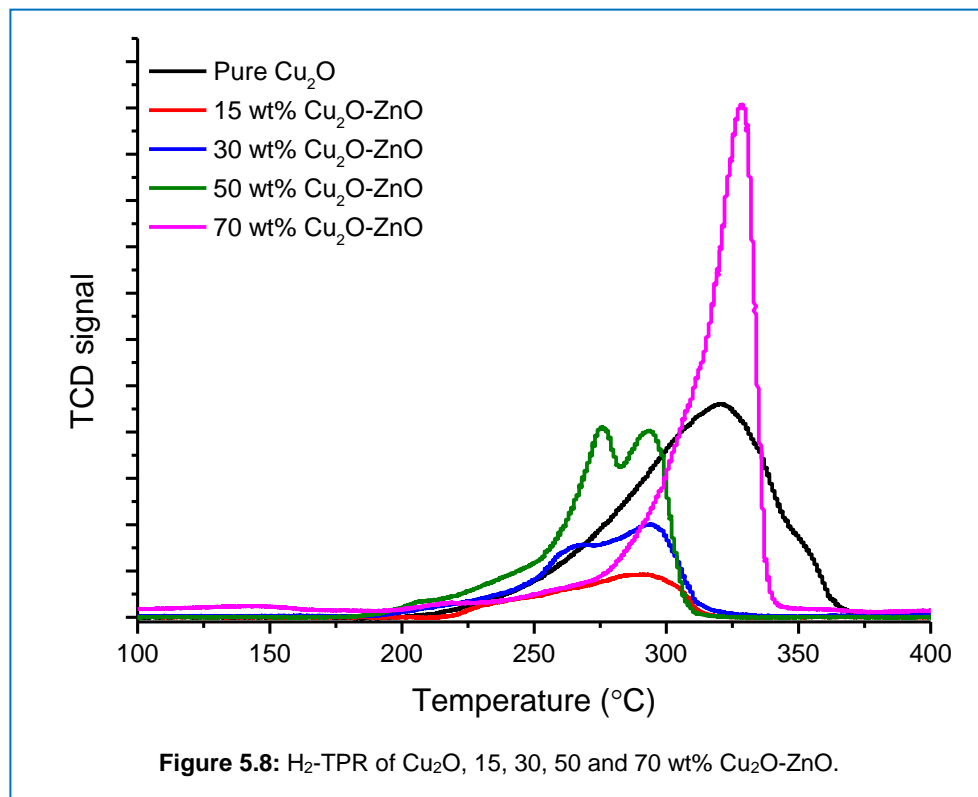
crystallite size up to 23 nm, showing high thermal stability of the material against common sintering [22] due to the presence of the ZnO shell.



5.3.4 H₂-TPR

H₂-TPR was performed for all Cu₂O-ZnO core-shell materials including the pure Cu₂O sphere as reference. Their reduction profiles are shown in Figure 5.8. The TPR profile of pure Cu₂O shows a broad peak with a maximum at a relatively high temperature (320 °C). When ZnO was added and covers the Cu₂O core, the reduction profile drastically changed. When a small amount of Zn was added (30 wt% Cu₂O-ZnO), the reduction temperature was identical but the profile became much more defined. At further increased loading of ZnO, the

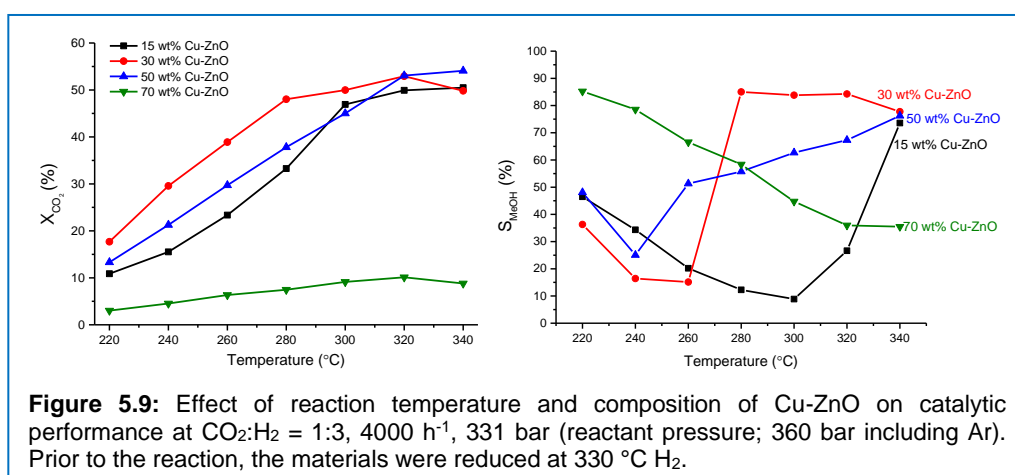
Cu-ZnO core-shell catalysts prepared by non-aqueous sol-gel method



reduction temperature maxima dropped by 30-50 °C, showing two distinguishable peaks for Cu₂O reduction, which could be assigned to surface and bulk Cu₂O reduction. XRD showed that ZnO was not reduced and remained as ZnO thus the peaks originate only from Cu₂O reduction. It is important to highlight that the presence of ZnO, more precisely Cu₂O-ZnO interaction, strongly enhanced the reducibility of Cu₂O, which could be beneficial for CO₂ hydrogenation to methanol.

5.3.5 Catalyst evaluation: Effects of Cu-Zn ratio

The catalytic activity of the Cu-ZnO core-shell materials (since the material is pre-reduced; the materials are simply denoted as Cu-ZnO instead of Cu₂O-ZnO hereafter) was evaluated under high-pressure conditions in a wide temperature range of 220-340 °C (Figure 5.9). Obviously, the catalytic activity of the four core-shell materials were very different in terms of CO₂ conversion and methanol selectivity. Generally, CO₂ conversion monotonously increased with temperature, and in contrast, the trends of methanol selectivity against reaction temperature was very different depending on the materials; 50 wt% Cu-ZnO showing steady increase, 70 wt% Cu-ZnO showing steady decrease and 15 and 30 wt% Cu-ZnO showing remarkable alternation from drop to increase in methanol selectivity with temperature. The material with the highest Cu content, 70 wt% Cu-ZnO, showed the lowest CO₂ conversion, although at low temperatures the catalyst exhibited the highest methanol selectivity, similar to the behavior of the commercial methanol synthesis catalyst (Chapter 4). Upon increasing the Zn content, with 50 wt% Cu-ZnO, the catalytic activity was boosted significantly, and strikingly the methanol selectivity trend was reversed, with an initial drop followed by a monotonous increase with temperature. Further increase in the Zn content, with 30 wt% Cu-ZnO, the highest CO₂ conversion



below 320 °C was observed. In this case, the initial drop in selectivity was obvious and then upon increase in the reaction temperature the reaction

Cu-ZnO core-shell catalysts prepared by non-aqueous sol-gel method

selectivity was suddenly reversed from CO to methanol between 260-280 °C. The highest Zn content material, 15 wt% Cu-ZnO, showed reasonably high catalytic activity and again the same trends in methanol selectivity, but more prominently with a large gradual drop and then gradual increase at higher temperature. The Cu surface area for these materials were 7.7, 10.6, 5.2, and 1.2 m² g⁻¹ for 15, 30, 50 and 70 wt% Cu-ZnO materials, respectively. This explains the low catalytic activity of 70 wt% Cu-ZnO, but it does not account for the unique selectivity changes. Thus, the Cu-ZnO interfaces are speculated to play important roles in directing the selectivity to methanol or CO. Interestingly, at the highest temperature examined, 340 °C, CO₂ conversion (ca. 50%) as well as methanol selectivity (ca. 80%) converges for 15, 30 and 50 wt% Cu-ZnO.

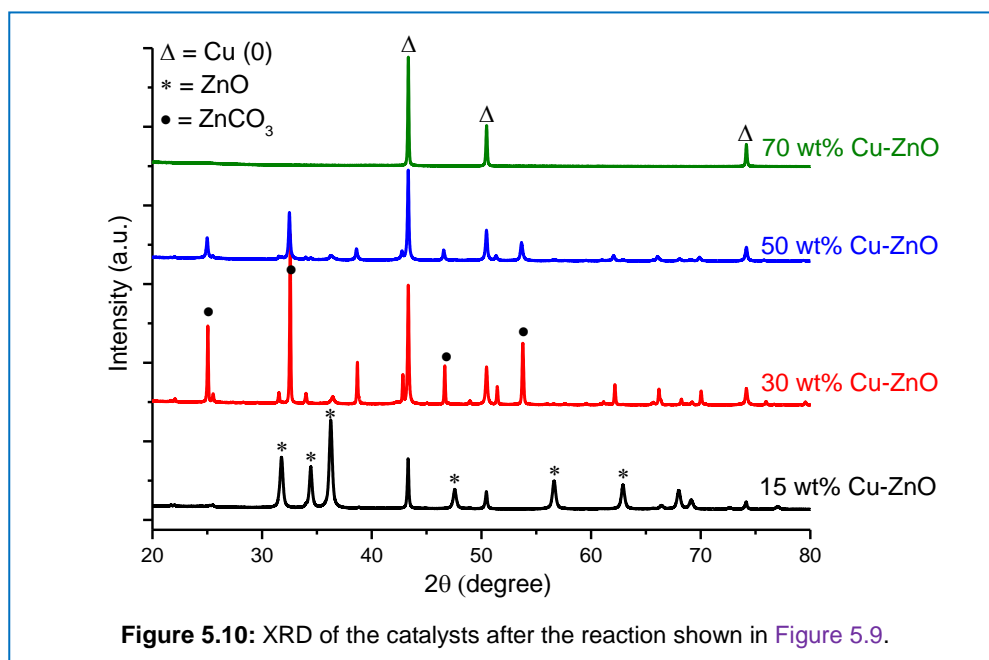
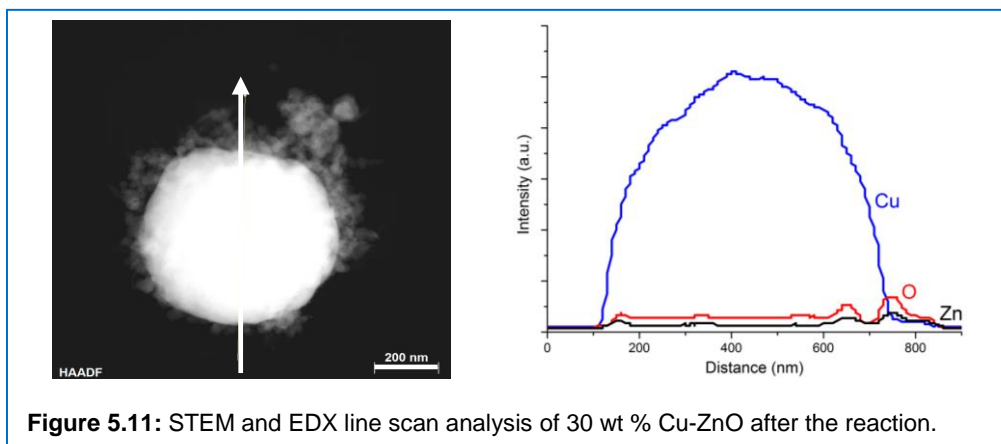


Figure 5.10: XRD of the catalysts after the reaction shown in Figure 5.9.

These values are in accordance with the thermodynamic expectation (Figure 4.4) and thus we can conclude that the reaction reached thermodynamic equilibrium over the three catalysts at 340 °C temperature. From the catalytic performance point of view, 30 wt% Cu-ZnO is the most interesting material since it shows relatively high CO₂ conversion (ca. 50%) with high methanol selectivity (ca. 85%) at 280 °C.

Chapter 5

In order to understand the distinct catalytic performance of the Cu-ZnO materials, the materials were studied by XRD after the catalytic reaction and the results are compared in [Figure 5.10](#). 70 wt% Cu-ZnO presented mainly the reflections due to Cu (0). In contrast, at the highest amount of Zn content (15



wt% Cu-ZnO), mainly ZnO phase was observed in addition to comparably small amount of Cu (0). Intriguingly, there was a clear formation of ZnCO_3 , which is not well reported for methanol synthesis catalysts, for 30 and 50 wt% Cu-ZnO besides the observation of the ZnO and Cu (0) phases. [Table 5.1](#) presents quantitative analysis of crystal phases observed for the two samples. This shows that most Cu_2O was transformed to Cu (0) as expected and, to our surprise, ZnO was transformed to ZnCO_3 . Assuming that all Zn components are crystalline and observable by XRD, notably 98% and 99 % of Zn are found in the form of ZnCO_3 for 30 and 50 wt% Cu-ZnO, respectively. These results show that the presence of ZnO and its interaction with Cu may not be the requisite for high catalytic activity and a unique form of Cu may be more decisive in determining the catalytic activity.

Cu-ZnO core-shell catalysts prepared by non-aqueous sol-gel method

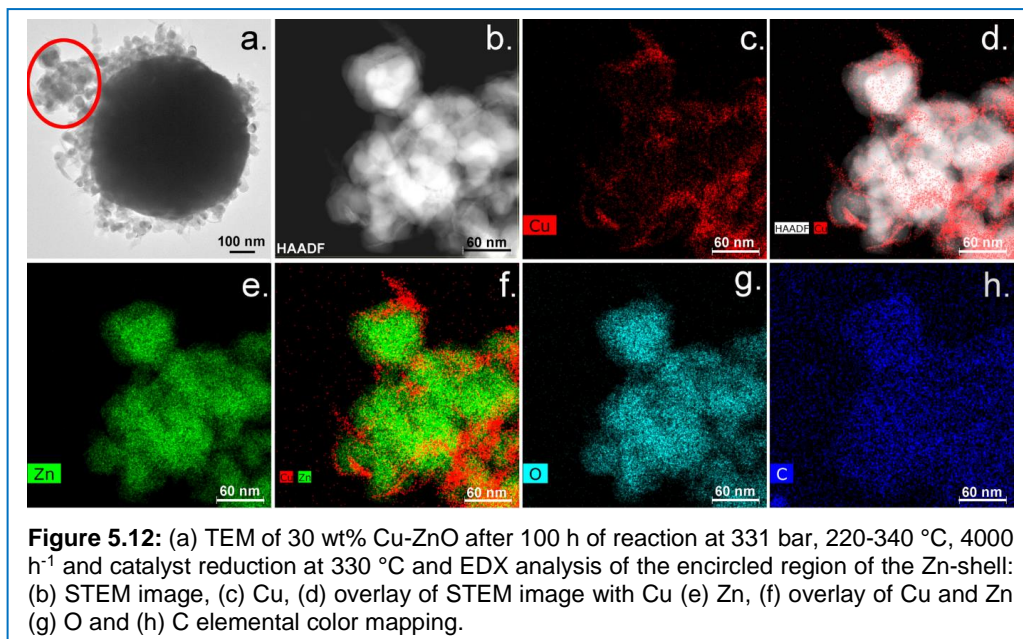
Table 5.1: Quantitative phase analysis of 30 and 50 wt% Cu-ZnO before and after the reaction.

Components	Before reaction		After reaction	
	30 wt%	50 wt%	30 wt%	50 wt%
Cu ₂ O	30.8	44.1	1.8	1.4
ZnO	69.2	55.9	0.4	1.3
Cu (0)	-	-	29.2	42.0
ZnCO ₃	-	-	68.4	55.4

To gain further structural and morphological insights, the best performing material, 30 wt% Cu-ZnO, after the reaction was studied by TEM and EDX line scan (Figure 5.11, 5.12a). First, the Cu core which was partially filled sphere, upon synthesis was fully filled with metallic Cu. The deformation of shell layer was not observed, although the consisting ZnO particles became sintered and more crystalline. Importantly, no agglomeration of copper particles was observed even after 100 h of reaction at 331 bar under varying the temperature from 220 to 340 °C, showing outstanding thermal stability of the Cu-ZnO core-shell structure.

In addition, STEM (Figure 5.12b) and EDX (Figure 5.12c-h) studies of the shell layer around the Cu core were performed to identify its structure after the reaction. The co-presence of Zn, O, and C with similar distribution (Figure 5.12e, g, h) confirms that the Zn-shell is transformed to ZnCO₃, taking also the XRD results (Figure 5.10) into account. Interestingly, some amount of Cu was also found in this shell region (Figure 5.12c) and its spatial distribution was remarkably different from that of Zn. The overlay of the Cu element distribution with the STEM image (Figure 5.12d) and with the Zn distribution (Figure 5.12f) clearly shows that Cu is supported over Zn component (i.e. ZnCO₃), preferentially extended over the surface and entering the cavities created by the ZnCO₃ particles. Such spread distribution of Cu is reasonable since both Cu and Zn precursors are present in the solution during the synthesis and some Cu species may have actually be located in the shell. Furthermore, the high Cu surface area of this material after activation (10.6 m² g⁻¹) indicates the presence

Chapter 5



of small Cu particles. Assumption of smooth spherical Cu particles with the diameter of 200, 500 and 1000 nm would give 3.3, 1.3 and 0.7 m² g⁻¹, respectively, confirming that highly dispersed Cu particles are present in the material and most likely contribute to its high catalytic performance of 30 wt% Cu-ZnO. On the other hand, the Cu surface area of the low catalytic activity material, 70 wt% Cu-ZnO, was 1.2 m² g⁻¹ and this is close to the surface area of smooth sphere of ca. 500 nm. This implies that in this case, catalytic activity originates from the surface of the Cu core and high methanol selectivity was observed at lower temperatures. This may be the characteristics of large crystallites, i.e. extended Cu surface [23].

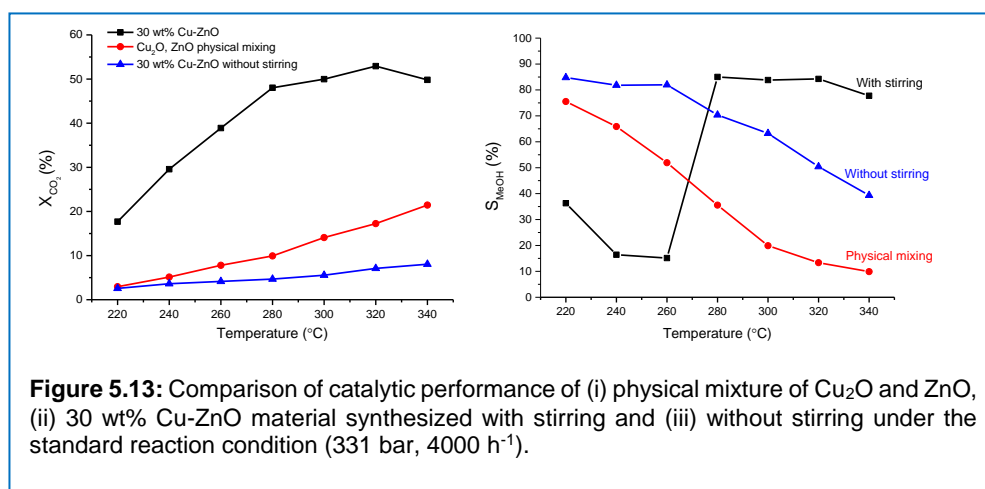
In literature, ZnCO₃ (smithsonite) phase has rarely been reported to be formed or present in methanol synthesis reaction from CO/CO₂, although recently Ash-Kurlander et al. identified such phase in CO₂-based methanol synthesis and reported that the acidic pH during the reaction was responsible for dissolution of ZnO in aqueous carbonic acid solution and its transformation from ZnO to ZnCO₃ [24]. However, effects of the ZnCO₃ phase on the catalytic activity are not known to date. To understand the relations between the ZnCO₃ formation and catalytic activity, 30 wt% Cu-ZnO was evaluated for its catalytic

Cu-ZnO core-shell catalysts prepared by non-aqueous sol-gel method

performance under different pressure and temperature conditions (Appendix Figure B5.3) and by XRD after the reaction (Appendix Figure B5.4). The great effects of reaction pressure on the catalytic performance were evident as described in Chapter 3. The selectivity changes from CO to methanol under the high pressure condition (331 bar) as discussed previously seems related to the reaction pressure and/or resulting catalytic activity (Appendix Figure B5.3). The XRD results (Appendix Figure B5.4) clearly show that the material structure is markedly different with a clear appearance of ZnCO_3 after the catalytic test at 331 bar in comparison to those after the tests at 27 and 184 bar. The origin of ZnCO_3 formation and also its impacts on the catalytic performance are further discussed in section 5.3.9.

5.3.6 Catalyst evaluation: Effects of Cu-Zn proximity

The above study where Cu and Zn contents in the core-shell structure are varied indicated that the interaction between Cu and Zn is indeed important for the catalytic activity, even suggesting a formation of highly dispersed Cu particle/layer over the Zn-containing phase. To further verify this synergetic function of Cu-ZnO, two materials, the catalytic performance of (i) physical mixture of Cu_2O and ZnO and (ii) Cu-ZnO synthesized without stirring (Figure 5.1c) was evaluated and the results are shown in Figure 5.13.

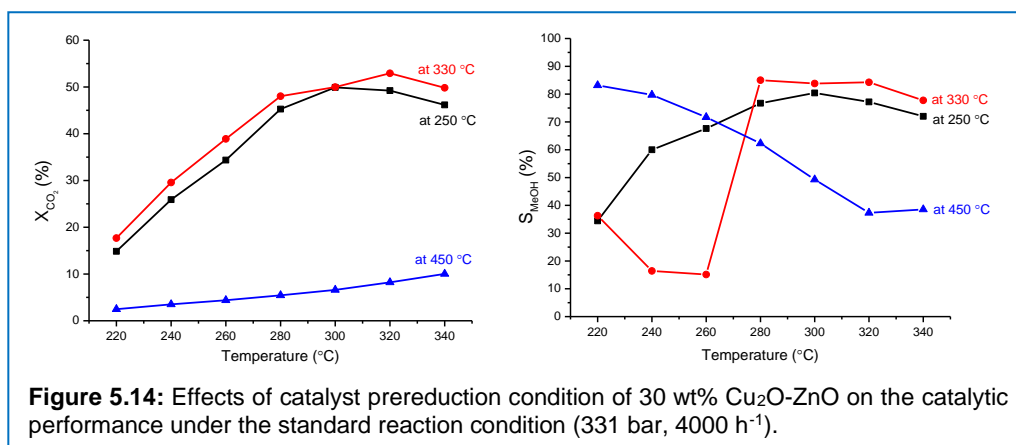


Chapter 5

Considerably lower catalytic activity was observed for the physical mixture of Cu_2O and ZnO as well as Cu-ZnO synthesized without stirring compared to Cu-ZnO synthesized with stirring, although the first two materials showed higher methanol selectivity at low CO_2 conversion (low temperature), indicating direct methanol synthesis as the main path at this temperature (Chapter 4), which was not the case for the core-shell material. These results show that the morphology and/or the close contact between Cu and Zn components are highly beneficial and important for high-performance methanol synthesis, providing Cu-Zn interface sites considered as the very active phase [10]. Also, the findings are in line with the high methanol selectivity at low temperature of extended Cu surface suggested previously for 70 wt% Cu-ZnO .

5.3.7 Catalyst evaluation: Effects of pre-reduction temperature

An experimental factor known to influence the catalytic performance in methanol synthesis using Cu -based catalysts is the reduction pretreatment condition under hydrogen atmosphere. Therefore, the effects were examined for the best performing material in methanol synthesis, 30 wt% $\text{Cu}_2\text{O-ZnO}$, reduced at three temperatures (250, 330 and 450 °C). These temperatures were chosen because three representative catalyst states can be covered: prior to the reduction of Cu_2O phase (250 °C), right after the major completion of the Cu_2O phase (330 °C) and then thorough reduction of Cu_2O (450 °C) as indicated by *in situ* XRD (red boxes in Figure 5.7). The catalytic performance of the $\text{Cu}_2\text{O-}$



Cu-ZnO core-shell catalysts prepared by non-aqueous sol-gel method

ZnO material reduced at the three temperatures is shown in [Figure 5.14](#), evidencing great impacts of the pretreatment on the catalytic performance. The catalyst reduced at 250 and 330 °C exhibited similar catalytic performance with three differences: (i) generally higher CO₂ conversion when reduced at 330 °C, (ii) higher methanol selectivity at lower temperature (<270 °C) for the material reduced at 250 °C and (iii) higher methanol selectivity at higher temperature (>270 °C) for the material reduced at 330 °C. Although the material reduced at 250 °C was not fully reduced to Cu (0) from the bulk point of view, the surface of the material was likely reduced and thus it showed the high activity. In contrast, when the material was reduced at 450 °C the catalytic performance dropped significantly, although the highest methanol selectivity was observed below 270 °C. This may be again the effect of Cu sintering and formation of extended Cu surface promoting direct methanol synthesis despite the low CO₂ conversion. The materials reduced at the three temperatures were studied by XRD after the reaction and the results are shown in [Figure 5.15](#). What is striking is that the same material reduced at three different temperatures shows largely

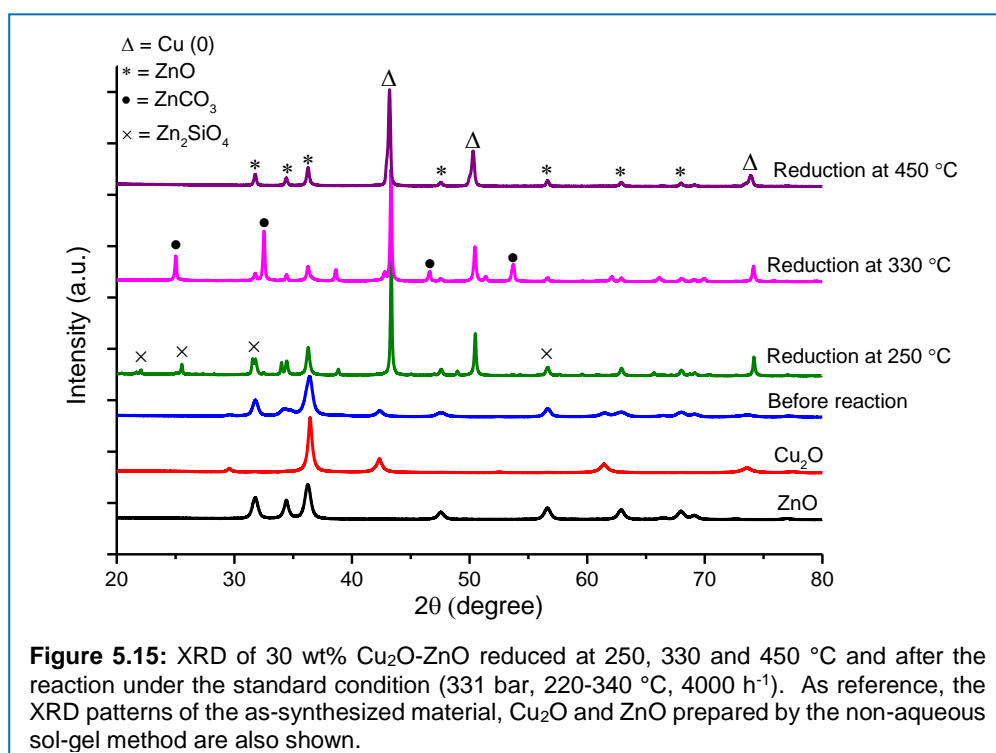


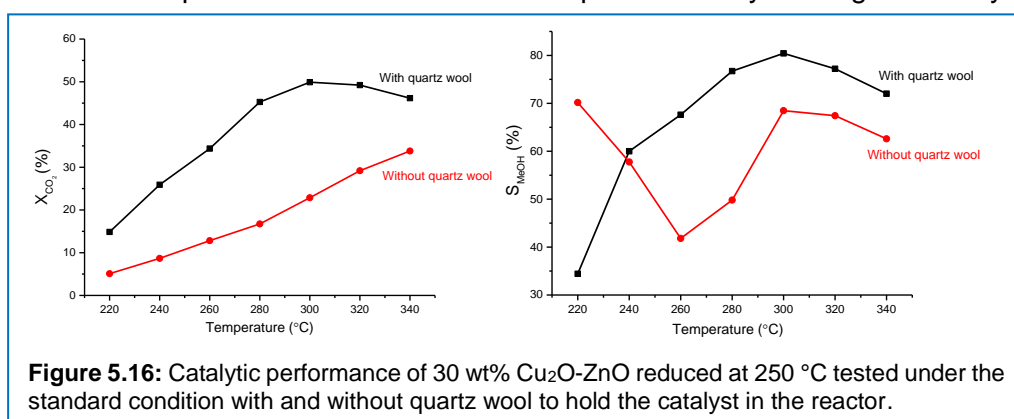
Figure 5.15: XRD of 30 wt% Cu₂O-ZnO reduced at 250, 330 and 450 °C and after the reaction under the standard condition (331 bar, 220-340 °C, 4000 h⁻¹). As reference, the XRD patterns of the as-synthesized material, Cu₂O and ZnO prepared by the non-aqueous sol-gel method are also shown.

Chapter 5

different XRD patterns after the reaction. As discussed above, for the material reduced at 330 °C, there was a dominant formation of ZnCO_3 .

To our surprise, this phase was not observed for the other two materials. When the material was reduced at 250 °C, there was a formation of Zn_2SiO_4 (JCPDS: 00-008-0492), although Si source was not fed into the reactor. On the contrary, there was no new phase formed upon reduction at 450 °C and Zn component was present as ZnO. The reduction treatment at this high temperature has led to the formation of stable ZnO as discussed above, likely with a loss of highly dispersed Cu under the reaction condition. All these observations strongly suggest that ZnO present in the 30 wt% Cu_2O -ZnO material is highly reactive, especially when reduced at lower temperature, and dynamically readjust its state according to its environment.

The formation of Zn_2SiO_4 has never been reported and the fact is intriguing. As explained in [Chapter 2](#) (Catalyst packing) quartz wool used to fix the catalyst bed in the reactor is the only source of silicon in the reactor system. Thus it is speculated that the ZnO after the low temperature reduction is so active that it reacts with the quartz which is in contact with the material. To examine the effects of this Zn_2SiO_4 phase formation on catalytic activity (or *vice versa*), the reaction was performed without the use of quartz wool by holding the catalyst



with 10 μm stainless steel frit. [Figure 5.16](#) compares the catalytic performance with and without quartz wool to fix the catalyst bed.

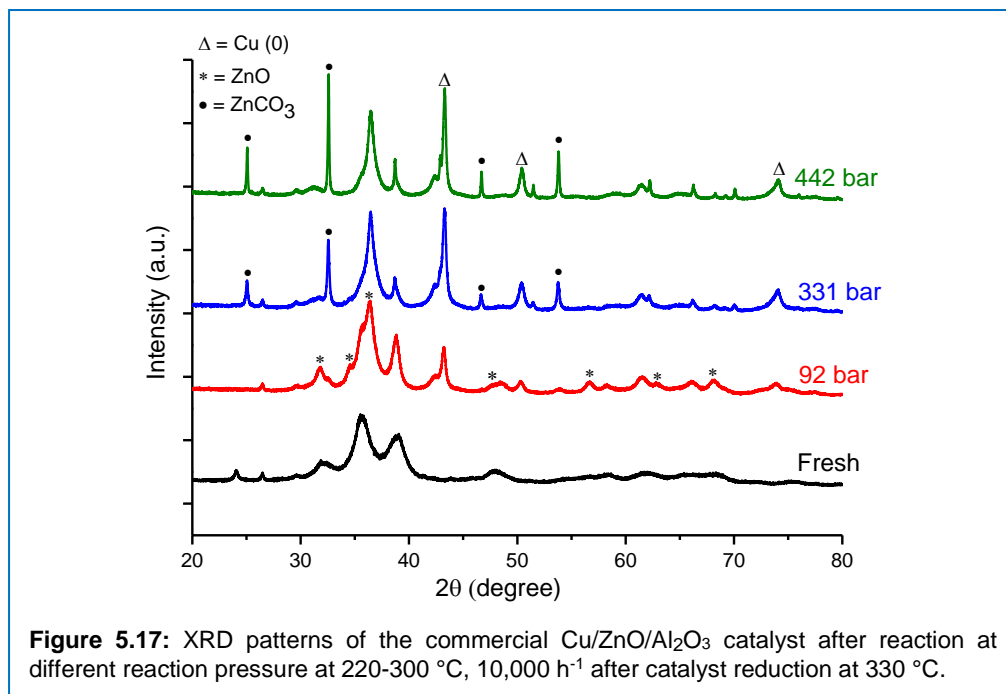
Cu-ZnO core-shell catalysts prepared by non-aqueous sol-gel method

Evidently, the results are different and higher catalytic performance was observed with quartz wool to hold the catalyst bed. No Zn_2SiO_4 phase was observed after the reaction without quartz wool and, instead, only ZnO was detected (Appendix B, Figure B5.5). The exact role of Zn_2SiO_4 is out of the scope of this work, but the rather similar catalytic performance of the materials reduced at 250 and 330 °C points out that actually the state of Zn component may not be of the critical importance for catalytic performance and rather the influence of their state and morphology on that of Cu is more critical. The structural effects of Zn_2SiO_4 and ZnCO_3 are likely similar, assisting higher dispersion of Cu sites over these Zn materials (crystallite size of ZnCO_3 and Zn_2SiO_4 was 72 nm and 60 nm respectively) (Figure 5.12). On the contrary, although Cu core does not sinter after the reduction at 450 °C, the reactivity drops markedly. Most probably, this is due to the higher crystallinity of the ZnO in the shell, as ZnO agglomerates and crystallite size of ZnO increases from 20 nm to 229 nm and thus lowering its surface area and consequently lowering the dispersion of active Cu species.

5.3.8 *Operando* XRD

To understand further the criteria for the ZnCO_3 phase formation observed only under highly performing high-pressure conditions, *operando* high-pressure XRD measurements were performed (Appendix Figure B5.6). The study was first attempted with 30 wt% Cu-ZnO, but due to the small particle nature (<10 μm particle size and filled in 150 μm ID capillary reactor), the pressure drop was too high and the catalytic performance was very low; thus no phase change of ZnO was observed. For this reason, the structural change of the commercial methanol catalyst before and after the reaction was investigated to verify whether the formation of ZnCO_3 is generic for Cu- and Zn-containing catalyst or

Chapter 5

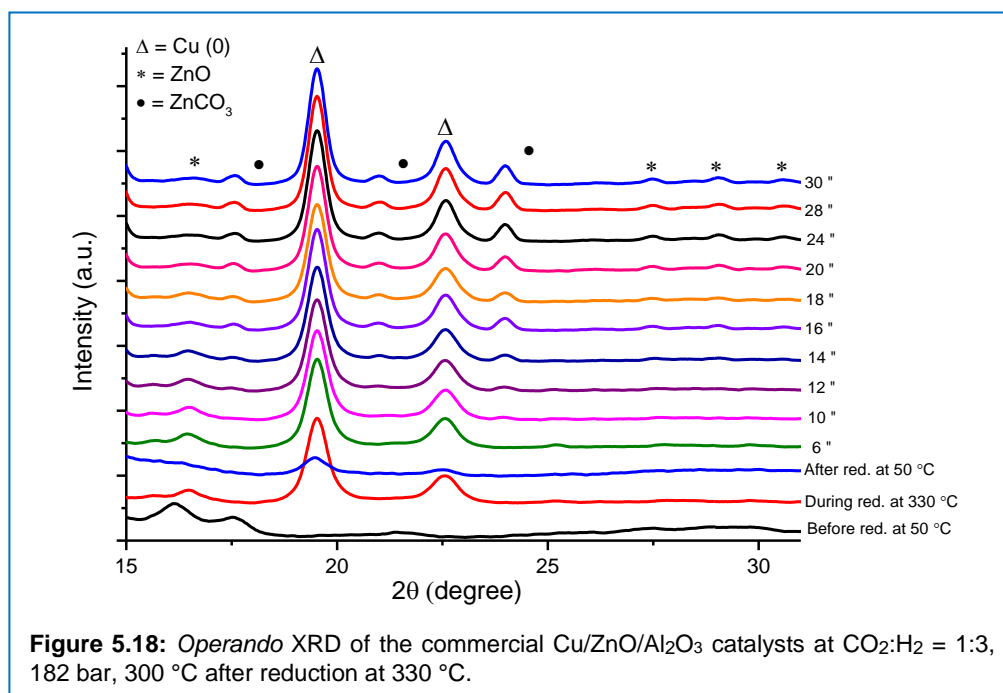


not. **Figure 5.17** shows the catalyst before and after the reaction performed at different pressure conditions (92, 331 and 442 bar).

The results confirm that the formation of ZnCO₃ is indeed generic to the Cu-Zn catalytic systems and the formation is more prominent at high pressure conditions. A closer look at the XRD patterns indicates that the initial ZnO phase is replaced to a greater extent by ZnCO₃ at higher reaction pressure, accompanying higher crystallinity of both Cu and Zn phases.

Figure 5.18 shows *operando* XRD patterns of the commercial Cu/ZnO/Al₂O₃ catalyst during the stoichiometric CO₂ hydrogenation to methanol at 182 bar at the reaction temperature of 300 °C after the reduction treatment at 330 °C. This study clearly confirms the rapid and gradual formation of ZnCO₃ and that the phase is formed during the reaction under the high-pressure condition and not after the reaction and exposing the catalyst to the air.

Cu-ZnO core-shell catalysts prepared by non-aqueous sol-gel method



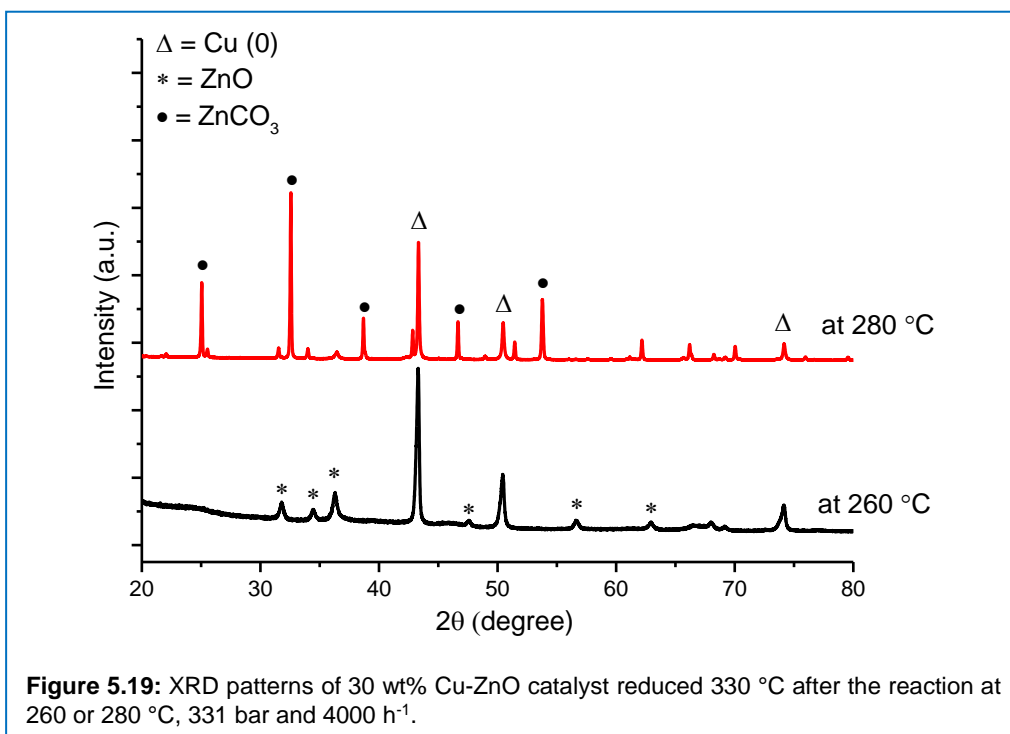
5.3.9 Relation between ZnCO₃ formation and catalytic activity

Figure B5.6 (Appendix B) and Figure 5.17 clearly showed ZnCO₃ formation under high-pressure conditions, but at the same time the formation was observed at lower pressure for the commercial catalyst (e.g. 92 bar). This implies that the formation may not be induced by the high pressure conditions, but rather induced by the high reactivity, more precisely by the formation of the dense product phase (liquid/supercritical) which is expected under high-pressure conditions.

There was a drastic selectivity change in a narrow temperature range of 260-280 °C from CO to methanol when the reaction temperature was raised using 30 wt% Cu-ZnO reduced at 330 °C (e.g. Figure 5.9). To elucidate the material factors directing the product selectivity, the representative materials, namely after the reaction at 260 and 280 °C, were studied by XRD. Figure 5.19 shows the results, highlighting the striking differences in the two XRD patterns with a clear formation of ZnCO₃ at 280 °C. The portion of Zn-containing phases (ZnCO₃/ZnO) was 0.0/69.2 wt% at 260 °C vs. 66.4/2.4 wt% at 280 °C according

Chapter 5

to the quantitative phase analysis. This is indicative of the product induced phase transformation rather than the effect of reaction pressure.

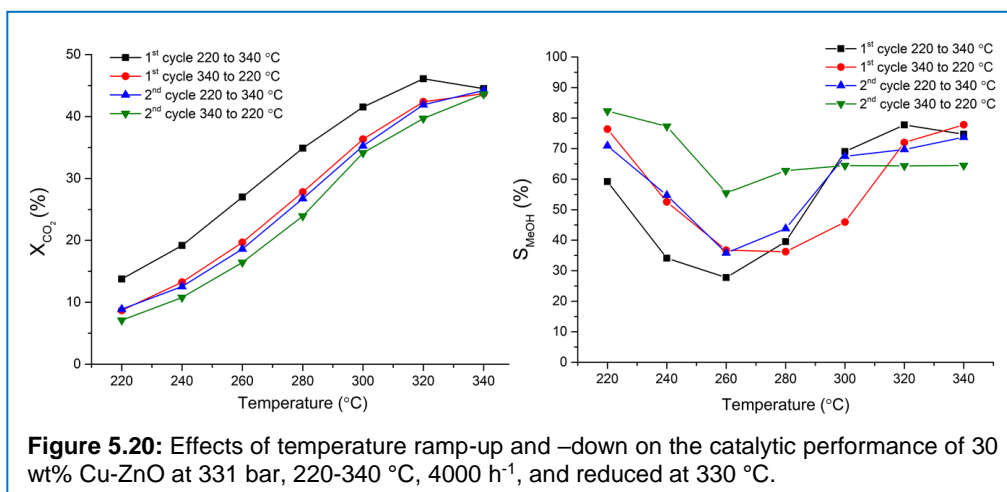


Above 280 °C, the methanol selectivity was remarkably enhanced for 30 wt% Cu-ZnO (Figure 5.9). Still one question remains: Is this state of Cu highly dispersed over ZnCO₃ (Figure 5.12) responsible for boosted methanol selectivity? To answer this question, the reaction was performed in a ramp-up and ramp-down cycle and repeated for 2 cycles. The catalytic results of this cycling study are presented in Figure 5.20. Based on the CO₂ conversion, some catalyst deactivation was observed after the first ramp-up, but then the catalytic activity remained relatively stable, although slight continuous decrease in CO₂ conversion could be noticed. This may be due to an irreversible structural change owing to the catalytic tests at up to relatively high temperature (340 °C). In contrast, the selectivity to methanol changed more drastically at each ramp-up and ramp-down step. During the first ramp-down, the drop in methanol selectivity in the middle temperature range was also observed, although the

Cu-ZnO core-shell catalysts prepared by non-aqueous sol-gel method

temperature at the minimum selectivity is shifted to a higher value. Further ramp-up (the second cycle) showed again the profile similar to the first cycle with somewhat higher selectivity to methanol. Interestingly, during the ramp-down of the second cycle, the drop in methanol selectivity was less pronounced and methanol selectivity became more constant.

The drop in methanol selectivity in the middle temperature range during the first ramp-down and the second ramp-up cycles as observed during the first ramp-up cycle indicates that the sudden selectivity change does not originate from the unique role of ZnCO_3 interacting with Cu and rather it originates most likely from the activity of the catalyst of that moment and phase behavior (product condensation) determined by the amount of products. Especially, during the first ramp-up step, due to the product water formation and high CO_2 pressure, highly acidic liquid/dense phase containing carbonic acid is likely formed, transforming most of ZnO into ZnCO_3 . This is in accordance with the pressure-dependent formation of ZnCO_3 observed for the commercial catalyst (Figure 5.20). However, as the cycle number increases, the catalyst loses its activity to some extent probably by further crystallization of ZnCO_3 and also consequent sintering of Cu. Notably, this stabilized state is beneficial to enhance methanol selectivity at low temperature range with a minor drop in CO_2 conversion. This is in agreement with the discussion above and the reported high selectivity to methanol over extended Cu surfaces in CO_2 hydrogenation.



Chapter 5

This porous but rigid structure of ZnCO_3 can be highly beneficial for the catalyst stability and methanol selectivity.

5.4 Conclusions

A surfactant-free, non-aqueous sol-gel method was developed to synthesize Cu-ZnO core-shell materials to investigate the unique Cu-Zn interface for methanol synthesis and to enhance thermal stability of active Cu sites. Through variation of the amount of Cu and Zn precursors, Cu_2O -ZnO core-shell structures were obtained. Materials with Cu_2O core and with highly dispersed ZnO nanoparticles layer were successfully synthesized.

30 wt% Cu_2O -ZnO showed the best catalytic performance with 52% CO_2 conversion and 84% methanol selectivity in the stoichiometric CO_2 hydrogenation to methanol at 331 bar. The high catalytic performance was attributed to the unique state of Cu in the shell of the catalyst rather than the core-shell structure. During the reaction, the core-shell structure was retained, but ZnO-shell structure underwent major phase transformation to ZnCO_3 . Electron microscopic studies showed that Cu, present in the shell layer, became well dispersed over the likely-rigid porous matrix consisting of ZnCO_3 nanomaterials. The formation of ZnCO_3 coincided with the selectivity boost towards methanol and also it was pressure-dependent; thus, this Zn phase transition was attributed to the highly acidic medium generated by CO_2 and H_2O contained in the feed/product under high-pressure conditions and therefore it was only observable above certain reaction pressure and CO_2 conversion. High-pressure *operando* XRD study using the commercial Cu/ZnO/ Al_2O_3 catalyst showed that ZnCO_3 is also observed for this case, showing the generality of this phase formation under high-pressure conditions.

The effects of Cu-ZnO proximity and pre-reduction temperature were examined. In both studies, Cu-ZnO proximity on nano-scale was found critical for the catalytic activity, although high methanol selectivity at low temperature was consistently observed for the materials where Cu is agglomerated (e.g. less

Cu-ZnO core-shell catalysts prepared by non-aqueous sol-gel method

Cu-ZnO contact or high reduction temperature) despite low CO₂ conversion. The reduction temperature had striking effects on the reactivity of the ZnO shell itself. After the reaction at 331 bar, the formation of ZnCO₃ and Zn₂SiO₄ phases was identified for the materials (30 wt% Cu₂O-ZnO) reduced at 330 and 250 °C, respectively. Only ZnO was observed when reduced at 450 °C. The differences are significant, but the type of Zn phase seems unimportant for the catalytic activity and rather how Cu is dispersed, thus the sintering of Zn component, seems more decisive for the catalytic performance.

This study showed that Cu core and ZnO shell structures are beneficial to keep the dispersion of Cu at the size of Cu core. However, at the same time it also showed that the main catalytic activity arises from the Cu nanoparticles/layer closely interacting with the Zn-component matrix in the shell layer. Non-aqueous sol-gel method was found to be very effective and tunable in designing Cu-Zn containing nanomaterials. Further future research directions using the synthesis method are expected to maximize the Cu dispersion in the form of simple Cu-Zn nanocomposites or to reduce the size of Cu core maximally to enhance the activity and stability of Cu-ZnO catalysts.

Chapter 5

Bibliography

- [1] W. Wang, S. Wang, X. Ma, J. Gong, *Chem. Soc. Rev.*, 40 (2011) 3703-3727.
- [2] O. Martin, C. Mondelli, A. Cervellino, D. Ferri, D. Curulla-Ferre, J. Perez-Ramírez, *Angew. Chem. Int. Ed.*, 55(21), (2016), pp. 6261-5.
- [3] L. Martinez-Suarez, J. Frenzel, D. Marx, B. Meyer, *Phys. Rev. Lett.*, 110 (2013) 086108.
- [4] G. Prieto, J. Zecevic, H. Friedrich, K.P. de Jong, P.E. de Jongh, *Nat. Mater.*, 12 (2013) pp. 34-39.
- [5] A. Karelavic, A. Bargibant, C. Fernandez, P. Ruiz, *Catal. Today.*, 197 (2012) pp. 109-118.
- [6] S. Natesakhawat, J.W. Lekse, J.P. Baltrus, P.R. Ohodnicki, B.H. Howard, X. Deng, C. Matranga, *ACS Catal.*, 2 (2012) pp. 1667-1676.
- [7] F.C. Meunier, *Angew. Chem. Int. Ed.*, 50 (2011) pp. 4053-4054.
- [8] S. Kuhl, A. Tarasov, S. Zander, I. Kasatkin, M. Behrens, *Chemistry*, 20 (2014) pp. 3782-3792.
- [9] C. Tisseraud, C. Comminges, S. Pronier, Y. Pouilloux, A. Le Valant, *J. Catal.*, 343, (2016), pp. 106-114.
- [10] C. Tisseraud, C. Comminges, T. Belin, H. Ahouari, A. Soualah, Y. Pouilloux, A. Le Valant, *J. Catal.*, 330 (2015) pp. 533-544.
- [11] S. Kattel, P.J. Ramírez, J.G. Chen, J.A. Rodriguez, P. Liu, *Science*, 355 (2017) pp. 1296-1299.
- [12] G.J. Millar, C.H. Rochester, S. Bailey, K.C. Waugh, *J. Chem. Soc. Faraday Trans.*, 89 (1993) pp. 1109-1115.
- [13] M. Sano, T. Adaniya, T. Fujitani, J. Nakamura, *J. Phys. Chem. B*, 106 (2002) pp. 7627-7633.
- [14] Z. Wang, H. Fu, Z. Tian, D. Han, F. Gu, *Nanoscale*, 8 (2016) pp. 5865-5872.
- [15] B.L. Cushing, V.L. Kolesnichenko, C.J. O'Connor, *Chem. Rev.*, 104 (2004) pp. 3893-3946.
- [16] M. Niederberger, G. Garnweitner, *Chem. Eur. J.*, 12 (2006) pp. 7282-7302.
- [17] G. Garnweitner, M. Niederberger, *J. Am. Ceram. Soc.*, 89 (2006) pp. 1801-1808.
- [18] M. Niederberger, M.H. Bartl, G.D. Stucky, *J. Am. Ceram. Soc.*, 124 (2002) pp. 13642-13643.
- [19] M. Niederberger, N. Pinna, J. Polleux, M. Antonietti, *Angew. Chem. Int. Ed.*, 43 (2004) pp. 2270-2273.
- [20] I. Bilecka, I. Djerdj, M. Niederberger, *ChemComm*, (2008) pp. 886-888.
- [21] N. Pinna, G. Garnweitner, M. Antonietti, M. Niederberger, *Adv. Mater.*, 16 (2004) pp. 2196-2200.
- [22] H.H. Kung, *Catal. Today.*, 11 (1992) pp. 443-453.
- [23] A. Bansode, B. Tidona, P.R. von Rohr, A. Urakawa, *Catal. Sci. Technol.*, 3 (2013) pp. 767-778.
- [24] U. Ash-Kurlander, O. Martin, L.D. Fontana, V.R. Patil, M. Bernegger, C. Mondelli, J. Pérez-Ramírez, A. Steinfeld, *Energy Technology*, 4 (2016) pp. 565-572.

6.

Conclusions and outlook

Chapter 6

6.1 General conclusions

CO₂ utilization for the synthesis of chemicals or fuels is expected to significantly contribute to reduce anthropogenic CO₂ emission and thus limit its substantial impact on global warming. Methanol, among other chemicals, is one of the most promising future chemical energy carriers as well as C1 feedstock, thus drawing global attention as the target molecule produced from CO₂. High-pressure advantages under over-stoichiometric CO₂:H₂ ratio (1:>3) have been reported previously by drastically increasing the reaction kinetics and even reaching the thermodynamic conversion. However, the major drawback of such processes is the treatment of unreacted hydrogen. In addition, there are obvious necessities to improve the catalyst and also to understand reaction mechanisms towards rational catalyst and process development. Reflecting this background, this thesis aims to (i) critically evaluate the advantages of the high pressure approach in stoichiometric CO₂:H₂ (1:3) ratio by examining different reaction and process parameters, (ii) investigate the reaction mechanism characteristic to high-pressure conditions, and (iii) develop thermally stable and highly active catalysts comprising of Cu-ZnO core-shell nanomaterials.

First, a high-pressure lab scale reactor setup for the continuous catalytic hydrogenation of CO₂ to methanol at pressures up to 510 bar was successfully constructed. The operation of the reactor system was controlled by software implementing safety measures, thus allowing unattended catalytic tests for a long period of time. Using this reactor system, advantages of high-pressure conditions under the stoichiometric reaction condition were evaluated in-depth using a commercial Cu/ZnO/Al₂O₃ catalyst. A strong interplay between kinetics and thermodynamics in the reaction performance were evidenced. At kinetically favorable high temperature (>260 °C) especially at lower GHSV, it was possible to enter the regime where thermodynamic equilibrium plays dominant roles in determining the catalytic activity. A good weight time yield (WTY) of 0.92 g_{MeOH} g_{cat}⁻¹ h⁻¹ was achieved at 442 bar with 88.5% CO₂

conversion and 97.2% methanol selectivity using our standard size of catalyst particles (100-300 μm). However, above 331 bar there was a formation of dense reaction mixture due to product condensation and thus the overall reaction rate was limited by internal mass transfer. When smaller catalyst particles (10-20 μm) were used instead, the limitation could be effectively removed. Thus obtained catalytic performance fully benefited from the high-pressure advantages of high reaction rate (kinetics), high equilibrium conversion (thermodynamics) and enhanced conversion (phase separation). Under these conditions of negligible mass transfer limitations at 442 bar, a very good WTY of 2.4 $\text{g}_{\text{MeOH}} \text{g}_{\text{cat}}^{-1} \text{h}^{-1}$ could be observed with 87.7% CO_2 conversion and 97.6% methanol selectivity. At a very high GHSV (100000 h^{-1}), an extraordinary WTY of 15.2 $\text{g}_{\text{MeOH}} \text{g}_{\text{cat}}^{-1} \text{h}^{-1}$ could be achieved.

To gain insights into the reaction mechanisms under high pressure, a mechanistic study using the commercial $\text{Cu}/\text{ZnO}/\text{Al}_2\text{O}_3$ catalyst was performed by space-resolved sampling of the reaction mixture from three different locations along the axial direction of the catalytic reactor. The results showed that CO_2 was directly converted to methanol at low temperature (180 $^\circ\text{C}$) and a small amount of detected CO resulted from methanol decomposition. A contrasting mechanism was observed at 340 $^\circ\text{C}$, where the endothermic reverse water-gas shift (RWGS) reaction dominated, producing CO as the major product. Importantly, this CO could then be hydrogenated to produce methanol. At 260 $^\circ\text{C}$ catalytic activity was high, the results showed RWGS and CO to methanol reactions are in equilibrium and resulted into high methanol concentration. These mechanistic insights were further verified by *operando* Raman concentration profiling using a sapphire capillary reactor and looking into the void space between the catalyst beds at 184 bar. A similar trend as the case sampled by GC was confirmed; at 180 $^\circ\text{C}$ preferential direct methanol formation and later methanol decomposition took place as confirmed by the change in H_2/CO_2 ratio. At higher temperature (260 $^\circ\text{C}$) initially H_2/CO_2 ratio was increased due to CO formation by RWGS and later lowering ratio

Chapter 6

indicates CO transformation to methanol. A liquid product condensation was observed at this condition at the end of the reactor, which was beneficial and responsible for high catalytic activity.

Cu-based catalysts are widely known for their excellent activity in the methanol synthesis reaction; however, copper agglomeration at higher temperature can lead to catalyst deactivation. With the aim to enhance the stability of Cu-based catalysts, Cu-ZnO core-shell catalyst, where Cu₂O spherical core is coated with ZnO nanoparticles, was synthesized by a newly designed protocol based on the non-aqueous sol-gel method. This morphology separates the Cu particles by thermally stable Zn component and also provides high Cu-ZnO interfacial area, which is considered to be an important factor for methanol synthesis. A series of 15, 30, 50 and 70 wt% Cu₂O-ZnO catalysts were synthesized and tested under various methanol synthesis conditions. 30 wt% Cu-ZnO showed the highest CO₂ conversion (52%) and methanol selectivity (84%) at 300 °C, 331 bar. The high catalytic performance was attributed to the unique state of Cu in the shell of the catalyst rather than the core-shell structure. The catalysts before and after the reaction was characterized by XRD, STEM-EDX. Interestingly, 30 wt% and 50 wt% Cu-ZnO catalyst showed emergence of ZnCO₃ phase after the reaction. Electron microscopic studies showed that Cu, present in the shell layer, became well dispersed over the likely-rigid porous matrix consisting of ZnCO₃ nanomaterials. The Zn phase transition was attributed to the highly acidic medium generated by CO₂ and H₂O contained in the feed/product under high-pressure conditions and therefore it was only observable above certain reaction pressure and CO₂ conversion. High-pressure *operando* XRD study using the commercial Cu/ZnO/Al₂O₃ catalyst showed that ZnCO₃ is also observed for this case, showing the generality of this phase formation under high-pressure conditions.

6.2 Outlook

During this study, many interesting questions arose which might encourage further research in this direction. As aforementioned, methanol synthesis was investigated at stoichiometric $\text{CO}_2:\text{H}_2$ ratio (1:3) under a wide range of process. The most striking results were obtained at the highest examined pressure (442 bar) due to the product condensation, i.e. phase separation [1]. However, mass transfer limitations were also observed under such conditions, restricting the efficiency of the catalyst. The limitations were minimized by reducing catalyst particle size, but the reduction in particle size increases the pressure drop and thus become irrelevant in practice. Lowering space velocity significantly improves the internal mass transfer, but methanol WTY is consequently lowered. Considering the unique advantages of high pressure conditions, it would be very interesting to develop a catalyst or a catalytic system which will intrinsically minimize mass transfer limitations as well as pressure drop. One of the promising approaches is to use structured catalysts like honeycomb-shape monolith, which can offer minimum pressure drop, high geometric surface, high surface to volume ratio and importantly good heat distribution [2, 3]. Hence the use of thermally conductive Cu, Al-based monolith catalysts are likely advantageous over powder packed-bed catalyst to manage precisely the mass transfer properties.

In addition to mass transfer limitations, agglomeration of copper particles during the reaction is observed due to the low thermal stability of Cu. Although the developed core-shell Cu-ZnO shows excellent catalytic activity with high Cu-ZnO interfacial area and high thermal stability at elevated temperatures, the large particle size of the materials reduces active copper surface area for methanol synthesis. At the end, to achieve better catalytic activity, especially to reach equilibrium conversion at low reaction temperature, one needs a catalyst with a very high active Cu surface area which is protected against sintering. Interestingly, during catalytic testing using Cu-ZnO core-shell nanomaterials, we observed formation of ZnCO_3 phase from ZnO. Detailed

Chapter 6

investigation of ZnCO_3 phase formation by high pressure *operando* XRD revealed that the phase transformation took place due to dissolution of ZnO in dense high pressure aqueous phase of reaction mixture. This phase helps to isolate the copper particles and avoid agglomeration by forming solid ZnCO_3 coating. Hence, when a nano-sized Cu is well protected by e.g. nano-ZnO layer, great enhancement of catalytic activity is expected. If the aforementioned mass transfer limitation is also minimized, the catalyst would be ideal for CO_2 to methanol conversion.

Thus, a promising catalyst would be a structured one with high Cu surface area and at the same time maximally avoiding sintering of active Cu metal. I envision that a nano-foam catalyst coated over a monolith structure can offer great potential to boost the methanol yield under high-pressure conditions. In this regard, use of self-assembled multilayered colloidal arrays by the vertical deposition technique is a promising option. By the self-assembly of polymer opals, e.g. made of polystyrene and PMMA monodisperse nano-/micro-spheres, the synthesis method can provide a long-range 3-D arrangement of nanomaterials deposited on a desired substrate.

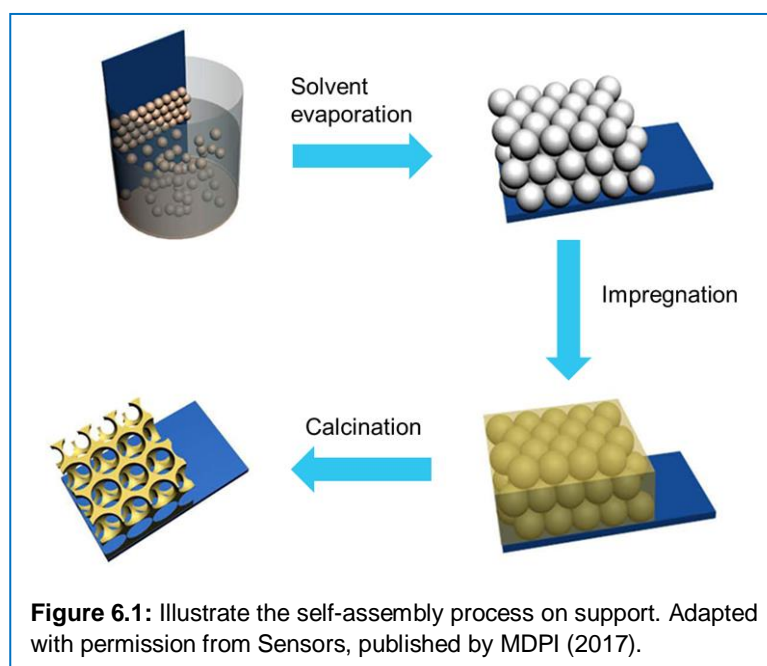


Figure 6.1: Illustrate the self-assembly process on support. Adapted with permission from Sensors, published by MDPI (2017).

Figure 6.1 illustrates the synthesis method; first a self-assembly process of polymer opals on a support and solvent drying, followed by precursor addition and calcination treatment, resulting in a foam material with 3D-structured hollows with the size of the nano-/micro-spheres [4]. The high tenability of porosity of such materials is obvious and it is possible to incorporate materials of different sizes into the interstices of the structure. In case of methanol synthesis the hollow 3D structure can be made of either Cu or ZnO and then the surface of the hollow structure can be coated with ZnO or Cu nanoparticles, respectively thus, maximizing the contact between Cu and ZnO while attaining the path for fluid transport thus preventing mass transfer limitations.

The mechanistic study of high-pressure CO₂ hydrogenation to methanol presented in the thesis shows that methanol decomposition becomes more prominent at higher temperature, although high-pressure conditions can suppress the unfavored methanol decomposition to a good extent. Thus performing the reaction at lower temperature is advantageous but in this case highly active catalyst is demanded to be kinetically enabled to reach the beneficial equilibrium conversion. If the above structured catalyst with an extraordinarily high Cu-ZnO active surface area could be synthesized, it is expected that the catalytic performance will be boosted significantly because of the excellent low-temperature activity as well as facilitated phase condensation at low temperature (hence the enhanced equilibrium shift toward methanol takes place), thus leading to boosted methanol yield.

Bibliography

- [1] J.G. van Bennekom, R.H. Venderbosch, J.G.M. Winkelman, E. Wilbers, D. Assink, K.P.J. Lemmens, H.J. Heeres, *Chem. Eng. Sci.*, 87 (2013) pp. 204-208.
- [2] M. Johansson, D. Papadias, P.O. Thevenin, A.G. Ersson, R. Gabrielson, P.G. Menon, P.H. Bjornborn, S.G. Jaras, *Catalytic combustion for gas turbine applications*, *Catalysis: Volume 14*, RSC, 1999, pp. 183-235.
- [3] G. Groppi, E. Tronconi, *Catal. Today*, 69 (2001) pp. 63-73.
- [4] R. Xing, Y. Du, X. Zhao, X. Zhang, *Sensors*, 17 (2017) pp. 710-721.

Chapter 6

Appendix

A

Supplementary information of Chapter 3

Table A3.1: Effect of GHSV on CO₂ and H₂ conversions, product selectivity and WTY of methanol using Cu/ZnO/Al₂O₃ catalyst at 442 bar, 280 °C, and CO₂:H₂ = 1:3.

GHSV (h ⁻¹)	Conv. (%)		Sel. (%)			WTY (mg _{MeOH} g _{cat} ⁻¹ h ⁻¹)		
	CO ₂	H ₂	CO	CH ₄	MeOH	CO	CH ₄	MeOH
650	89.9	87.8	6.2	6.2	87.6	8.3	4.6	133.7
2000	90.7	86.5	3.9	1.4	94.8	17.4	3.3	487.6
4000	88.5	86.8	1.9	0.9	97.2	37.5	5.2	920.4
6000	88.0	84.3	3.0	0.5	96.5	61.0	3.4	1402.6
8000	86.1	84.2	5.5	0.4	94.1	88.9	3.6	1776.4
10000	84.7	81.9	6.6	0.4	93.1	135.1	4.1	2177.8
30000	61.3	59.0	18.3	0.0	81.7	708.3	0.0	3948.1
60000	45.1	41.1	39.7	0.0	60.3	2664.7	0.0	4465.9
100000	31.8	27.2	42.8	0.0	57.2	3427.5	0.0	4964.2

Appendix A

Table A3.2: Effect of GHSV on CO₂ and H₂ conversions, product selectivity and WTY of methanol using Cu/ZnO/Al₂O₃ catalyst at 331 bar, 260 °C, and CO₂:H₂ = 1:3.

GHSV (h ⁻¹)	Conv. (%)		Sel. (%)			WTY (mg _{MeOH} g _{cat} ⁻¹ h ⁻¹)		
	CO ₂	H ₂	CO	CH ₄	MeOH	CO	CH ₄	MeOH
650	89.0	85.0	1.4	0.7	97.8	1.9	0.6	154.5
2000	86.5	85.1	2.2	0.4	97.4	9.4	1.1	477.8
4000	83.3	83.2	3.0	0.2	96.8	12.2	0.5	885.4
6000	74.8	72.3	3.9	0.1	96.0	14.5	0.2	1187.2
8000	69.5	66.8	4.3	0.1	95.5	14.8	0.3	1590.9
10000	61.0	58.8	6.1	0.1	93.7	97.0	1.3	1692.8
30000	40.2	37.6	13.9	0.0	86.2	397.8	0.0	2826.6
60000	33.2	27.9	23.8	0.1	76.1	564.0	0.7	4082.6
100000	25.3	20.4	30.0	0.0	70.0	541.5	0.2	4867.8

Table A3.3: Effect of GHSV on CO₂ and H₂ conversions, product selectivity and WTY of methanol using Cu/ZnO/Al₂O₃ catalyst at 184 bar, 280 °C, and CO₂:H₂ = 1:3.

GHSV (h ⁻¹)	Conv. (%)		Sel. (%)			WTY (mg _{MeOH} g _{cat} ⁻¹ h ⁻¹)		
	CO ₂	H ₂	CO	CH ₄	MeOH	CO	CH ₄	MeOH
650	37.3	33.3	7.0	1.7	91.0	4.1	0.5	60.2
2000	44.1	41.7	8.5	0.6	90.9	18.9	0.7	228.3
4000	47.1	43.5	11.9	0.3	87.8	55.3	0.8	460.4
6000	46.4	43.6	13.5	0.4	86.1	91.8	1.0	662.4
8000	47.0	44.4	15.1	0.1	84.8	142.4	0.0	876.9
10000	45.5	40.4	13.9	0.3	85.8	147.3	2.2	1031.6
30000	37.1	28.8	22.7	0.1	77.3	599.3	0.0	2352.5
60000	32.8	22.8	33.7	0.0	66.3	1610.6	0.0	3559.6
100000	26.6	15.2	36.3	0.0	63.7	2342.5	0.0	4592.6

Supplementary information of Chapter 3

Table A3.4: Effect of GHSV on CO₂ and H₂ conversions, product selectivity and WTY of methanol using Cu/ZnO/Al₂O₃ catalyst at 92 bar, 280 °C, and CO₂:H₂ = 1:3.

GHSV (h ⁻¹)	Conv. (%)		Sel. (%)			WTY (mg _{MeOH} g _{cat} ⁻¹ h ⁻¹)		
	CO ₂	H ₂	CO	CH ₄	MeOH	CO	CH ₄	MeOH
650	32.3	23.6	78.1	8.6	13.0	39.4	2.5	7.4
2000	33.2	25.8	27.4	0.8	71.8	43.1	0.5	128.9
4000	32.9	26.7	26.3	0.4	73.3	82.5	0.8	261.7
6000	32.6	25.8	36.1	0.4	69.7	167.5	1.2	337.3
8000	30.9	27.6	26.4	0.4	64.9	169.9	1.6	537.5
10000	30.0	21.3	45.4	0.2	54.9	326.6	0.9	450.1
30000	28.6	22.8	49.8	0.4	53.6	1124.7	3.8	1293.7
60000	25.9	18.3	44.6	0.8	51.2	1635.9	17.6	2312.6
100000	22.4	13.7	52.3	0.6	47.7	2795.6	22.1	2892.6

Table A3.5: Effect of GHSV on CO₂ and H₂ conversions, product selectivity and WTY of methanol using Cu/ZnO/Al₂O₃ catalyst at 46 bar, 280 °C, and CO₂:H₂ = 1:3.

GHSV (h ⁻¹)	Conv. (%)		Sel. (%)			WTY (mg _{MeOH} g _{cat} ⁻¹ h ⁻¹)		
	CO ₂	H ₂	CO	EtOH	MeOH	CO	EtOH	MeOH
650	21.4	12.7	93.6	0.0	6.4	30.66	0.0	2.4
2000	25.4	14.7	92.6	0.1	8.4	111.3	0.2	11.5
4000	24.3	14.3	73.6	0.2	26.3	169.8	0.9	69.4
6000	24.0	14.4	73.9	0.2	26.0	252.3	1.1	101.5
8000	23.8	14.1	75.4	0.2	24.5	340.0	1.4	126.5
10000	23.8	14.3	77.2	0.2	22.8	444.3	2.5	150.0
30000	25.1	11.2	76.8	0.2	22.3	2116.6	6.5	651.6
60000	24.0	11.0	70.1	0.2	23.3	2542.1	12.2	908.4
100000	20.2	10.0	80.3	0.2	19.7	4255.5	17.4	1191.1

Appendix A

Table A3.6: Effect of GHSV on CO₂ and H₂ conversions, product selectivity and WTY of methanol using Cu/ZnO/Al₂O₃ catalyst, 280 °C, and CO₂:H₂ = 1:3 using 10-20 µm catalyst particles at three pressure conditions (92, 331, and 442 bar).

92 bar

GHSV (h ⁻¹)	Conv. (%)		Sel. (%)		WTY (mg _{MeOH} g _{cat} ⁻¹ h ⁻¹)	
	CO ₂	H ₂	CO	MeOH	CO	MeOH
10000	34.1	27.4	46.5	53.5	382.6	503.7
30000	29.3	21.0	45.1	52.5	958.4	1331.1
60000	25.1	16.5	51.9	48.1	1887.6	2003.2
100000	25.9	17.2	36.8	63.2	2262.4	4449.5

331 bar

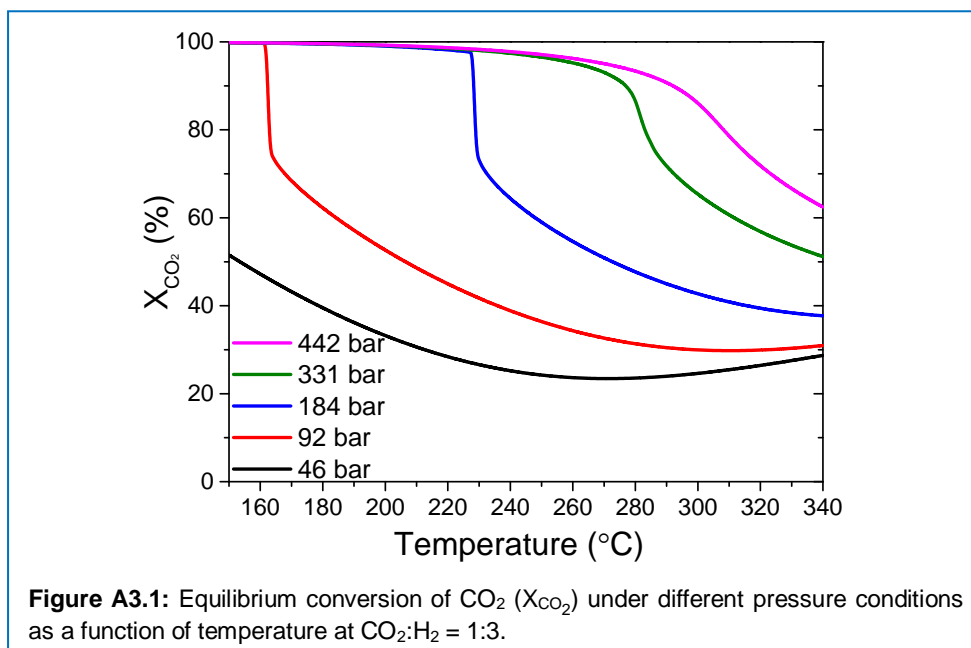
GHSV (h ⁻¹)	Conv. (%)		Sel. (%)		WTY (mg _{MeOH} g _{cat} ⁻¹ h ⁻¹)	
	CO ₂	H ₂	CO	MeOH	CO	MeOH
10000	63.7	57.2	6.5	93.5	100.1	1644.8
30000	46.4	38.2	11.9	88.1	418.4	3545.3
60000	33.8	25.8	18.7	81.3	912.6	4545.1
100000	27.2	22.4	25.0	75.0	1606.1	5513.5

442 bar

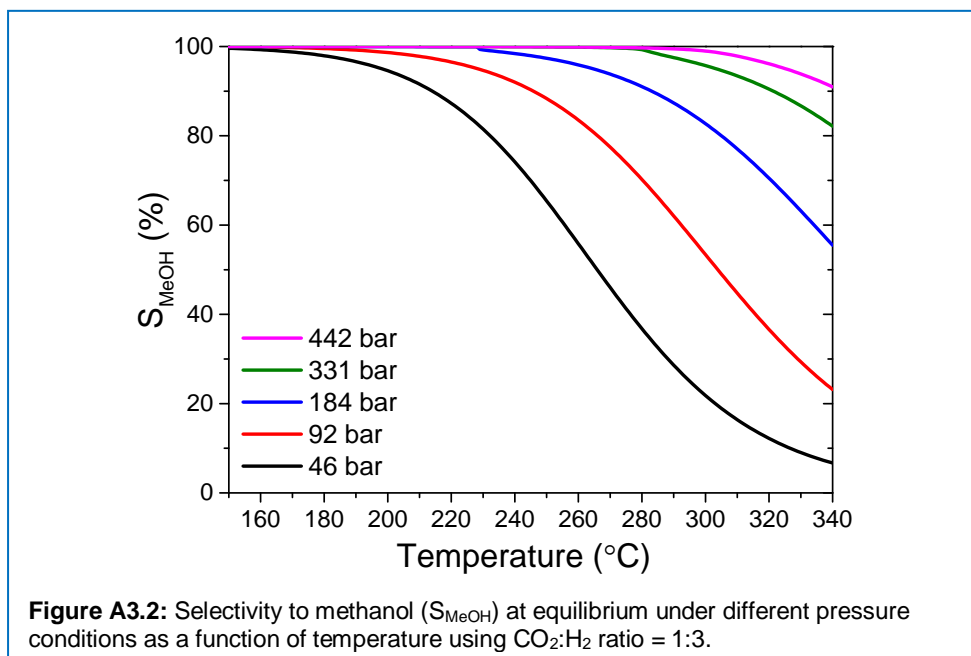
GHSV (h ⁻¹)	Conv. (%)		Sel. (%)			WTY (mg _{MeOH} g _{cat} ⁻¹ h ⁻¹)		
	CO ₂	H ₂	CO	CH ₄	MeOH	CO	CH ₄	MeOH
10000	87.7	83.8	2.2	0.2	97.6	47.3	2.1	2364.8
30000	80.0	73.9	3.2	0.1	96.7	196.8	1.6	6714.8
60000	67.9	61.5	10.0	0.0	93.9	601.2	0.8	10554.7
100000	65.3	58.7	7.9	0.1	91.9	1242.8	12.5	15253.7

Table A3.7: Binary interaction parameters (k_{ij}) for the modified SRK EOS [1]

	CO	CO ₂	Methanol	H ₂	Water	CH ₄
CO	-	0.1164	-0.370	-0.0007	-0.474	0.0204
CO ₂	0.1164	-	0.100	0.1164	0.300	0.0956
Methanol	-0.3700	0.1000	-	-0.1250	-0.075	0.046
H ₂	-0.0007	0.1164	-0.125	-	-0.745	0.001
Water	-0.4740	0.3000	-0.075	-0.7450	-	0.014
CH ₄	0.0204	0.0956	0.046	0.0010	0.014	-



Appendix A



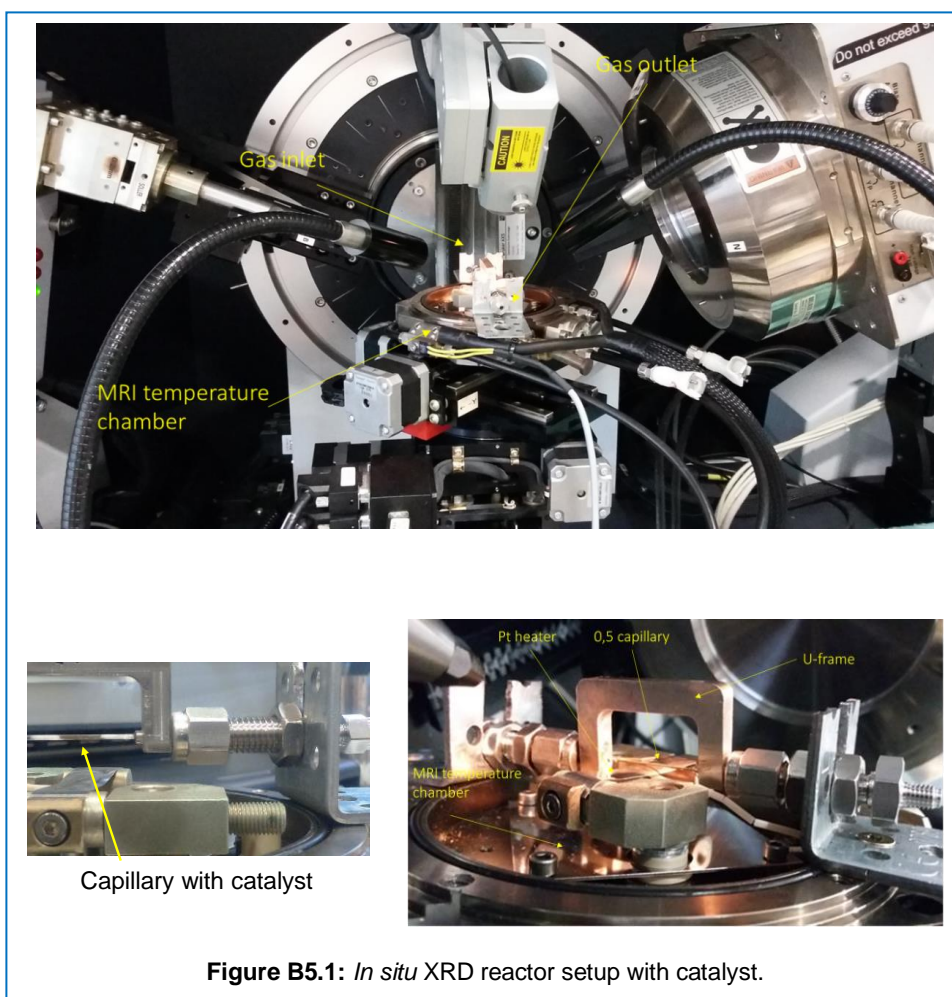
Bibliography

- [1] J.G.v. Bennekom, J.G.M. Winkelman, R.H. Venderbosch, S.D.G.B. Nieland, H.J. Heeres, *Ind. Eng. Chem. Res.*, 51 (2012) pp. 12233-12243.

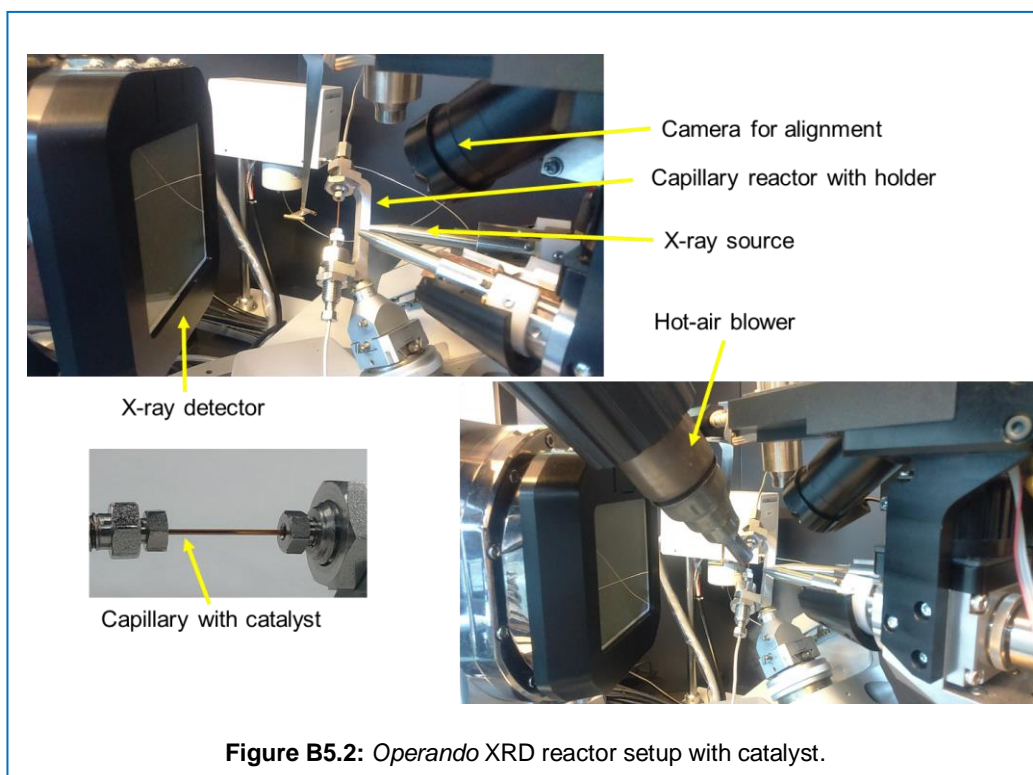
Appendix

B

Supplementary information of Chapter 5



Appendix B

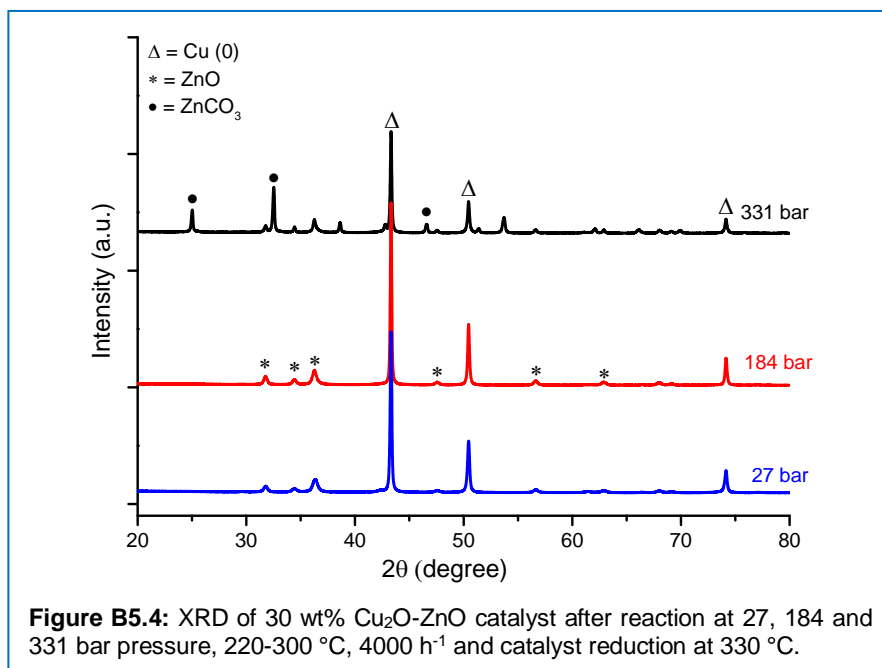
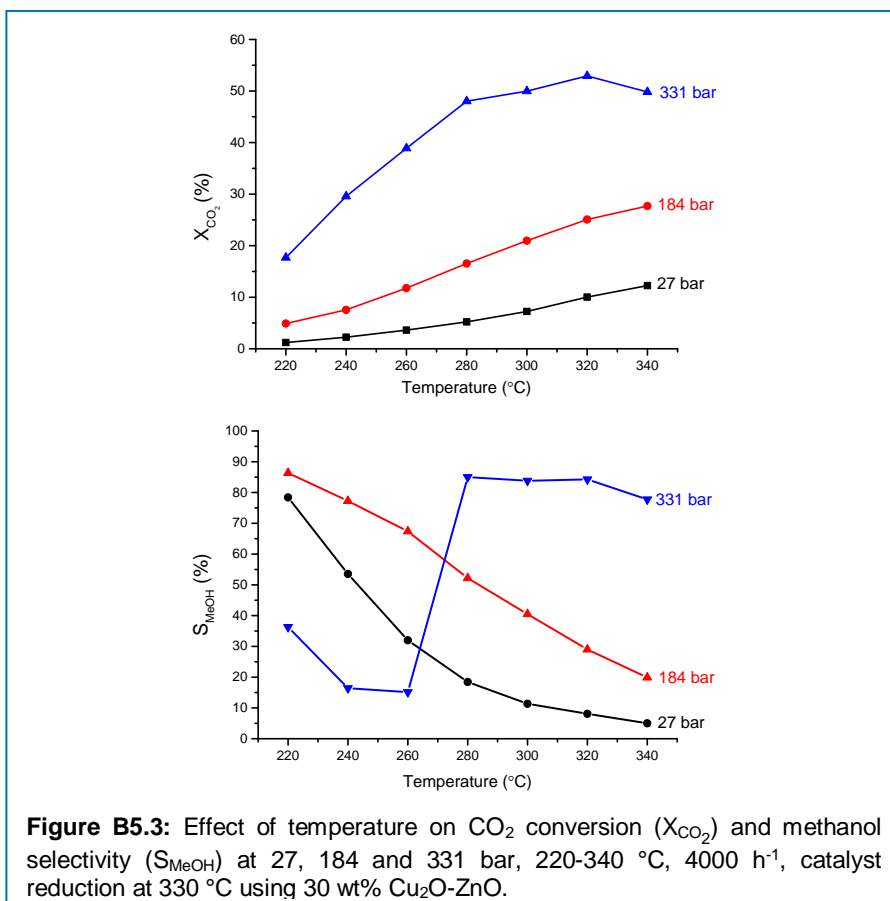


Physicochemical properties

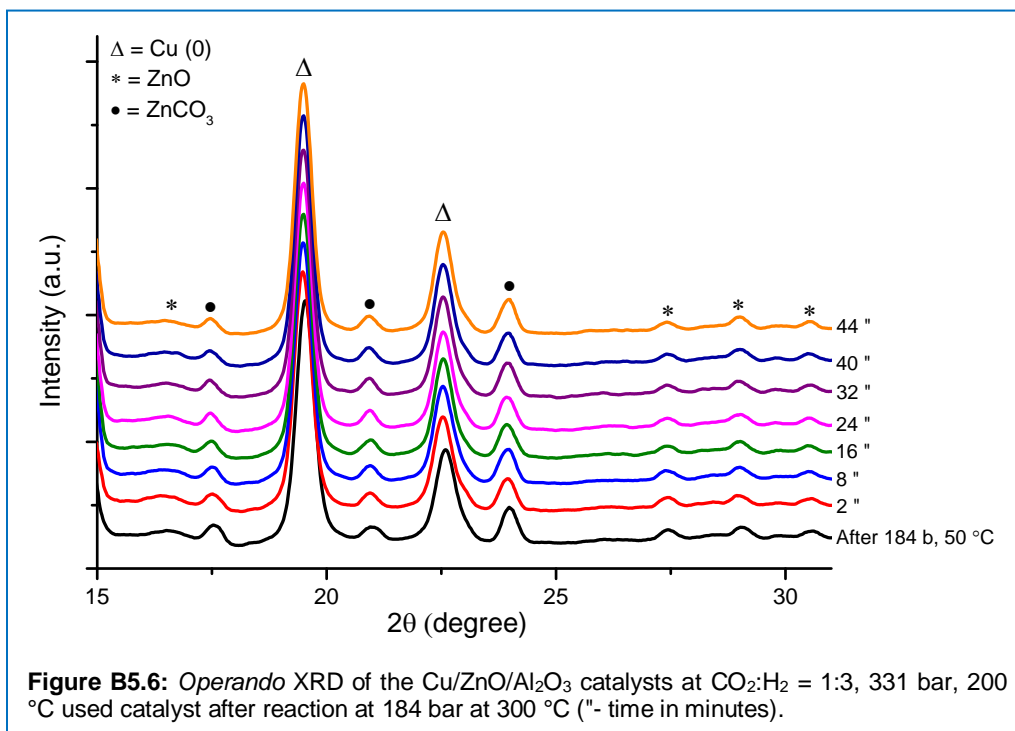
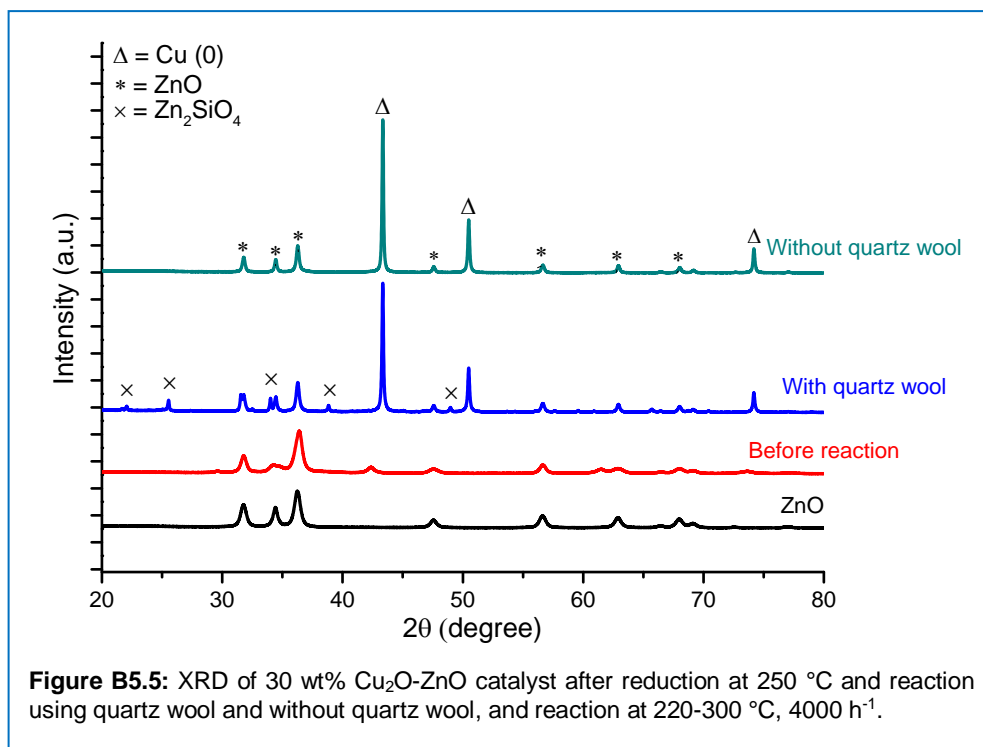
Table B5.1 Copper surface area and crystallite size of catalyst using different wt% loading of Cu₂O-ZnO

Catalyst	Cu (wt %)	Zn (wt %)	S _{Cu} (m ² g ⁻¹)	D _{Cu} (nm)
15 wt% Cu ₂ O-ZnO	15	85	7.7	62
30 wt% Cu ₂ O-ZnO	30	70	10.6	67
50 wt% Cu ₂ O-ZnO	50	50	5.2	71
70 wt% Cu ₂ O-ZnO	70	30	1.2	81

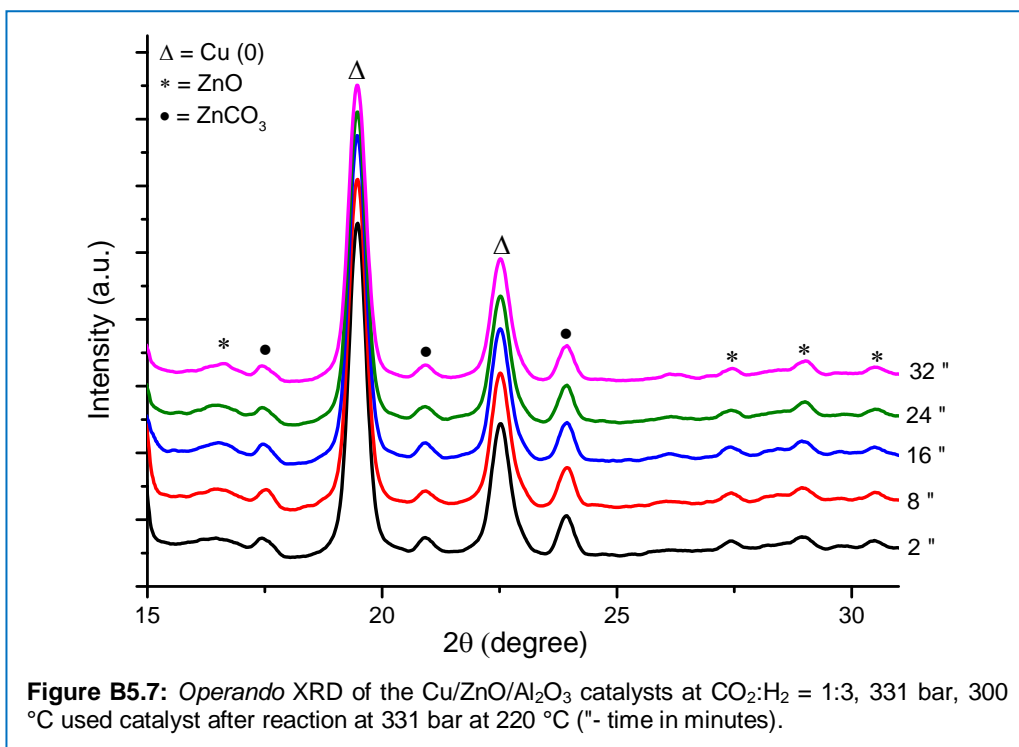
Supplementary information of Chapter 5



Appendix B



Supplementary information of Chapter 5



Appendix B

Shorthand glossary

Abbreviations

Acac	Acetyl Acetonates
AU	Arbitrary Unit
BE	Binding Energy
BET	Brunauer–Emmett–Teller theory for measurement of surface area of material ($\text{m}^2 \text{g}^{-1}$)
BJH	Barrett-Joyner-Halenda method used for pore size and volume measurement ($\text{cm}^3 \text{g}^{-1}$)
BnOH	Benzyl Alcohol
BPR	Back Pressure Regulator
BV	Ball Valve
CCS	Carbon Capture and Storage
CCU	Carbon Capture and Utilization
CV	Check Valve
DFT	Density Functional Theory
EDX	Energy Dispersive X-ray Spectroscopy
EtOH	Ethanol
EXAFS	Extended X-ray Absorption Fine Structure
FID	Flame Ionization Detector
FTIR	Fourier Transform Infrared Spectroscopy
FWHM	Full Width at Half Maximum
GC	Gas Chromatography
GC-MS	Gas Chromatography with Mass Spectroscopy
GHSV	Gas Hourly Space Velocity

Shorthand glossary

HAADF	High-Angle Annular Dark Field
HRTEM	High Resolution Transmission Electron Microscopy
ICI	Imperial Chemical Industries
ID	Inner Diameter
IEA	International Energy Agency
IPCC	Intergovernmental Panel on Climate Change
IR	Infrared Spectroscopy
JCPDS	Joint Committee on Powder Diffraction Standards
MeOH	Methanol
MFC	Mass Flow Meter
MS	Mass Spectroscopy
NL	Normal Liter
OAc	Acetate
OD	Outer Diameter
P	Pressure
PI	Pressure Indicator
PID	A Proportional Integral Derivative
PPM	Parts Per Million
Raman	Raman Spectroscopy technique named after Sir C. V. Raman
RD	Ruptured Disc
RPM	Rotations Per Minute
RT	Retention Time (min)
RWGS	Reverse Water Gas Shift
S	Selectivity
SA	Surface Area
SMSI	Strong Metal Support Interaction
SS	Stainless Steel

STEM	Scanning Transmission Electron Microscopy
T	Temperature
TCD	Thermal Conductivity Detector
TEM	Transmission Electron Microscopy
TGA	Thermogravimetric Analysis
TPD	Temperature Programmed Desorption
W	Watt (Power)
WTY	Weight Time Yield
X	Conversion
XRD	X-ray Diffraction
Y	Yield

Latin Letters

r'_{AS}	Intrinsic Reaction Rate of the Surface Reaction of A
r_A	Reaction Rate (A is CO ₂ in this case)
ϕ_1	Thiele Modulus
C_{surf}	Concentration of A at the Outer Surface
C_{WP}	Weisz-Prater Criterion
D_{eff}	Effective Diffusion
R	Catalyst Particle Size
η	Effectiveness Factor
ρ	Catalyst Density

Shorthand glossary

List of publications

Journal publications

1. “High-pressure advantages in stoichiometric hydrogenation of carbon dioxide to methanol”

Rohit Gaikwad, Atul Bansode, and Atsushi Urakawa. *Journal of Catalysis*, 343 (2016) 127-132.

2. “Cu-ZnO core-shell structure for methanol synthesis: Structure-Activity relationship”

Rohit Gaikwad, Niklaus Kranzlin, Markus Niederberger, Jordi Benet, Dorota Koziej, and Atsushi Urakawa, *manuscript in preparation*

3. “Space-resolved gas analysis of high-pressure CO₂ hydrogenation to methanol”

Rohit Gaikwad, Helena Reymond, Philipp Rudolf von Rohr, and Atsushi Urakawa, *manuscript in preparation*

Conference contribution

1. High-pressure advantages in stoichiometric hydrogenation of carbon dioxide to methanol- **Oral Presentation**

Rohit Gaikwad, Atul Bansode, and Atsushi Urakawa, 253rd American Chemical Society (ACS) conference, held on April 2017 in San Francisco, USA.

2. Cu-ZnO core-shell structure for methanol synthesis: Structure-Activity relationship- **Oral Presentation**

List of publications

Rohit Gaikwad, Niklaus Kranzlin, Markus Niederberger, Jordi Benet, Dorota Koziej, and Atsushi Urakawa, PhD day June 2017, Spain .

3. High-pressure advantages in stoichiometric hydrogenation of carbon dioxide to methanol- **Poster Presentation**

Rohit Gaikwad, Atul Bansode, and Atsushi Urakawa, Zing Conference on, "Carbon Dioxide Catalysis" April 2016, Portugal.

4. CO₂ hydrogenation to methanol synthesis using Cu-ZnO core-shell structure- **Poster Presentation**

Rohit Gaikwad, Niklaus Kranzlin, Markus Niederberger, Jordi Benet, Dorota Koziej, and Atsushi Urakawa, 253rd American Chemical Society (ACS) conference, held on April 2017 in San Francisco, USA.

Curriculum vitae

Personal information

Name	Rohit Vilas Gaikwad
Date of Birth	3 rd August 1987
Place of Birth	Pune, Maharashtra, India
Nationality	Indian
Email	rgaikwad@icmq.es , rvagaikwad@gmail.com

Education

03.2014 - Present	PhD student Institute of Chemical Research of Catalonia (ICIQ) Tarragona, Spain <u>PhD Thesis:</u> "Carbon Dioxide to Methanol: Stoichiometric Catalytic Hydrogenation under High Pressure Conditions" Supervisor: Prof. Dr. Atsushi Urakawa
06.2008 – 05.2010	MSc. In Organic Chemistry University of Pune, India <u>Master Thesis:</u> "Oxidation of benzene to phenol using mixed transition metal oxide catalysts" Supervisor: Dr. V. H. Rane CEPD, National Chemical Laboratory, Pune
06.2005 – 05.2008	BSc. in Chemistry University of Pune

Curriculum vitae

Grants

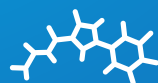
1. FPI fellowship for doctoral study, Spanish government – 2014
2. Research mobility grant from Spanish government – 2015
3. Short research stay grant, Spanish government – 2017

Work experience

10.2013 – 02.2014	Research Intern, Shell Technology Center, Bangalore, India
03.2011 – 10.2013	Research Project Fellow, Chemical Engineering Department, National Chemical Laboratory, Pune, India
10.2010 – 10.2013	E-tutor, TechKnit Enabled PVT LTD



UNIVERSITAT
ROVIRA i VIRGILI



ICIQ'

Institut
Català
d'Investigació
Química